NTNU
Det skapende universitet

Gjenvinning av Sjeldne Jordarter fra Elektronisk Avfall

Berit Johansen Vinje

Materialteknologi
Innlevert: februar 2016
Hovedveileder: Gabriella Tranell, IMTE
Medveileder: Ragnhild Elizabeth Aune, IMTE

Norges teknisk-naturvitenskapelige universitet
Institutt for materialteknologi

PREFACE AND ACKNOWLEDGEMENTS

This thesis was carried out at the Department of Materials Science and Engineering, and was funded by the EU project REEcover, research grant FP7-603564. It is part of work package 3, which aims to upgrade dilute rare earth oxide streams through a pyrometallurgical approach. The goal of the project was to upconcentrate and separate rare earth oxides from the ferrous fraction from WEEE recycling. Initial demagnetization of two of the material inputs was done at Luleå University of Technology by Bertil Pålsson. Those materials were also analysed prior to the experiments described here. The analyses were done by Tecnalia. All other experimental work has been done in the labs of the Department of Materials Science and Engineering, and the results are presented at the end of this report. Students Cathrine Kyung Won Solem, Lene Jensberg Hansen, Ingrid Meling, Oda Marie Ellefsen, Erlend Sverdrup and Martin Storli Værnes did the rough work on the part of the material that was demagnetized at NTNU, as well as the large-scale experiments with the same material.

My biggest thanks go to Lars Klemet Jakobsson for his invaluable help and guidance throughout the whole thesis. Torill Sørløkk did the XRF analyses, Morten Raaness did the EPMA-WDS analyses and Tone Anzjøn helped me with the sessile drop method. The off-gas measurements were done by Ole Kjos. I would like to thank my supervisor Gabriella Tranell for her guidance through this project. I am also grateful to Trygve Lindahl Schanche, Jonas Einan Gjøvik and Dmitry Slizovskiy for their patience with my many questions and requests for help in their labs.

Last, but not least, I would like to thank Kristine Bakken and Jarle Andre Kramer for proof-reading and for their support all the way through.

Berit Johansen Vinje

Trondheim, 31.01.2016

ABSTRACT

The rare earth elements (REE) are a group of chemically similar elements consisting of scandium, yttrium and the lanthanides. They are essential to most new and "green" technologies, but their production is anything but green. Today, China produces more of these elements than the rest of the world together, and dominates the market. Demand is rapidly exceeding supply, yet only about 1% of rare earths are recycled. Because the main use for rare earths is in electrical applications, efficient recycling of electrical waste will soon be vital to the continued use of these elements. Rare earths occur naturally as oxides, and good methods have been established for their extraction. The purpose of this project was to examine if rare earth elements could be effectively separated from electrical and electronic waste as oxides using a pyrometallurgical method.

This project only dealt with the ferrous fraction of electrical waste. Rare earth magnets follow the ferrous stream, and need to be demagnetized to be separated from the iron. A total of three different inputs were examined, collected at different times and from an industrial WEEE recycling process. The material was initially demagnetized and sieved, then melted in a graphite crucible in a graphite tube furnace. The resulting metal and slag phases were consequently examined using SEM and EDS, EPMA, XRF, XRD and the sessile drop method.

The resulting metal and slag fractions were easy to separate, and analyses indicate that all of the neodymium had gone to the slag. Dysprosium and mangenese were found in both slag and metal, however the amounts have not been established. The three different inputs were very different, and conclusions are hard to draw on the economical feasibility of the method until more samples have been collected which establish the average composition of the waste.

SAMMENDRAG

De sjeldne jordartene er en gruppe av grunnstoffer med like kjemiske egenskaper som omfatter lantanoidene og scandium og yttrium. I løpet av de siste tiårene har de blitt essensielle for moderne og "grønn" teknologi, men de er alt annet miljøvennlige å fremstille. Kina dominerer i dag markedet, og produserer mer enn resten av verden til sammen. Etterspørselen etter sjeldne jordarter vokser uten at markedet holder tritt. Bare omkring 1 % av sjeldne jordarter blir resirkulert. Ettersom sjeldne jordarter naturlig forekommer som oksider, er metodene for ekstrahering fra oksider gode og veletablerte. Målet for dette prosjektet var derfor å finne ut om sjeldne jordarter kunne seprareres fra el-avfall som oksider ved bruk av en pyrometallurgisk metode.

Denne oppgaven er kun konsentrert rundt den jernholdige fraksjonen fra el-avfallssortering. Magneter laget av sjeldne jordarter følger denne fraksjonen og må avmagnetiseres for å kunne sorteres vekk fra jernet. Prøver ble hentet totalt tre ganger til forskjellige tider fra en industriell prosess for el-avfallssortering. Materialet ble først avmagnetisert og deretter siktet, før det ble smeltet i grafittdigler i en grafittrørovn. Resultatene ble studert med SEM og EDS, EPMA, XRF, XRD og sessile drop-metoden.

Materialet smeltet i lett separerbare metall- og slaggfaser. Analysene antyder at all neodym har gått til slaggfasen, mens noen stoffer som dysprosium og mangan er å finne i begge fasene. De tre utgangsprøvene hadde svært ulik sammensetning og ga vidt forskjellige resultat, og det er vanskelig å avgjøre om metoden har noe for seg industrielt sett før flere prøver er blitt tatt for å avgjøre hvor gjennomsnittlig sammensetning ligger.

LIST OF ABBREVIATIONS

ABS - Acrylonitrile Butadiene Styrene

CG-MS - Gas Chromatography-Mass Spectrometry

EDS - Energy-Dispersive X-ray Spectroscopy

EPMA-WDS - Electron Probe Microscopy-Wavelength Dispersive Spectrometry

HDD - Hard Disk Drives

HIPS - High Impact Polystyrene

HREE – Heavy Rare Earth Elements

ICP-OES - Inductively Coupled Plasma Optical Emission Spectrometry

LREE – Light Rare Earth Elements

PAH - Polycyclic Aromatic Hydrocarbons

PBB – Polybrominated Biphenyls

PBDE - Polybrominated Diphenyl

PBDD/F - Polybrominated Dibenzo-p-Dioxins and Furans

PC – Polycarbonate

PCB - Printed Circuit Boards

PE – Polyethylene

PHAH - Polyhalogenated Aromatic Hydrocarbons

PP – Polypropylene

REE – Rare Earth Elements

REO – Rare Earth Oxides

RoHS – Restriction of Hazardous Substances

SEM - Scanning Electron Microscope

WEEE – Waste of Electrical and Electronic Equiment

XRD - X-Ray Diffraction

XRF - X-Ray Fluorescence

1 TABLE OF CONTENTS

2 INTRODUCTION

2.1 BACKGROUND

The rare earth elements are a group of metals that are essential to green technologies. In later years, China has moved to dominate the market, making other countries concerned with becoming too dependent on Chinese export. The EU project REEcover aims to find new and sustainable routes of producing rare earth elements. The two routes considered within REEcover are recycling of magnetic waste from waste of electrical and electronic equipment (WEEE) and extraction of rare earth elements from tailing from Swedish iron ores. In this thesis, only the former has been considered. Currently, rare earths are hardly being recycled. The recycling is made difficult by the fact that although there are vast amounts of electrical and electronic waste, only small amounts of rare earths are needed inside each piece of equipment. This needs to be collected and dismantled to access the rare earths, but at present, the rare earths are mostly dispersed into other waste streams. The reduced environmental impact of recycling rare earths would be substantial.

2.2 OBJECTIVE

The goal of this project was to separate the rare earths from iron as oxides for further hydrometallurgical processing. The experiments were conducted using a graphite tube furnace for the smaller-scale experiments on all inputs, and using an induction furnace for the larger-scale smelting of input 2c only. The samples were demagnetized and sieved before melting, then analysed by SEM and EDS, EPMA-WDS, XRD, XRF and the sessile drop method.

3 LITERATURE SURVEY

The rare earth elements are a group of important elements with whom many are unfamiliar. This chapter looks into the chemistry, uses and production of the rare earth elements, before going into some detail on electrical and electronic waste.

3.1 RARE EARTH ELEMENTS

The group of elements that are called rare earth elements (REE) consists of 17 elements that are chemically similar. These are the 15 lanthanides as well as scandium and yttrium, as shown in Figure 3-1. All of the elements occur in nature, except promethium, which only has radioactive isotopes.

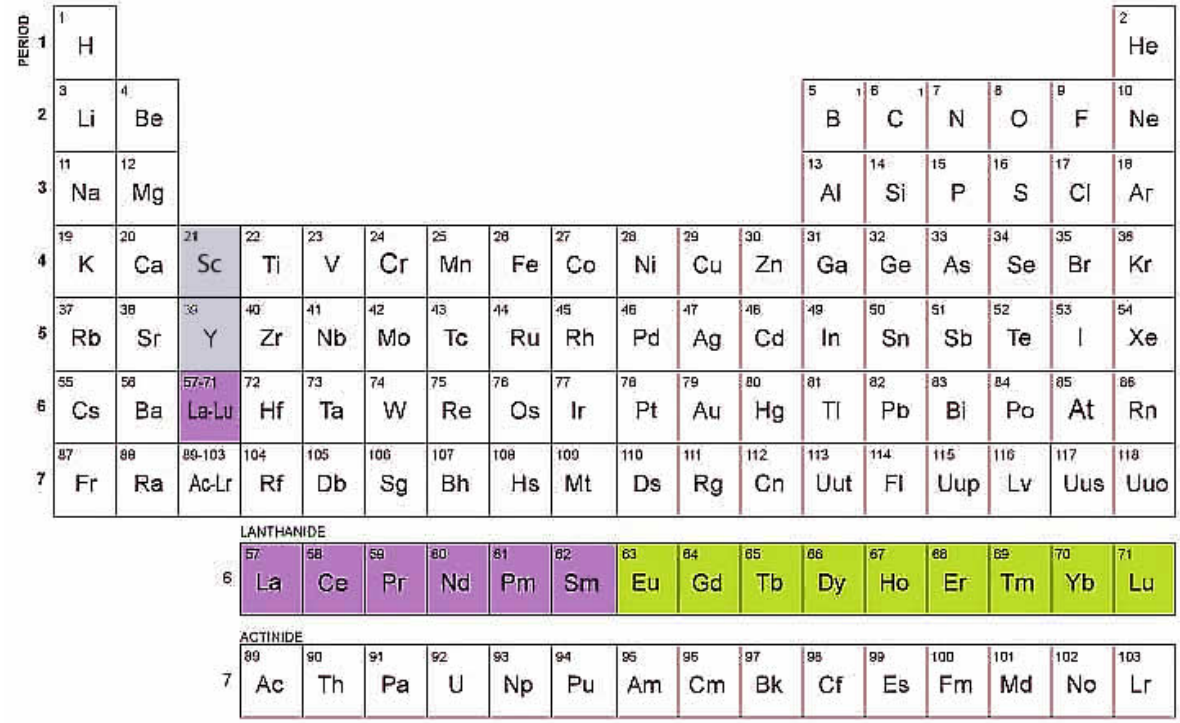

Figure 3-1 The Periodic Table highlighting Sc and Y in grey, the light rare earth elements (LREE) in purple and the heavy rare earth elements (HREE) in green. [1]

When referring to production, demand or abundance of the rare earth elements, common practice is to refer to the amounts of rare earth oxides (REO) rather than rare earth metals, as they never occur as pure metals in nature. The rare earth elements are divided into light rare earth elements (LREE) and heavy rare earth elements (HREE). A common convention is that the LREE include scandium and the elements from lanthanum to europium, while the HREE are yttrium and gadolinium to lutetium. Rare earth minerals are generally high in either LREE or HREE.[2] The most important LREE ores are bastnäsite ($(Ce,La,Y)CO_3F$) and monazite ($(Ce,La)PO_4$), and the most important HREE ore is xenotime (YPO_4). About 95 % of the world's rare earths are found in these three minerals.[3]

The name "rare earths" stems from their discovery, as chemical substances that were thought to be pure elements were once called earths. They are quite abundant, and their name reflects unfamiliarity rather than rarity. However, their occurrence is scattered, and

they invariably occur together in minerals as very stable oxides and behave as an entity. In fact, most of the rare earth minerals that were first assumed to be new elements have later been shown to consist of several, illustrating how difficult they are to separate.[3]

3.1.1 World resources

Seen from the 2014 demand for rare earth elements, the world resources are large enough to last for at least 1000 years for all elements but Eu, which has around 600 years resource. However, the demand is increasing rapidly and the world production is unable to meet the current demand. For Eu, the peak production, i.e. the production rate and year at which the production starts to decline, might be only 10 to 30 years away. Figure 3-2 shows a comparison of the abundance of several elements.

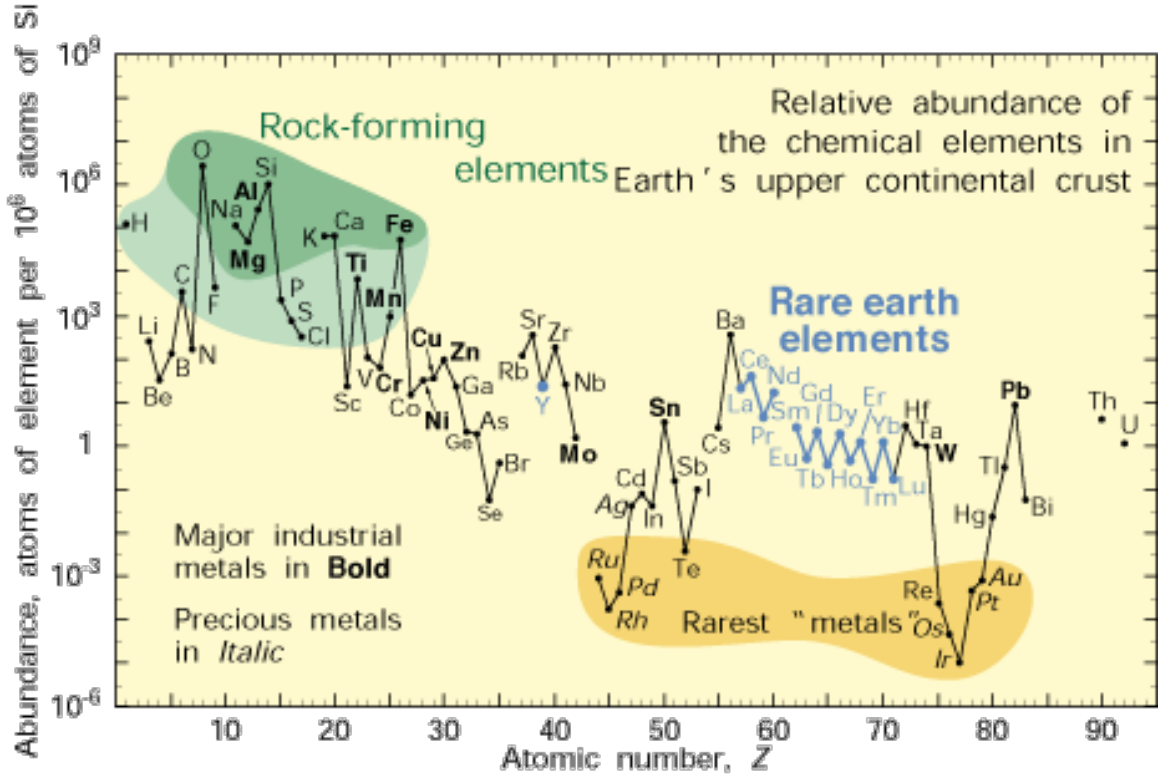

Figure 3-2 The abundance of the elements of the Earth's upper continental crust, with the rare earths marked in blue [4].

3.1.2 Uses

The REEs are becoming increasingly important due to their applications in green technologies, as they are essential to permanent magnets, lamp phosphors, rechargeable NiMH batteries and catalysts. The rare earth permanent magnets are 3-10 times stronger than those that are either ceramic based or aluminium based permanent magnets. Smaller sized technology such as cell phones and laptops would not be possible without rare earths.[5] The U.S. Department of Energy lists dysprosium, neodymium, terbium, europium and yttrium as critical elements for further advances in clean energy technology. [6] As an example, in the new generation of wind turbines, two tons of rare earth magnets is needed for the permanent magnet generator on top of the turbine. Table 3-1 shows the main uses of the rare earth elements.

Table 3-1 Applications of the rare earth elements, again marked in grey, purple and green, referring to Sc and Y, the LREE and the HREE, respectively [3]

Rare Earth Element	Applications
Scandium (Sc)	Ceramics, lasers, phosphors, high performance alloys
Yttrium (Y)	Highest affinity for oxygen of all elements. Used in fluorescent lighting phosphors, computer displays, automotive fuel consumption censors, and ceramics as crucible for reactive, molten metals.
Lanthanum (La)	Catalysts, hydrogen storage batteries, green phosphors, laser crystals
Cerium (Ce)	Phosphors, ceramics, catalysts, UV-blocking in glass, polishing agent in precision optical polishing
Praseodymium (Pr)	Yellow pigment in ceramics
Neodymium (Nd)	Purple colouring of glass, welding goggle tinting, lasers, dielectrics. Neodymium-iron-boron permanent magnets ($Nd_2Fe_{14}B$) are the strongest permanent magnets available.
Samarium (Sm)	Samarium-cobalt permanent magnets (Sm_2Co_{17}) for lightweight or high-temperature electrical applications, lasers, dielectrics
Europium (Eu)	Unique luminescent behaviour used in red phosphors and medical and biochemical applications
Gadolinium (Gd)	Phosphors and scintillated materials, contrast agent for MRI due to high magnetic moment
Terbium (Tb)	Phosphors
Dysprosium (Dy)	Essential additive in NdFeB production due to very high magnetic moment
Holmium (Ho)	Highest magnetic moment of all elements, used as pole piece or magnetic flux concentrator in high strength magnets. Also in lasers for medical uses.
Erbium (Er)	Glass colouring, amplifier in fiber optics, lasers for medical use
Thulium (Tm)	Crystals, lasers, portable x-ray sources
Ytterbium (Yb)	Fiber amplifier and fiber optics technologies, lasers, silicon photocells, stress gauges exploiting ytterbium's increased electrical resistance when exposed to very high stress
Lutetium (Lu)	Lacks magnetic moment, host for x-ray phosphors due to forming the densest known white material, $LuTaO_4$.

3.1.3 Production

For a long time, Mountain Pass, California was the most important rare earth elements deposit, but China now dominates the production, controlling 85 % of the world supply. 45 % of the world supply is produced at the world's richest rare earth deposit, Bayan Obo, near Baotou, China. The newly opened Mount Weld in Australia is also one of the most promising deposits in the world. Kvanefjeld, Greenland, has a very large deposit of both LREE and uranium, and are doing pilot testing for the production of both.[7] REE supplies are limited in part to the fact that although the elements occur together, the concentrations of the individual elements can be very different, and vary between deposits of the same type of mineral. The light rare earth elements are more abundant than the heavy rare earth elements. Another factor is that rare earths are often by-products dependent on the market value of the main product, and they often contain significant amounts of thorium, making them undesirable or unprofitable to produce.[3] Figure 3-3 shows the distribution of rare earths between countries.

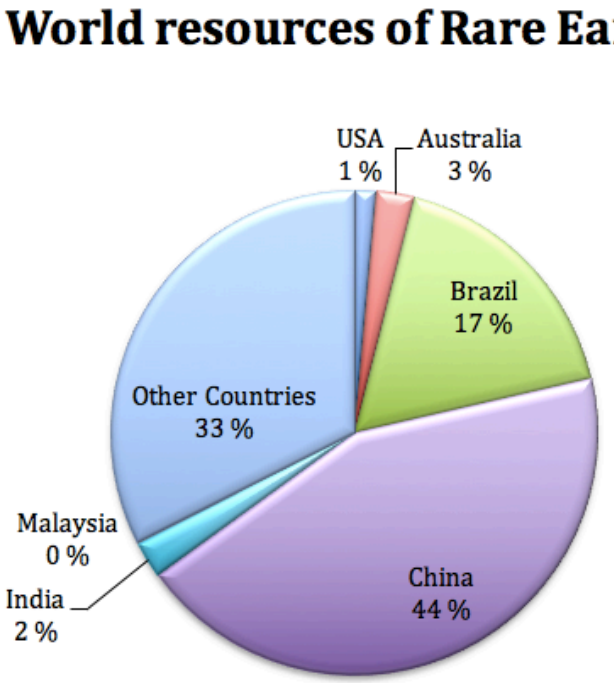

Figure 3-3 World rare earth resources [8].

Most rare earth mining is either open pit, underground or *in-situ* leaching. Figure 3-4 shows the overall steps for the extraction, very simplified. These steps are energy, water and chemical intensive, and pose large risks to the environment. For adjacent water basins and rivers, the greatest hazard is radioactive substances (thorium and uranium), acids, fluorides and heavy metals. Air emissions also include thorium and uranium, as well as hydrofluoric acid, hydrochloric acid, sulphur dioxide, sulphur trioxide and dust. There is also the issue of tailing management. However, this has mostly been due to bad regulations of the industry. There are estimates indicating that for the production of 1 ton of REE, 60,000 m^3 of gases mixed with H_2SO_4 and HF is produced, as well as 200 m^3 of acid water and 1.4 tons of radioactive waste. [7]

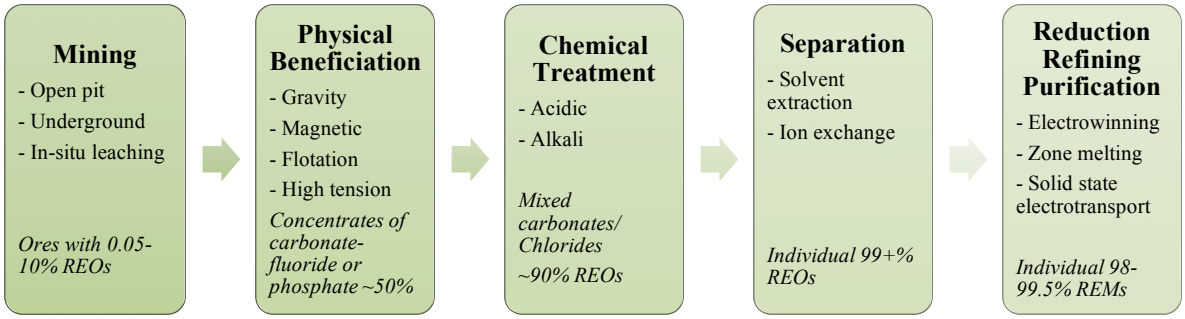

Figure 3-4 Processing routes for REE ores [3]. Adapted from [9].

The process typically starts, as shown in Figure 3-4, with an ore with a REO concentration of between 0.05-10 %. The second step is then to beneficiate the ore by separating the different minerals from each other through either magnetic, high tension or electrostatic separation, gravity or froth flotation, depending on the ore and its constituent minerals. The resulting concentrates have a rare earth oxide concentration of approximately 50-60 %.[3] In some of these processes, there is little environmental impact due to low energy consumption and no use of chemicals, however from for instance flotation, this step can lead to large tailing ponds and release of heavy amounts of wastewater, ground-up materials and chemicals.[7]

The third step involves chemical treatment, and is the step with the highest environmental impact. The acidic route stands for at least 90 % of the extraction methods. In the case of monazite, the mineral is treated with caustic soda, leaving a marketable phosphate by-product. Thorium is then separated from the rare earth oxides by fractional precipitation through leaching with hydrochloric acid. Bastnäsite is first treated with hydrochloric acid to remove calcium and strontium carbonates. It is then calcined to remove carbon dioxide. The resulting rare earth oxide concentration is 85-90 %. For xenotime, the acid treatment involves concentrated sulphuric acid at 300°C.

In the fourth step, the individual rare earth oxides are separated from each other using the small differences in basicity that is due to the decrease in ionic radius from lanthanum to lutetium. These differences have an influence on the solubility of salts, the hydrolysis of ions and the formation of complex species. The separation processes include selective oxidation, fractional crystallization, fractional precipitation, ion exchange and solvent extraction.

After these four steps, the resulting products are the rare earth oxides. As these oxides are extremely stable, reducing them to metals is very difficult. The pure metals can be produced through the reduction of anhydrous chlorides or fluorides or reduction of rare earth oxides. Rare earth chlorides or chloride-oxide mixtures may also be reduced through fused salt electrolysis.[3]

As described in detail by Krishnamurthy and Gupta [3], under standard conditions and according to the Ellingham diagram shown in Figure 3-5, the only elements that can reduce rare earth oxides or rare earth fluorides are calcium and, at high temperatures,

carbon. However, the melting temperature of calcium oxide is very high (2570°C), making it an unsuitable process. Carbothermic reduction under vacuum and at high temperatures should be effective because it makes $p_{CO}<<1$ and thereby $a_{CO}<<1$. However, carbides are formed along with the reduction, which form very stable compounds with oxygen and nitrogen, complicating the process. The activity of the oxides can be lowered to change the free energy of the reaction. This can be done by forming a product metal with a low boiling point so that it vaporizes in the metallothermic reaction (lowering the partial pressure, p, and the activity, a, of the metal), recovering the reduced metal as an alloy (lowering the activity of the metal), or by trapping the compound formed by the reductant in a complex slag (lowering the activity of the slag).

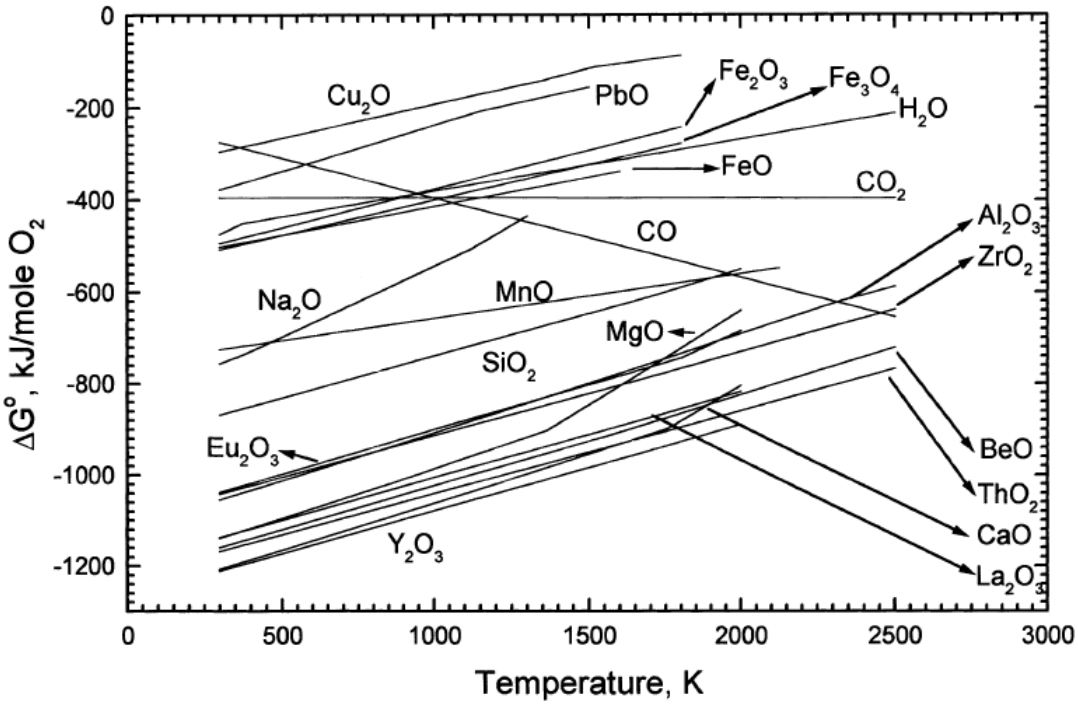

Figure 3-5 Standard free energy of formation as function of temperature of selected oxides of rare earth and some common metals [3].

The halide route is the preferable route for most of the rare earths. A rare earth chloride or fluoride needs to be prepared first. The fluorides can be reduced by calcium oxide to a high purity, while the chlorides can be reduced by potassium, sodium and lithium as well as calcium. Using fluoride gives the best result but is the most costly. For the elements samarium, europium and ytterbium, the best way to reduce their oxides is through lanthanothermy, that is, metallothermic reduction by lanthanum. Most rare earths are electrolytically reduced by recovering the rare earths as binary alloys with low melting temperatures, which can further be distilled to pure metal.

For some applications, the reduced metal is pure enough after the reduction step. Others may need refining. Refining is done with a sequence of different processes to remove all the different impurities. This step is very difficult because, as the rare earths are so reactive, impurities may come from the refining container itself. After for instance fluoride reduction, the sequence may consist of vacuum melting, vacuum sublimation and

solid-state electrotransport to give metals of over 99.5 % purity. Ultrapure metals may be achieved through zone melting, in which the impurities are not removed but redistributed, creating zones that are 99.99 % pure.[3]

3.1.4 China and environmental concern

The United States led the research efforts and innovations within the field of rare earths up until the 1980s, when China gradually began to take over the market as illustrated in Figure 3-6. Since the 1980s, China has invested large amounts of money into technological research, in particular to rare earth elements. They now have two state key laboratories as well as two institutes dedicated to rare earth elements. The only two journals in the world that focus almost exclusively on rare earths are both published by the Chinese Society of Rare Earths.

The bastnäsite deposit at Bayan Obo in Inner Mongolia, China has been known since the 1930s. The rare earth production there is only a by-product of the iron production that has been going on since the 1950s, and is a result of China's focus on maximising the output from the mine. Between 1978 and 1989, their production of rare earths increased by an average of 40 % every year.[10] As exports grew through the 90s, China outperformed other producers such as Molycorp, owner of the Mountain Pass mine, California, and the latter closed in 2002. This was also in no small part due to environmental concerns.

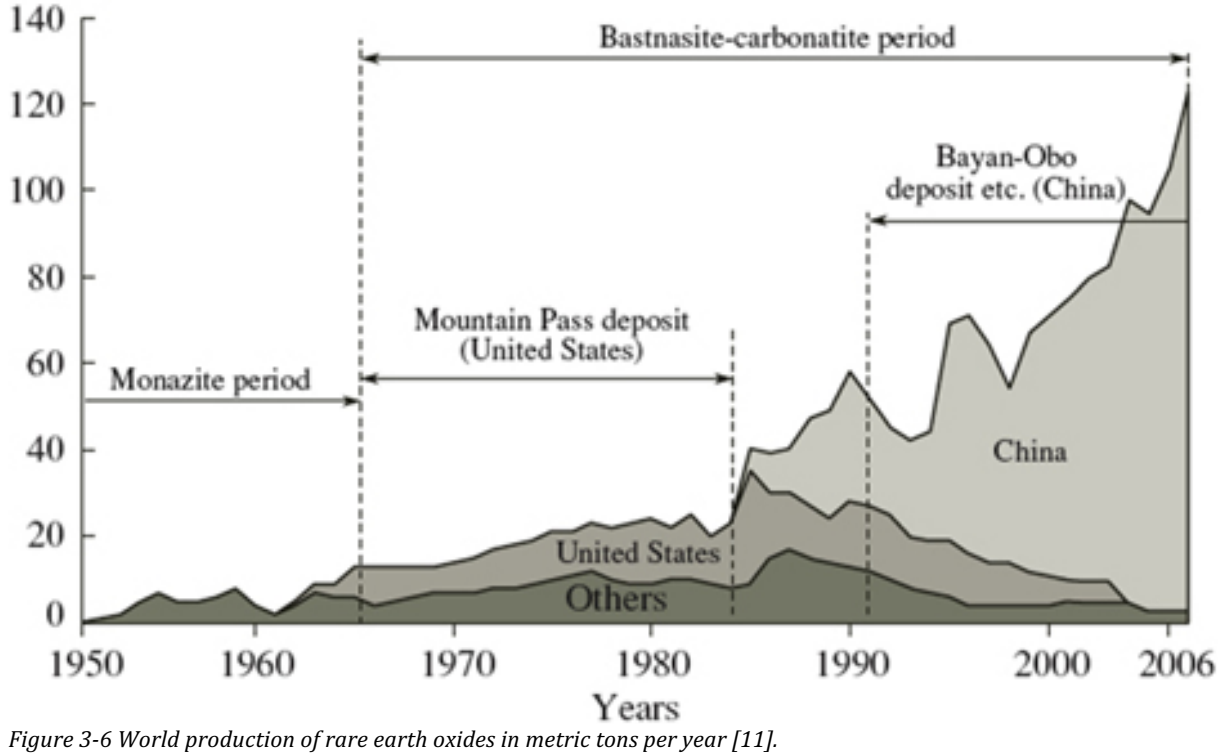

Figure 3-6 World production of rare earth oxides in metric tons per year [11].

In 1995 China National Non-Ferrous Metals Import & Export Corporation managed to acquire GM's NdFeB magnet division by agreeing to the U.S. government demand to keep the production in the U.S. for at least five more years, only to move the entire production to China five years later. In less than a decade the permanent magnet market shifted, and

from being mostly produced in Japan, the U.S. and Europe in 1998, permanent magnets were by 2007 almost exclusively made in China. In 2005, China nearly managed to purchase Unocal, which owns Molycorp. If the sale had gone through, China would have had monopoly over all the greatest rare earth resources in the world. In 2009 they also came close to owning a major share in the Australian Mount Weld mining company, Lynas Corporation. The Australian government stopped the sale.[10]

The Chinese rare earths industry has been poorly regulated, with extensive smuggling from illegal mines and vast environmental damage. In 2008, one third of the export was through smuggling. This shows a serious lack of control over the industry. As the illegal export contributes to keeping prices low and depleting resources more quickly, it can be very harmful. It also leads to more environmental destruction.

Producing 1 tonne of rare earths generates 2,000 tons of tailings, which more often than not are radioactive. Most of the ten million tons of acidic and radioactive wastewater from the rare earth mining activities at Bayan Obo are discharged without being effectively treated, and a lot of this is dumped into the Yellow River. The Yellow River serves as irrigation water for the around 150 million people living along it between Baotou and the Yellow Sea.[10] In a 2012 interview with Le Monde, an old farmer living near Baotou described how crops began to die in the late 90s on the once lush farmland. Animals became sick and died, and the neighbouring villages to Baotou have been mostly deserted.[12] China has general pollution control standards, but until 2009 they had no specific pollution discharge standards for the rare earths industry.[10] The risk of losing investments to the government is one of the factors hindering the development of environmentally friendly mining activities. In China, the land is owned by the government and could at any time be seized, for instance to make a new railroad through the premises. There is no economical support offered as incentive to make improvements.

Because of the sheer size of the industry, China has also had great difficulties in enforcing their not very strict safety regulations. This is not made easier by the fact that people and companies cannot be held accountable for accidents. Workers at the rare earth refineries are exposed to chemicals such as ammonium bicarbonate, oxalic acid, hydrofluoric acid, sulphuric acid and radioactive dust, and pneumoconiosis, or black lung, is the most common disease in Baotou.[10]

Due to the expected increase in domestic consumption and the wish to take control over its own industry, as well as the fear of depleting its resources too fast, China began restricting export quotas in 2009. This move was also to control more of the global production, as the export of semi-finished goods is being limited while the export of finished products is encouraged, forcing more and more companies to move their production to China. This led to a spike in prices in 2011 that amplified the fears of other countries that they would become too dependent on China. Some also predict a disproportion in supply and demand as consumption, not only from consumer goods but also green technology such as wind mills, continues to increase rapidly in the years to come.

3.2 WASTE OF ELECTRICAL AND ELECTRONIC EQUIMENT (WEEE)

3.2.1 Problems associated with e-waste

E-waste is a generic term which covers all end-of-life products with either a battery or circuitry. It includes everything from large and small household appliances and toys to sound systems, computers, small electrical devices and medical equipment. Actual global amounts of e-waste are hard to calculate because different countries define differently what e-waste comprises, and also because not all electric and electronic equipment enters the proper recycling chain. Estimates are made based on the amounts of EEE put on the market. This was approximately 20 million tons in 1990 and 80 million tons in 2015. The global amount of e-waste in 2015 has been estimated to 50 million tons.[13] In Europe alone, it is expected to be more than 12 million tonnes by 2020.[14] Figure 3-7 shows a pile of WEEE. The WEEE man, shown in Figure 3-8, is a product of the environment awareness initiative of RSA and Canon Europe in 2006, and is built from the estimated amount of WEEE that each UK citizen will produce in a lifetime.

Figure 3-7 Pile of WEEE at Coolrec recycling plant [15].

Figure 3-8 The WEEE Man: A 7m tall sculpture made from the 3.3 tonnes of WEEE generated in a lifetime by an average UK citizen. [16]

E-waste contains a range of hazardous materials, but also valuable and precious metals. The waste requires careful handling, and advanced technologies have been developed that minimize harm to humans and the environment, whilst maximizing the recovery of resources. However, much e-waste is rather sent to underdeveloped countries where it is dismantled manually and with low and selective resource recovery.[13] The e-waste is

sent under the pretence that everything is reusable and helps bridge the digital gap between developed and developing countries, but up to 75 % of what is sent is useless scrap. The crude dismantling methods expose the workers to toxic or carcinogenic substances, and because useless waste is sent to landfills or incinerated, it causes great and lasting harm to the local environment. [17]

Several initiatives have been made to steer e-waste handling into a sustainable future, notably StEP and the Basel Convention. The Solving the E-waste Problem (StEP) Initiative of 2004 is a global platform for cooperation and sharing of knowledge on e-waste management. [13] The Basel Convention on the Control of Transboundary Movements of Hazardous Wastes and Their Disposal, a United Nations treaty, intends to prevent movement of hazardous waste between countries, specifically from developed to developing countries. While 182 states and the European Union have signed the convention, the U.S. have not. The Basel Ban Amendment bans export of hazardous waste for any reason including recycling, from certain developed countries to developing countries. The amendment has not been accepted by enough states to make it to enter into force, as countries such as Canada and Australia have strongly opposed it. It has however been adopted by the EU and made legally binding to all member states. [18]

3.2.2 The WEEE and RoHS Directives

The EU Waste Framework Directive was first launched in 1975. The trouble with it was that concepts such as “waste” were only loosely defined and opened up to many different interpretations among the member states. It has since been amended with clearer definitions to ensure the practices in different member states are the same. The intention of the directive is to reduce landfill levels by promoting waste as a secondary resource. The directive emphasises a hierarchy in which the main goal is to not create waste at all, then to recycle and reuse the waste that has been created. It also focuses on energy recovery and the need for proper disposal. The costs of disposal of waste is placed on the producer, and the more waste a producer creates, the more they have to pay to have it disposed of.

The Waste Electrical and Electronic Equipment (WEEE) directive follows the same hierarchy as the Waste Framework Directive. It was introduced in 2002. Producers and distributors have to pay for the costs of WEEE collection, treatment, recycling and recovery. The producer has to comply with the laws and regulations of the country from which their product is bought, and the return of WEEE must be free of charge for the consumer. All though the directive was introduced in 2002, it took until 2008 before it had been implemented by all member states.[13] The directive lists WEEE into ten different categories:

- Large household appliances
- Small household appliances
- IT and telecommunications equipment
- Consumer equipment
- Lighting equipment
- Electrical and electronic tools
- Toys, leisure and sports equipment
- Medical devices

- Monitoring and control instruments
- Automatic dispensers

It also specifies which kinds of equipment are included within each category.[13]

The Directive on the Restriction of Hazardous Substances (RoHS) of 2006 aims to ensure that the recycling and disposal of WEEE not pose any risks to health or the environment. The directive bans lead, mercury, cadmium, hexavalent chromium, polybrominated biphenyls (PBB) and polybrominated diphenyl ether (PBDE) from use in EEE. In certain situations, and where no substitutions exist, some of these substances are however permitted. One significant effect of the overlap of products older and newer than 2006 is that old parts containing prohibited substances cannot be reused in new products.[13]

3.2.3 The material content of WEEE

In general, WEEE contains a mixture of ferrous and non-ferrous metals including precious metals, and different types of plastics and ceramics. The material content of WEEE is rapidly changing and is very different for products made before and after 2006. Not only is the composition changing because of the prohibition of certain substances, such as in the switch from lead-based to lead-free solders; the products themselves are also evolving rapidly, as with the change from CRT-based televisions to LCD screens. Due to this as well as the vast range of products that are covered by the term WEEE, the composition of WEEE is extremely varied and inhomogeneous. The material distribution reported by Hense et al. [19] is shown in Figure 3-9, though it is worth noting that different researchers have found highly disparate numbers [20].

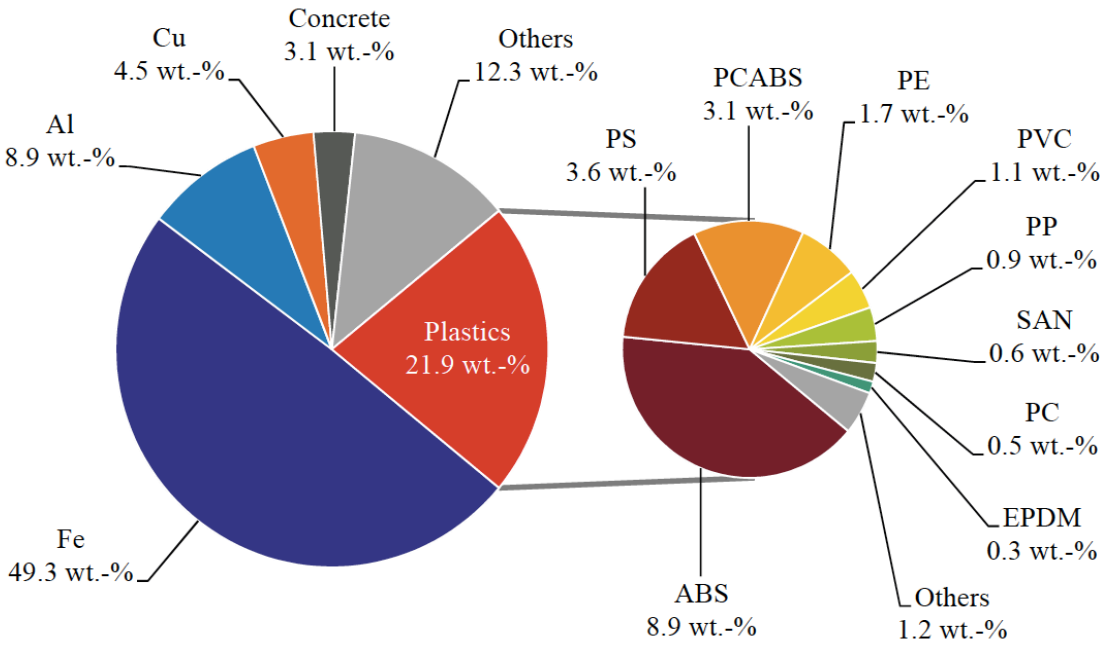

Figure 3-9 Material content of WEEE.[19]

3.2.4 Current reuse, handling, sorting and recycling of WEEE

Traditional methods for WEEE recycling focus on separating metals from non-metals in high volumes. The WEEE must first be manually sorted to take out any easily removable parts as well as e.g. batteries, cables and separable plastic parts. The remaining scrap is

then mechanically shredded and comminuted, and the ferrous fraction is separated magnetically from the rest while eddy-current is used to separate non-ferrous metals from plastics and other fractions. With small domestic appliances, the process may be more complex and include manual removal of hazardous components in-between the above steps. Because the plastics are usually mixed and contaminated, their widespread fate in Europe has been incineration for energy recovery. They may also be sent to other countries for sorting and reuse. In Japan, the electronics manufacturers are more closely involved in the recycling of their own products through ownership of the recycling facilities, and the facilities are shaped more like reverse production lines, allowing the products to be dismantled with much less contamination and increasing the opportunities for reuse. [13, 21]

The chemistry of plastics was interesting to this project because of the amount of plastic that was present in one of the samples, input 2c MET-2. Studies on pyrolysis of WEEE plastics were examined since the sample was to be heated to 500°C.

In the recycling of WEEE plastics it is hard to obtain a product with the same quality and at the same price as new material, due in part to the varying quantities and types of plastics. As also seen in Figure 3-9, the most important plastics used in WEEE are acrylonitrile butadiene styrene (ABS), polypropylene (PP), high impact polystyrene (HIPS), polycarbonate (PC), PC/ABS blends and polyethylene (PE). All of these are relatively easy to separate and recycle, but small inclusions of other types of plastics, such as polyphenylene oxide blends (PPO) and polyvinylchloride (PVC), complicate things [13]. In addition, about one quarter of WEEE plastics contain flame retardants, and one third of these are halogen based [19]. These need to be identified and sorted out if the rest of the polymers are to be reused. Incineration of WEEE plastics for energy recovery requires extensive purification of the off-gases. When halogenated flame retardants are thermally decomposed, they may form highly toxic and persistent polycyclic aromatic hydrocarbons (PAH), polyhalogenated aromatic hydrocarbons (PHAH) and polybrominated dibenzo-p-dioxins and furans (PBDD/F). These form mainly in the temperature range of 250-450°C and in the presence of oxygen. The main bromine compound above 400°C is HBr [19]. Plastics pyrolysis is usually done in a fixed bed reactor. Other highly toxic and corrosive compounds that may form during pyrolysis are ammonia, hydrogen cyanide, hydrogen fluoride and hydrogen chloride. Aside from the health and environment hazards associated with these substances, they are also corrosive and influence the choice of materials for the reactor or furnace [13].

Printed circuit boards (PCBs) make up approximately 2 % of WEEE [22] and are especially problematic to recycle. PCBs contain 40% metals, 30 % ceramics and 30 % plastics, and their main value is in the recycling of copper. They also contain a lot of iron, SiO_2, Al_2O_3, epoxy and fiberglass, as well as a host of precious or problematic materials, such as gold, palladium, lead and antimony. Flame retarded thermosets are the main polymer type in PCBs. PCBs of size bigger than 10 cm^2 are sorted out manually before grinding to be processed separately, but those that are smaller continue into the general waste stream [13].

3.3 RARE EARTH ELEMENTS IN WEEE

Non-ferrous metal recycling plants mainly focus on copper and some precious metals. In the modern recycling of copper, processes are designed that allow recovery of up to 17 metals, however rare earths and most precious metals are lost to the slag [19]. The same is true for the ferrous stream. The rare earth magnets are brittle, and upon shredding they crush into a fine powder that sticks to iron, which is then lost in the slag in such low concentrations that recovery is not economically feasible.

3.3.1 Previous attempts to extract rare earths from e-waste

Quite a few studies have been made into the recycling of rare earths from either manufacturing scrap or from end-of-life scrap. The former can be relatively easy because the manufacturer already knows the scrap's composition, because the concentration is high and because it has not been polluted. End-of-life scrap needs to be collected and properly sorted and dismantled, and the product is likely degraded and of an unknown, complex composition. Krishnamurthy and Gupta [3] have presented an extensive overview on efforts within REE recycling from scrap. Most studies focus on batteries and magnets, and only few look at post-consumer scrap. Direct recycling and reuse is only relevant for large and easily accessible magnets from vehicles and wind turbines, while all others need further processing. Hard disk drives (HDDs) consume the most rare earth permanent magnets of all electronic equipment (6000-12000 tons), and because of the turnover rate and the fact that they are sorted out from other WEEE, HDDs may be the best source of NdFeB magnets from WEEE. Efficient separation of REE magnets from scrap was seen as one of the key barriers to magnet recycling during the EU-Japan-US Trilateral Conference on Critical Raw Materials of 2011[2]. It is easy to demagnetize the magnets by heating them above 300°C, but because the magnets may either be sintered or bound together with epoxy, demagnetization means melting organic binders and glue, resulting in the creation of hydrocarbon vapours. Many studies therefore look into other ways of collecting the magnets[2]. A recent and noteworthy study published by Hoshi *et al.*[23] employed the same method to pure Nd magnet manufacturing scrap as the one that was applied to end-of-life scrap in this project, except that graphite was added to the scrap to conserve the crucibles. They also achieved similar results as in this report.

NdFeB magnets are made from an $Nd_2Fe_{14}B$ matrix phase that is surrounded by a neodymium-rich grain boundary phase. The grain boundary phase may be alloyed with small amounts of praseodymium, gadolinium, terbium, and especially dysprosium, as well as other elements such as cobalt, vanadium, titanium, zirconium, molybdenum or niobium. It can also contain copper, aluminium or gallium. Dysprosium is added to magnets to increase their temperature stability against demagnetization[2].

NiMH batteries are an example of scrap that is sorted out for special treatment, and could have a high potential for rare earth recovery. Discarded batteries are currently used as a cheap source of nickel in steel recycling. They contain 8-10 % misch metal, which is a mixture of LREE with a composition resembling that of monazite. If melted in an electric arc furnace, a nickel-cobalt alloy has been obtained, with the REO forming as slag [3]. The Ames process uses liquid metal solvents to recycle NdFeB magnets by taking advantage of the fact that Nd is highly soluble in molten magnesium or silver, while iron and boron are not. The process produces very pure material, but is slow and cannot handle partially

oxidized scrap. Partly oxidized REE magnets from manufacturing scrap can be recycled using electroslag refining, in which impurities in the scrap are trapped in a reactive flux consisting of a mixture of $CaCl_2$, CaF_2 and a rare-earth fluoride [3]. In the case of homogenous scrap, for instance REE magnets from HDDs, alloys may be reprocessed after hydrogen decrepitation[2]. Hydrometallurgical processing generally works for all types of magnet scrap, and the methods are the same as for extraction from primary ores. However, it requires multiple steps and chemicals, and generates a lot of waste water.

4 EXPERIMENTAL PROCEDURES

In order to upgrade the material used in this project before smelting, it had to demagnetized to be separated from the iron fraction. This section first describes the input materials, then describes the demagnetization as it was done at NTNU, before explaining the setup for the smelting experiments.

4.1 INPUT MATERIALS

Within the REEcover project, three different types of inputs have been selected for research. **Input 1** contains general WEEE scrap, **Input 2** contains rare earth rich WEEE scrap, while **Input 3** contains hard disk drives. This project has only focused on Input 2. The material was collected at different times, denoted as **a**, **b** and **c**, where **a** was collected first. Figure 4-1 shows, very simplified, how the material was processed prior to the experiments described in this report. Only the ferrous fraction has been examined.

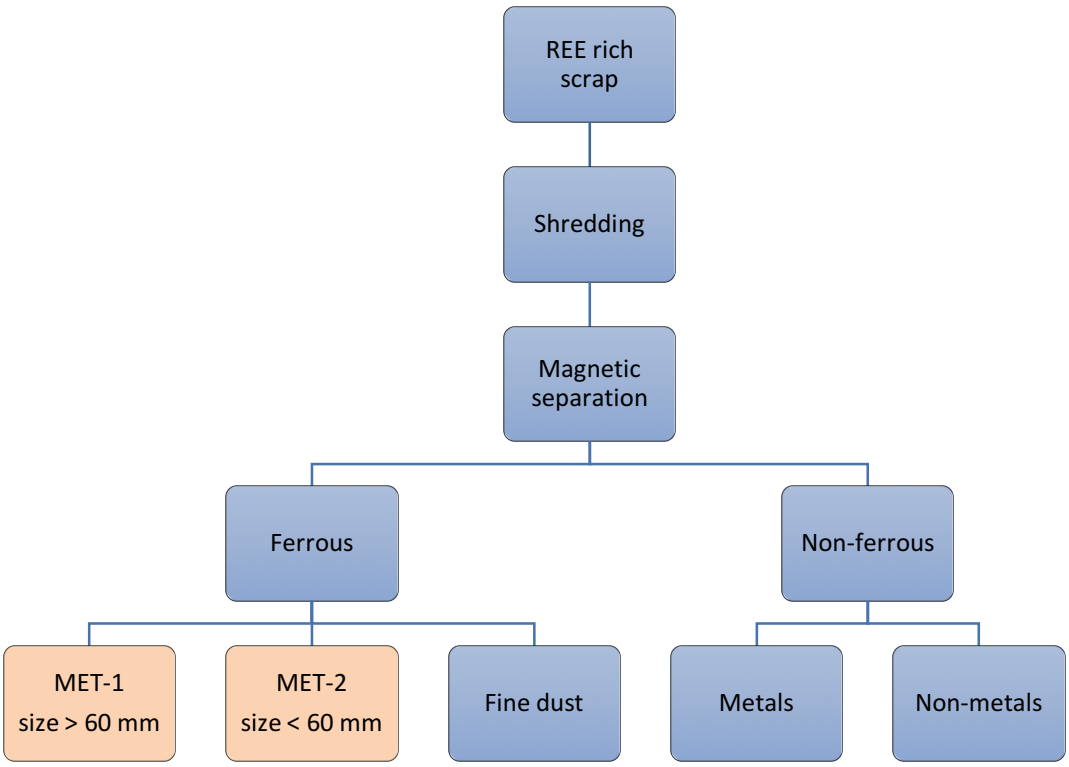

Figure 4-1 Simplified overview of the processing of the input materials before this project.

As illustrated in Figure 4-2, MET-1 and MET-2 were examined for all inputs except 2a, where only MET-1 was available. After demagnetization to separate magnets from iron, the fractions were sieved so as to collect as large a concentration as possible of crushed magnets. The plus and minus notation refers to the sieving. The three inputs were sieved to different sizes. 2a was sieved so that the material that was to be investigated (the minus fraction) was no bigger than 9.5 mm. 2b was sieved to 3.35 mm and 2c to 2 mm. The plus fraction has not been analysed.

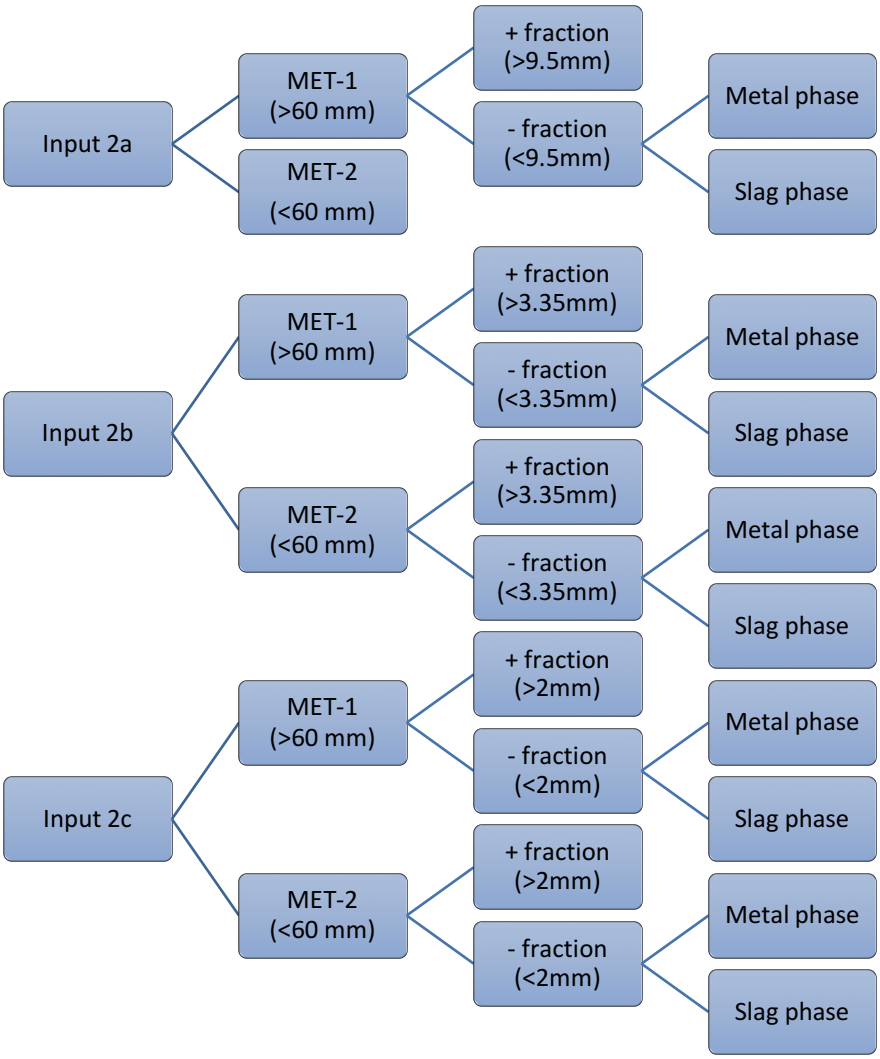

Figure 4-2 The input materials to this project.

Analyses have been done by an external laboratory on the demagnetized, but otherwise untreated, inputs 2a and 2b. The compositions were found using acid digestion and analysis by inductively coupled plasma optical emission spectrometry (ICP-OES). The results are shown in Table 4-1. Figures 3-3 to 3-7 show pictures of all of the minus fractions, while Figure 4-8 and Figure 4-9 show input 2c MET-1 and MET-2, respectively, before demagnetization.

Table 4-1 Analyses from Tecnalia of Input 2a MET-1, 2b MET-1 and 2b MET-2 using acid digestion and ICP-OES.

Input 2a MET-1			Input 2b MET-1			Input 2b MET-2		
Element	Amount		Element	Amount		Element	Amount	
Nd	**6489**	mg/kg	Nd	4039	mg/kg	Nd	2016	mg/kg
Dy	**246**	mg/kg	Dy	162	mg/kg	Ce	7	mg/kg
Gd	**24**	mg/kg	Ce	24	mg/kg	Dy	41	mg/kg
Y	**2**	mg/kg	Er	<2	mg/kg	Eu	<2	mg/kg
Eu	**9**	mg/kg	Eu	7	mg/kg	Gd	21	mg/kg
La	**31**	mg/kg	Gd	15	mg/kg	La	10	mg/kg
Ce	**<10**	mg/kg	La	21	mg/kg	Tb	<10	mg/kg
Tb	**43**	mg/kg	Pr	647	mg/kg	Y	19	mg/kg
In	**11**	mg/kg	Sm	<2	mg/kg	Pr	250	mg/kg
Ga	**<10**	mg/kg	Tb	<10	mg/kg	Cd	61	mg/kg
Cd	**46**	mg/kg	Y	6	mg/kg	Co	1050	mg/kg
Co	**808**	mg/kg	Cd	63	mg/kg	Ti	2265	mg/kg
Al	**0,15**	%	Co	473	mg/kg	In	<20	mg/kg
Cu	**0,5**	%	Ti	2286	mg/kg	Ga	<30	mg/kg
Fe	**80,3**	%	In	<20	mg/kg	Al	1,25	%
Mn	**0,76**	%	Ga	<30	mg/kg	Cu	3,59	%
Ni	**0,21**	%	Pb	1129	mg/kg	Fe	59,29	%
Pb	**0,1**	%	Cu	2,54	%	Mn	4,38	%
Sn	**0,17**	%	Fe	59,1	%	Ni	1,7	%
Zn	**0,74**	%	Mn	1,41	%	Pb	0,41	%
Ti	**0,02**	%	Ni	0,77	%	Sn	0,7	%
			Al	5,27	%	Zn	4,34	%
			Pb	0,11	%			
			Sn	0,18	%			
			Zn	2,28	%			

Figure 4-3 Input 2a MET-1, demagnetized and sieved to -9,5mm.

Figure 4-4 Input 2b MET-1, demagnetized and sieved to -3,35mm.

Figure 4-5 Input 2b MET-2, demagnetized and sieved to -3,35mm.

Figure 4-6 Input 2c MET-1, demagnetized and sieved to -2 mm.

Figure 4-7 Pictures of all fractions.

Figure 4-8 Input 2c MET-1 before demagnetization.

Figure 4-9 Input 2c MET-2 before demagnetization.

4.2 DEMAGNETIZATION

Inputs 2a MET-1, 2b MET-1 and 2b MET-2 were demagnetized and sieved prior to this project. With the help of students Cathrine Solem, Lene Hansen and Ingrid Meling, input 2c was demagnetized at NTNU.

The demagnetization was done using a chamber furnace and regular, store-bought roasting trays made from stainless steel, as shown in Figure 4-10. The furnace could take 2 trays at a time, and they were filled with 6-8 kg of scrap each time. The scrap was heated in air at 500°C for 1 hour. Afterwards, it was cooled and sieved to -2 mm.

Figure 4-10 Tray with scrap from Input 2c MET-2 after demagnetization. Most of the plastic parts were slightly deformed, but remained whole. The trays, of size 40x32 cm, suffered slight deformation, but were reused without trouble.

4.2.1 Measurements of off-gases.

The off-gases from the demagnetization of Input 2c MET-2 were measured using thermal desorption tubes, where the gas is sucked trough a tube containing an absorbent that binds most hydrocarbons. It was then analysed using gas chromatography-mass spectrometry (GC-MS). The method provides a good picture of the general type of substances contained in the gas, but because no calibration standard existed for the specific gas, there is some uncertainty with regards to amounts and the specific species that were present.

4.3 SMELTING

The minus fraction for Inputs 2a MET-1, 2b MET-1 and MET-2 and 2c MET-1 and MET-2 were all smelted in the graphite tube furnace shown in Figure 4-11 in argon atmosphere. Input 2c MET-1 and MET-2 were also melted in a larger scale in the induction furnace shown in Figure 4-12., with help from students Martin Værnes, Erlend Sverdrup and Oda Marie Ellefsen.

Figure 4-11 Graphite tube furnace.

Figure 4-12 Induction furnace.

The heating program for the small-scale melting of Inputs 2a MET-1, 2b MET-2 and 2c MET-1 and MET-2 is shown in Table 4-2. Also shown is the heating program for Input 2b MET-1, which required a higher temperature to melt. The temperature for the larger-scale melting of Input 2c MET-1 and MET-2 was controlled manually, and the temperature logs are shown under the results of the Smelting experiments.

Table 4-2 Heating programs for all small-scale experiments.

Heating program for inputs 2a, 2b MET-2, 2c MET-1 and 2c MET-2 (small-scale):		Heating program for Input 2b MET-1:	
0-1000°C:	60 min	0-1000°C:	60 min
1000°C hold:	30 min	1000°C hold:	30 min
1000-1550°C:	30 min	1000-1830°C:	45 min
1570°C hold:	60 min	1830°C hold:	60 min
1570-1000°C:	60 min	1830-1000°C:	60 min
1000°C-RT (furnace off):	3h 15min	1000°C-RT (furnace off):	3h 15min

In each of the smaller-scale experiments, the sample was weighed out and poured into an inner graphite crucible of the following dimensions: outer diameter: 40mm, inner diameter: 32mm, outer height: 54mm, inner depth 50mm. Please note that Input 2c MET-1 was heated in an even smaller crucible due to a shortage of the regular sized crucibles. The amount of material filled into each crucible was such as to reach about 1/3 up the crucible wall, because a preliminary experiment had proven it necessary in order to prevent it from boiling over. The inner crucible was then placed inside an outer graphite crucible and covered with a non-sealing lid. The set-up is shown in Figure 4-13 and Figure 4-14.

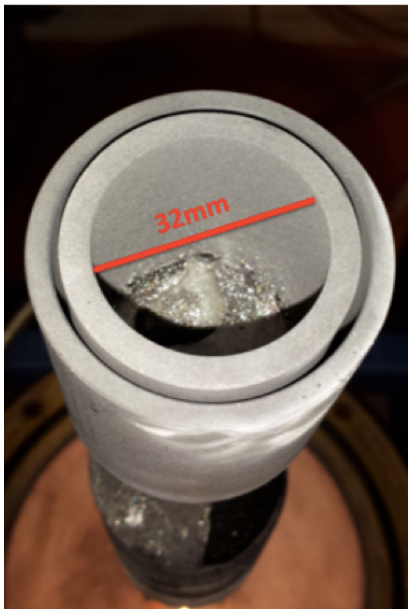

Figure 4-13 Inner crucible placed inside outer crucible and filled with material.

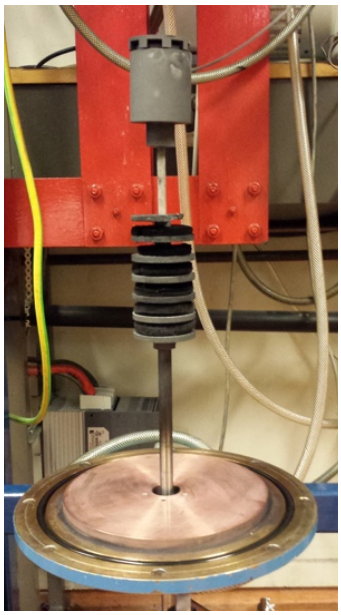

Figure 4-14 Crucibles mounted in furnace and under a lid.

Figure 4-15 Setup of large-scale experiments. The thermocouple was placed inside the graphite tube.

For the larger-scale experiments, the crucibles were filled with 2.5-3 kg. The crucible dimensions were: outer diameter: 15 cm, inner diameter: 11.4 cm, height: 40 cm. Based on the height of the crucibles and the amount of gas that evolved during the experiment, one may assume that the samples had little contact with air. A graphite tube was placed in the crucible as holder for the thermocouple. The set-up is shown in Figure 4-15.

4.4 ANALYSES

The metal and slag that formed during the melting experiments were easy to separate. The metal phases were analysed using electron probe microscopy-wavelength dispersive spectrometry (EPMA-WDS). The slag phases were analysed with EPMA, scanning electron microscope (SEM), energy-dispersive X-ray spectroscopy (EDS), X-ray fluorescence (XRF), X-ray diffraction (XRD) and the sessile drop technique.

4.4.1 SEM, EDS and EPMA

The samples were cast in epoxy and grinded and polished down to 1μm. They were then carbon coated and examined, first with a Zeiss Ultra 55 Limited Edition Field Emission SEM and EDS. EPMA-WDS was chosen in addition because no rare earths could be detected in the metal phase using EDS, and because EPMA could provide a better overall picture of the distribution of elements.

4.4.2 XRF

The X-ray fluorescence was performed using a Bruker S8 Tiger with the Bruker QuantExpress SpectraPlus software. XRF provides a semi-quantitative analysis of the composition of the samples. With both EDS and XRF there may be disturbances from other elements or overlapping characteristic peaks. The biggest source of insecurity for these results is that XRF results need to be compared to a standard, however no standard exists for these samples. The results and peaks were therefore reviewed and those that were dubious have been removed. Some of the peaks may still have been wrongly identified and belong to other elements.

4.4.3 XRD

The slags were crushed to fine powder to perform XRD. The XRD was done using a Bruker D8 Focus with the Diffrac.Eva software. It was performed mainly to establish whether or not Input 2b MET-2 had a glassy structure, but it was done for all slags. However, the results were hard to interpret due to the high amount of elements and phases in the samples.

4.4.4 Sessile drop technique

In the first experiment with Input 2b MET-1, the sample was not properly melted, and the sessile drop technique was used to establish which temperature it would have to reach. The other inputs were also tested to see whether it had in fact been necessary to heat them to 1570°C.

5 RESULTS

Although the off-gases from the demagnetization of Input 2c was not of major focus to this project, the results are important to a potential industrial-scale method, and the results are given here before the results of the main focus, the smelting, are given.

5.1 DEMAGNETIZATION

As each tray could only hold up to 8 kg scrap, 27 trays were needed to demagnetize Input 2c MET-1, while 11 trays were needed for MET-2. The sum of the weights of all of the trays before and after demagnetization, as well as the weight of the minus fractions, are given in Table 5-1.

Table 5-1 Weights of Input 2c MET-1 and MET-2 before and after demagnetization, including mass loss.

	Input 2c MET-1	Input 2c MET-2
Sum scrap before heat treatment	199 481 g	80 518 g
Sum scrap after heat treatment	199 387 g	78 917 g
Sum dust -2mm (minus fraction)	8 874 g	12 137 g
Av. Dust fraction	4.49%	15.35%
Av. Mass loss	0.06%	1.96%

5.1.1 Measurements of off-gases

The measurements were done over time and varied, but typical results are given in Table 5-2. Only hydrocarbons can be measured with this method, and it is not unlikely that HCl, HBr or HCN were produced (O. Kjos, personal communication, January 26, 2016). The specific components produced would probably differ between measurements and experiments, but the overall trend seems to be heavy hydrocarbons and polyaromatic hydrocarbons. Although the latter forms mainly between 250-450°C, they may also form above those temperatures. Also, the samples did not heat instantaneously or uniformly, since different materials have different heat capacities, and the hydrocarbons will have had ample time to form.

Table 5-2 Components measured in the off-gases from the demagnetization of Input 2c MET-2.

Suggested component	Signal strength	Comment
Benzene	Strong	
Trichloroethylene	Weak	Uncertain identification
Toluene	Middle	
Tetrachloroethylene	Weak	
Chlorobenzene	Middle	
Styrene	Strong	
Bromobenzene	Middle	
Phenol	Middle	Uncertain identification
Benzonitrille, Phenol 2-chloro, Bezofuran	3 components overlap	Uncertain identification, hard to tell apart
1,2-dichloro-benzene	Middle	
1-methylethylbenzene, 2-bromophenol, acetophenone	3 components overlap	Uncertain identification
1bromo-2chlorobenzene	Weak	
1bromo-3chlorobenzene	Middle	
1,3,5 Trichlorobenzene	Middle	
Naphthalene	Strong	
1,2,3-trichlorobenzene	Middle	
Biphenylene	Middle	
Dibenzofuran	Middle	

5.2 SMELTING

In the large-scale experiments on Input 2c, an endothermic reaction was observed at a temperature that varied between 1370°C and 1480°C, where the temperature dropped with 4-40°C. Up to this temperature, the reaction was fierce and the flames colourful and firework-like. Figure 5-1 shows the plot of the temperature logs from all of the large-scale experiments.

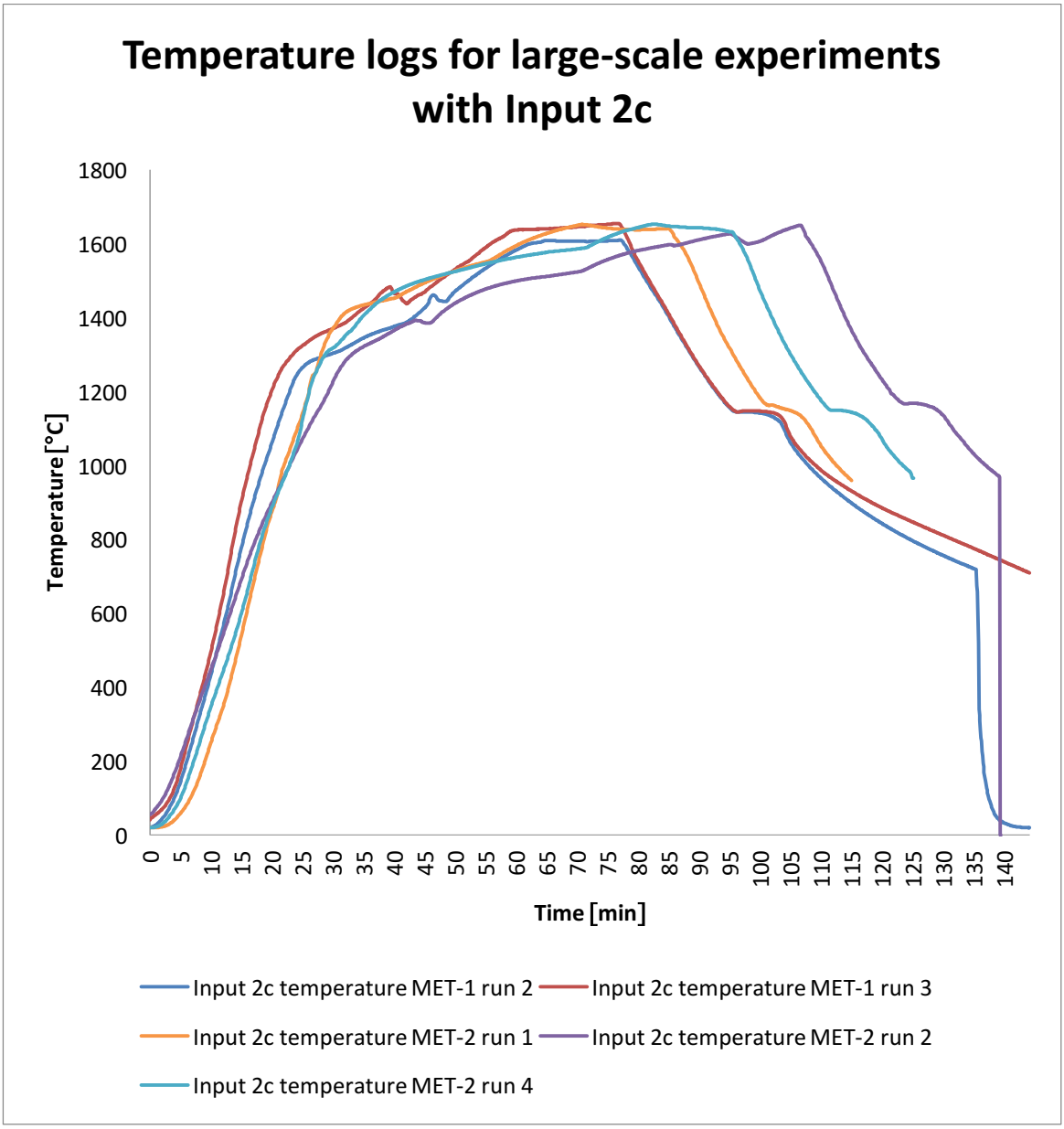

Figure 5-1 Temperature from large-scale smelting experiments. The logging was ended at different times, the crucibles were also cooled at different rates because some were removed from the furnace wile others were allowed to cool inside the furnace. Run 1 of MET-1 and run 3 of MET-2 are not included because the thermocouples failed.

Table 5-3 shows the weights of the samples before and after melting. Figure 5-2 shows all the samples after the smelting experiments. The temperature needed for the second experiment with Input 2b MET-1 was established using the sessile drop method. Notice especially the mass losses and fractions of slag from each experiment.

Table 5-3 Mass balances for all experiments.

Mass balance small-scale experiments							
Input	Input 2a	Input 2b				Input 2c	
Sieving	Met1, -9.5mm	Met 1, -3.35mm		Met 2, -3.35mm		Met 1, -2mm	Met 2, -2mm
Sample no	1	1	2	1	2	1	1
Initial weight (g)	31,89	36,01	36,66	46,92	30,67	11,55	25,77
Total weight after	30,34	32,4035	29,97	31,61	23,91	10,12	20,97
Weight of metal	28,61	N/A	16,89	29,08	20,98	8,81	15,77
Weight of slag	1,41	N/A	13,07	2,37	2,93	1,31	5,20
Inseparable metal and slag		32,4035					
Fraction slag	4,4 %		35,65 %	5,0 %	9,56 %	11,3 %	20,2 %

Mass balance large-scale experiments							
Input	Input 2c			Input 2c			
Sieving	MET-1, -2mm			MET-2, -2mm			
Sample no	2	3	4	2	3	4	5
Initial weight (g)	2500	3085	3076	2948	3047	3000	2844
Total weight after	2261	2765	2816	2350	2458	2261	2022
Weight of metal	1956	2418	2427	1940	2026	1862	1673
Weight of slag	305	347	389	410	432	399	349
Inseparable metal and slag							340
Fraction slag	12,20 %	11,25 %	12,65 %	13,91 %	14,18 %	13,30 %	

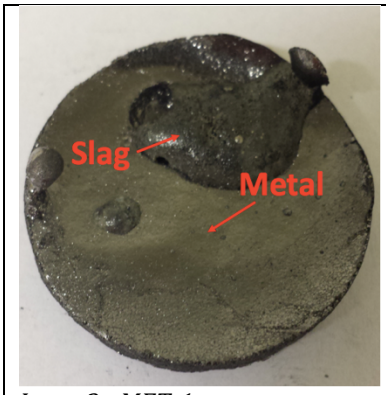

Input 2a MET-1

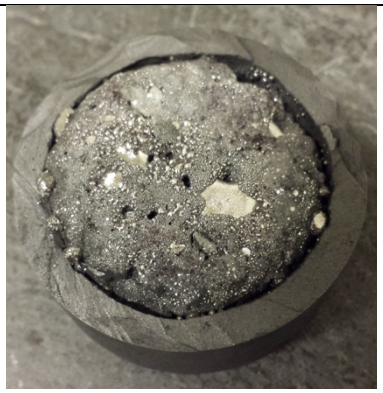

Input 2b MET-1 First experiment.

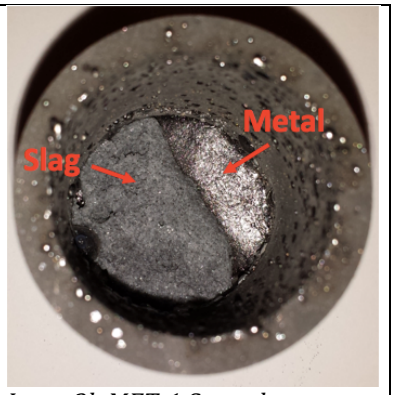

Input 2b MET-1 Second experiment.

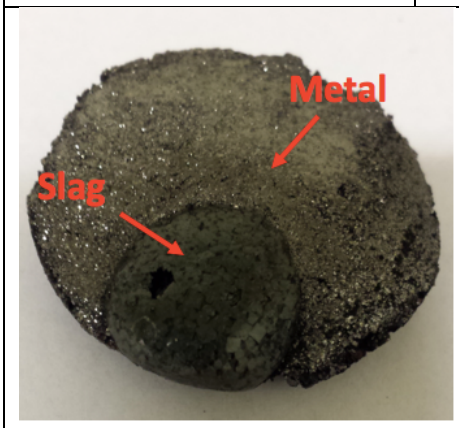

Input 2b MET-2

Input 2b MET-2 close-up on slag

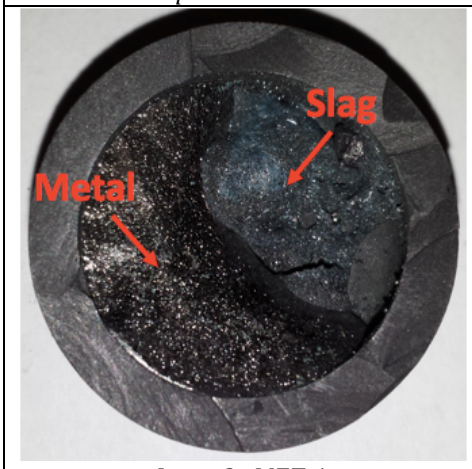

Input 2c MET-1

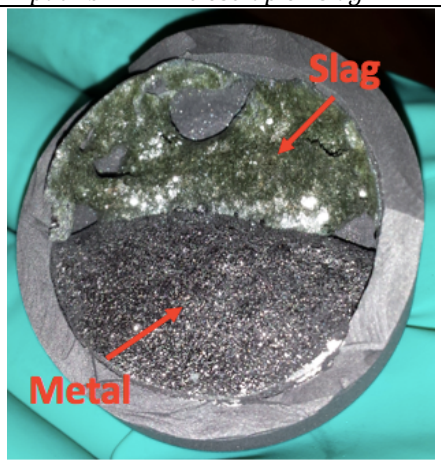

Input 2c MET-2

Figure 5-2 Pictures of all the fractions after small-scale smelting. Pictures are included from both experiments with Input 2b MET-1, because the first experiment did not reach a temperature high enough for phase separation. The second experiment was successful. A close-up on Input 2b MET-2 is also shown, were the assumed glassy phase is visible.

5.3 ANALYSES

5.3.1 SEM, EDS and EPMA

The images that are shown were considered representative of the structures of the materials. Only the slag of each input was analysed with EDS. Both slag and metal were analysed with EPMA. For the EPMA analyses, three points were selected for measuring the concentrations of each type of phase. The averages are given here.

5.3.1.1 Input 2a MET-1

Figure 5-3 shows a SEM image of the slag of Input 2a MET-1. Points 1-3 mark where the corresponding EDS points given in

Table 5-4 were measured.

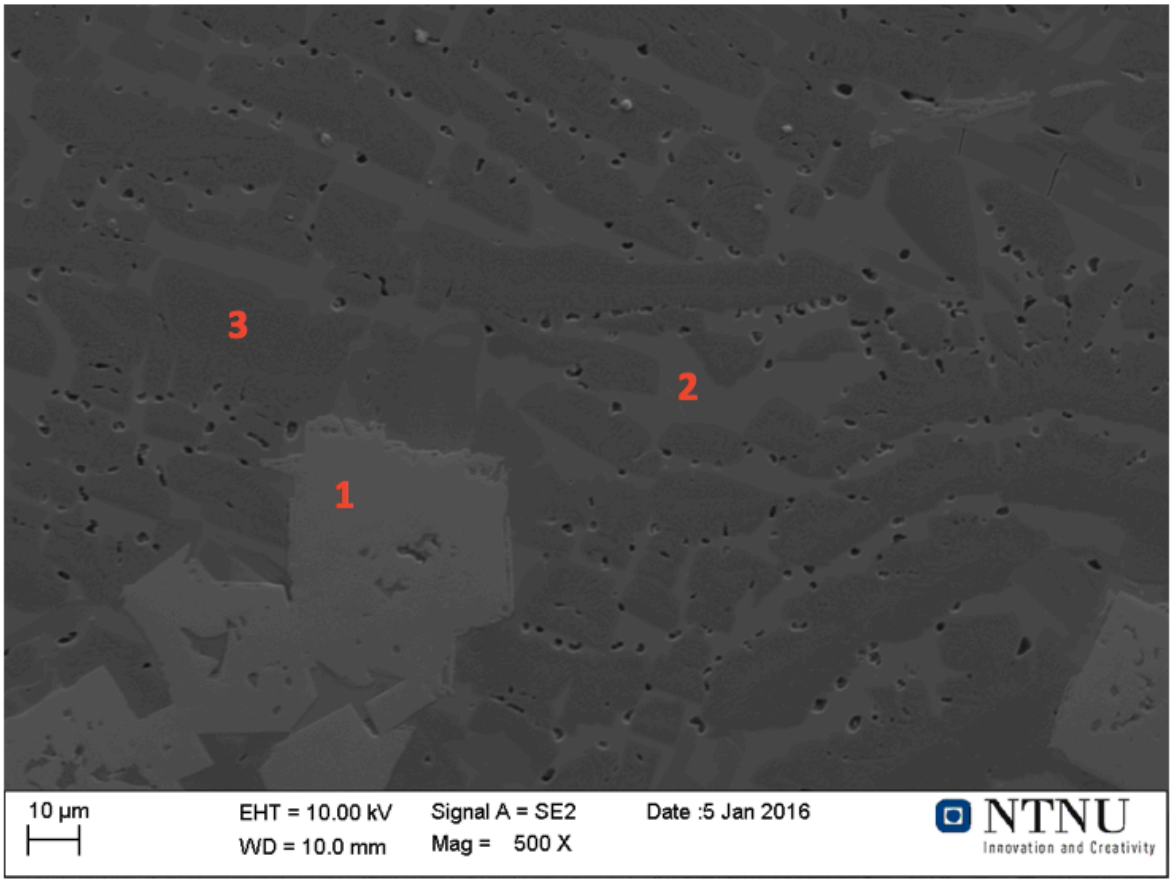

Figure 5-3 SEM image of the slag from Input 2a MET-1, with EDS points.

Table 5-4 EDS results for the slag of Input 2a MET-1.

Point 1			Point 2			Point 3		
Element	[wt.%]	[norm. wt.%]	Element	[wt.%]	(norm. wt.%]	Element	[wt.%]	[norm. wt.%]
Nd	40,96	39,23	O	20,48	24,49	Br	28,85	21,52
Br	20,89	20,01	Ti	13,04	15,60	Sr	28,37	21,16
O	18,00	17,24	W	12,93	15,47	O	26,27	19,60
Pr	5,94	5,69	Ce	9,55	11,42	W	16,50	12,31
Cr	4,24	4,06	Br	7,17	8,58	Te	7,71	5,75
C	4,04	3,87	Nd	5,56	6,65	Nd	7,27	5,43
La	3,35	3,21	Te	3,18	3,81	C	5,23	3,91
Zn	3,21	3,07	Ca	2,02	2,41	Ca	5,13	3,82
W	2,78	2,66	Ba	2,00	2,39	Ti	2,25	1,68
Ba	1,00	0,96	V	1,86	2,23	Ce	2,13	1,59
			C	1,85	2,22	Pr	1,61	1,20
			Ar	1,51	1,80	Zn	1,57	1,17
			Mg	1,35	1,62	Mg	1,17	0,87
			Cl	1,11	1,32			
Sum:	104,40	100,00	Sum:	83,61	100,00	Sum:	134,05	100,00

The slag of Input 2a MET-1, as analysed with EPMA, is shown in Figure 5-4. Point 4 had specks of darker shade, but these inclusions were too small to be distinguished by the electron probe, and the results may be considered an average of the area of darkest grey shade. The results are shown in Table 5-5. The metal is shown in Figure 5-5. The matrix is marked as point 4. Point 2 had a slightly different hue from the matrix and was surrounded by another phase, marked as point 3. The compositions of the points are given in Table 5-6.

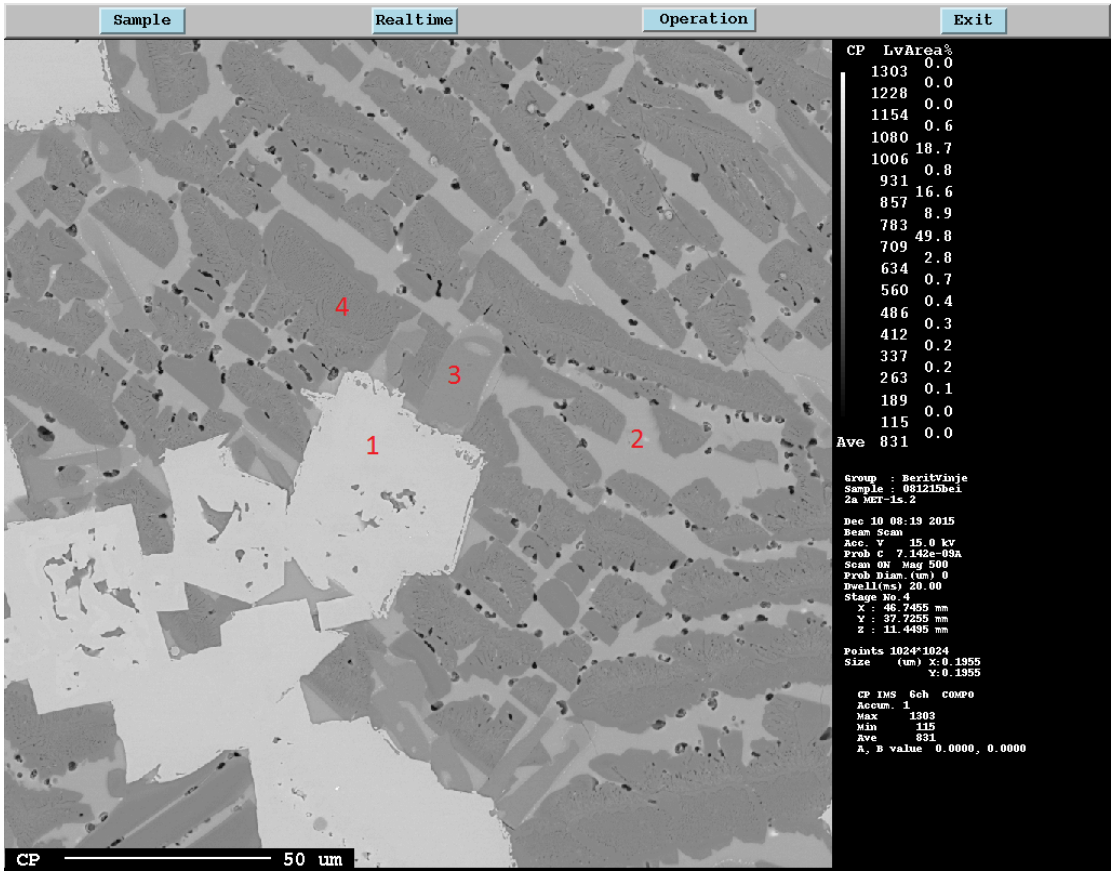

Figure 5-4 Input 2a MET-1 slag.

Table 5-5 EPMA results for slag from Input 2a MET-1.

Point 1			Point 2			Point 3			Point 4		
	(wt%)	Norm.		(wt%)	Norm.		(wt%)	Norm.		(wt%)	Norm.
O	23,96	34,85	Ba	32,29	35,73	Sr	35,84	37,59	O	29,78	33,23
Nd	21,63	31,46	O	25,25	27,94	O	25,36	26,60	Sr	23,08	25,74
Al	10,92	15,88	Sr	9,24	10,23	Si	11,12	11,66	Al	13,51	15,07
Sr	2,64	3,83	Al	5,40	5,98	Ba	10,07	10,57	Ba	6,56	7,32
Eu	2,62	3,80	Si	4,93	5,45	Mg	5,50	5,77	Si	6,25	6,97
Pr	2,23	3,24	Ca	3,56	3,94	Ca	5,07	5,32	Ca	6,03	6,73
Ti	2,20	3,19	Mg	2,84	3,15	C	0,79	0,83	Dy	1,25	1,39
Dy	1,39	2,02	Nd	2,23	2,47	Nd	0,57	0,60	Mg	0,96	1,07
Ca	0,86	1,26	Dy	1,74	1,93	Al	0,42	0,44	S	0,94	1,05
C	0,32	0,46	Ti	1,12	1,24	Ti	0,31	0,33	C	0,59	0,66
			S	0,67	0,74	Dy	0,18	0,19	Eu	0,36	0,41
			Zr	0,40	0,44	W	0,10	0,11	Pr	0,33	0,36
			Eu	0,35	0,39						
			Mn	0,34	0,37						
Total	68,75	100,0	Total	90,37	100,0	Total	95,35	100,0	Total	89,63	100,0

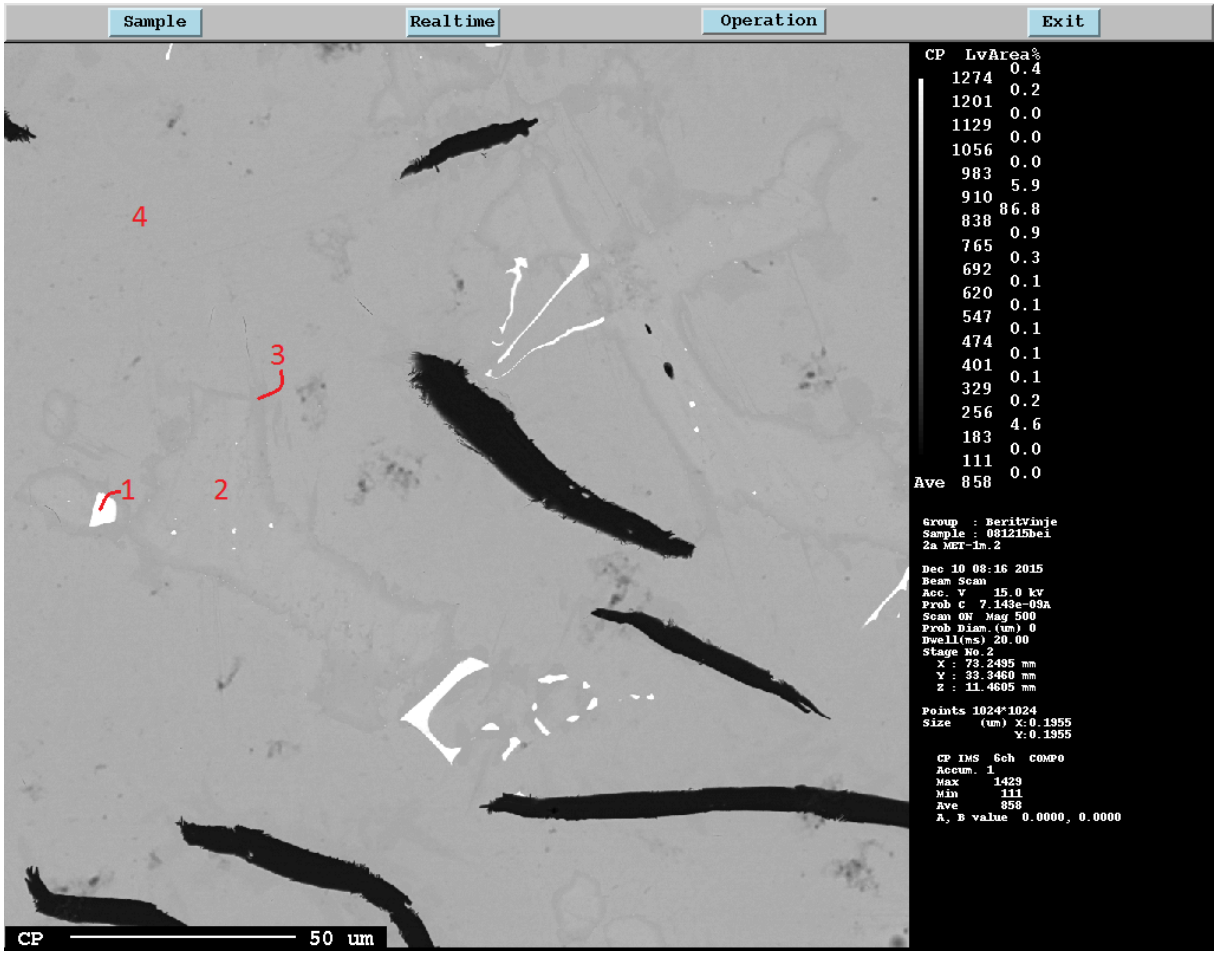

Figure 5-5 Input 2a MET-1 metal.

Table 5-6 EPMA results for metal from Input 2a MET-1.

Point 1			Point 2			Point 3			Point 4		
	(wt%)	Norm.		(wt%)	Norm.		(wt%)	Norm.		(wt%)	Norm.
W	59,07	63,16	Fe	85,42	87,45	Fe	96,91	94,49	Fe	95,71	94,69
Ti	18,25	19,52	W	5,98	6,13	Cu	2,49	2,43	Mn	1,40	1,39
Fe	6,52	6,97	Mn	2,26	2,32	Mn	0,89	0,87	Cu	0,93	0,92
Sr	3,26	3,49	Cr	1,28	1,31	Dy	0,58	0,56	Dy	0,79	0,78
Nb	2,87	3,07	Dy	1,27	1,30	C	0,49	0,47	C	0,57	0,57
C	1,27	1,36	C	0,90	0,92	Ni	0,44	0,42	W	0,47	0,46
Cr	1,05	1,12	Sr	0,31	0,31	O	0,28	0,27	Cr	0,36	0,36
Zr	0,36	0,38	O	0,25	0,26	Sn	0,22	0,21	Sn	0,31	0,31
O	0,35	0,38				Tb	0,15	0,15	Ni	0,28	0,28
Mn	0,19	0,20				Si	0,12	0,12	O	0,25	0,25
Ba	0,12	0,13									
Dy	0,11	0,12									
Mo	0,11	0,11									
Total	93,52	100,00	Total	97,68	100,00	Total	102,56	100,00	Total	101,08	100,00

5.3.1.2 Input 2b MET-1

The SEM image with EDS points is shown in Figure 5-6, with numbers 1-4 marking where EDS measurements have been made. The results of the EDS measurements are given in Table 5-7.

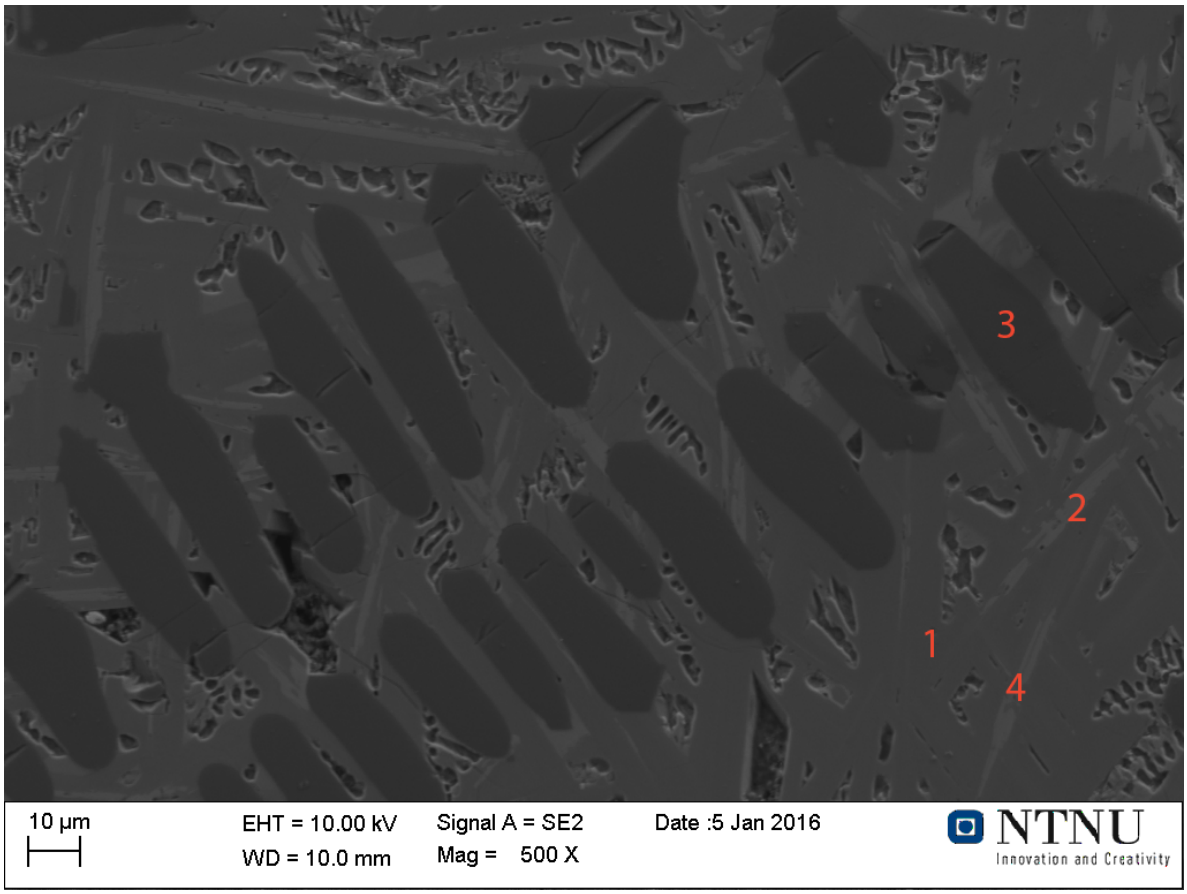

Figure 5-6 SEM image of slag from Input 2b MET-1.

Table 5-7 EDS points for the slag from Input 2b MET-1.

Point 1			Point 2			Point 3			Point 4		
Element	[wt.%]	(norm. wt.%]	Element	[wt.%]	(norm. wt.%]	Element	[wt.%]	[norm. wt.%]	Element	[wt.%]	[norm. wt.%]
Br	70,53	37,10	Br	43,83	32,05	Ar	55,55	36,08	Br	47,88	33,71
Te	40,01	21,05	O	22,52	16,47	Mg	44,08	28,64	Te	25,23	17,77
O	28,32	14,90	Te	22,27	16,28	O	40,15	26,08	O	23,48	16,53
Ca	25,49	13,41	Nd	16,82	12,30	C	14,17	9,20	Ca	15,45	10,88
C	12,15	6,39	Ca	13,56	9,91				Nd	14,32	10,09
W	9,05	4,76	C	10,81	7,90				C	11,16	7,86
Mg	2,74	1,44	Si	4,56	3,33				Si	4,49	3,16
Zn	1,82	0,96	Zn	2,39	1,75						
Sum:	190,11	100,00	Sum:	136,76	100,00	Sum:	153,94	100,00	Sum:	142,01	100,00

In the EPMA image shown in Figure 5-7, point 1 marks the white streaks within what is considered the matrix, while point 2 is the matrix. Points 3 and 4 are the grey and black phases, respectively, while the white spots marked with 5 appeared to be metallic iron. Results are shown in Table 5-8.

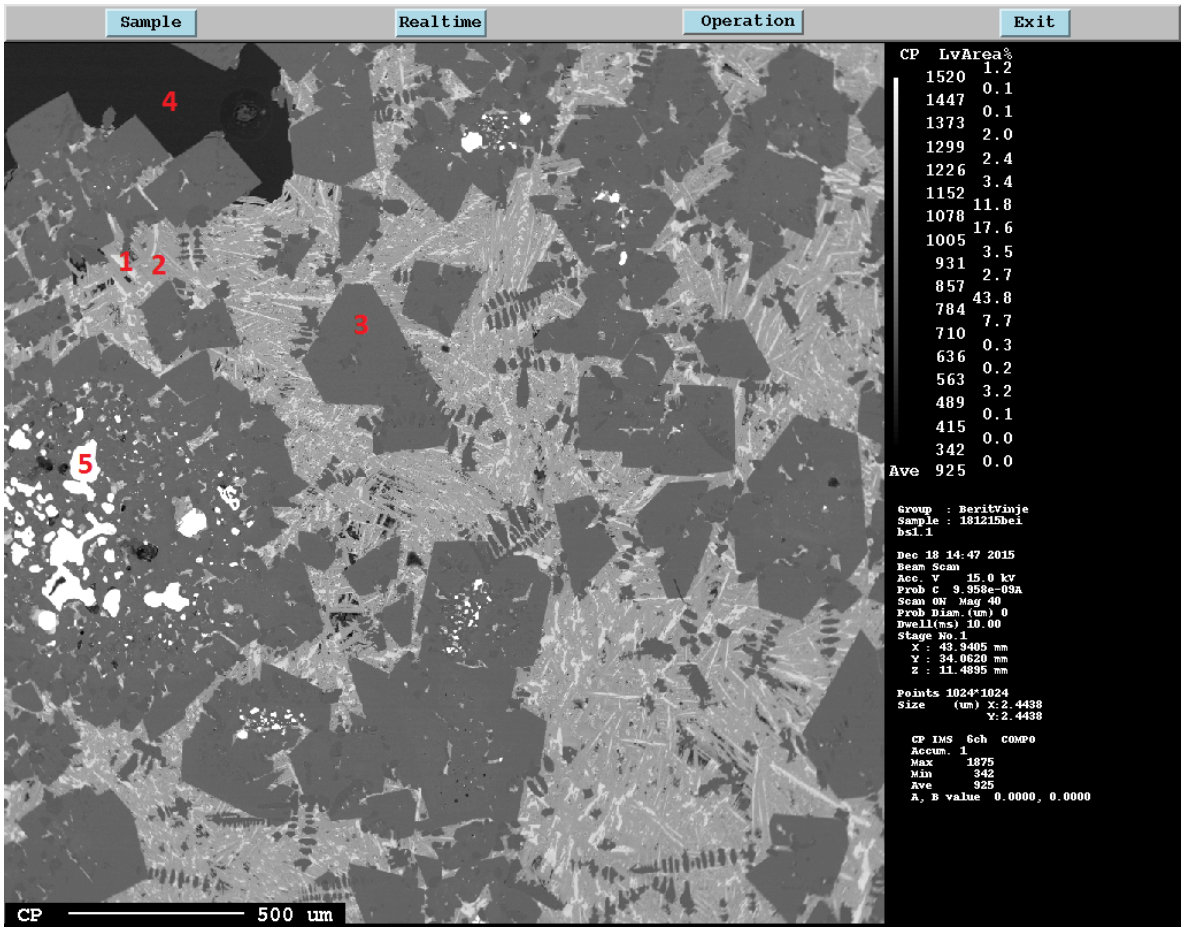

Figure 5-7 Input 2b MET-1 slag.

Table 5-8 EPMA results for slag from Input 2b MET-1.

Point 1			Point 2			Point 3		
	wt%	Normalized		wt%	Normalized		wt%	Normalized
O	34,69	39,02	O	35,62	37,86	O	44,11	44,00
Al	20,78	23,38	Al	26,13	27,77	Al	38,77	38,68
Ca	17,67	19,88	Ca	24,47	26,00	Mg	16,03	15,99
Nd	6,80	7,65	Mg	2,05	2,17	C	1,33	1,33
Si	3,23	3,63	Sr	1,78	1,89			
Sr	1,95	2,19	Si	1,56	1,66			
C	1,04	1,18	Nd	1,46	1,55			
Eu	0,83	0,94	C	1,03	1,10			
Dy	0,75	0,85						
Pr	0,69	0,78						
Mg	0,45	0,51						
Total	88,89	100,00	Total	94,08	100,00	Total	100,25	100,00

Point 4			Point 5		
	wt%	Normalized wt%		wt%	Normalized wt%
Mg	56,77	58,12	Fe	56,43	56,01
O	38,83	39,75	Cr	37,66	37,38
C	1,38	1,41	Cu	1,55	1,53
Al	0,69	0,71	Mn	1,42	1,41
			Si	1,17	1,16
			Ni	0,95	0,95
			C	0,83	0,83
			Dy	0,74	0,73
Total	97,67	100,00	Total	100,75	100,00

Figure 5-8 shows the metal phase of Input 2b MET-1. Point 1 is the lighter grey of the matrix, point 2 is the darker grey within the matrix. Within the white streak through the light phase is a shade that is hardly distinguishable, but darker than the white streak. The white streak is marked as point 3, the darker shade is point 4 and the matrix of the lighter phase is point 5. The compositions are given in Table 5-9.

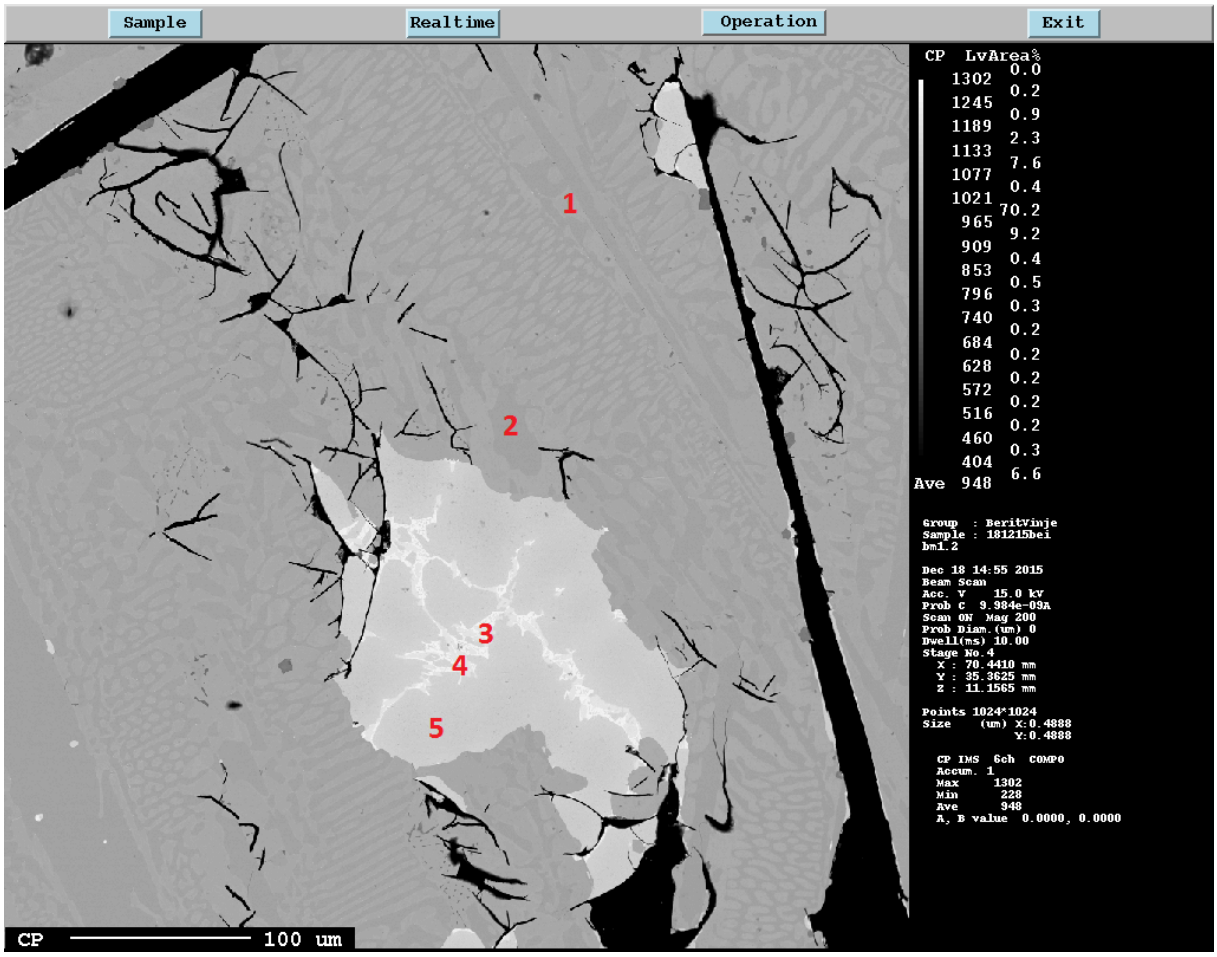

Figure 5-8 Input 2b MET-1 metal.

Table 5-9 EPMA results for metal from Input 2b MET-1.

Point 1			Point 2		
	(wt%)	Normalized wt%		(wt%)	Normalized wt%
Fe	84,64	84,25	Fe	78,60	83,17
Cu	5,69	5,66	Cr	8,62	9,12
Mn	2,55	2,53	Mn	3,59	3,80
Cr	1,85	1,84	Dy	1,87	1,98
Si	1,75	1,74	C	1,44	1,52
Ni	1,73	1,72	Ni	0,38	0,40
Dy	1,32	1,31			
C	0,94	0,94			
Total	100,46	100,00	Total	94,51	100,00

Point 3			Point 4			Point 5		
	wt%	Norm. wt%		wt%	Norm. wt%		wt%	Norm. wt%
Cu	66,56	63,44	Cu	62,07	57,86	Cu	86,41	82,51
Sn	33,24	31,68	Sn	29,91	27,88	Sn	9,48	9,05
Ni	1,63	1,55	Mn	8,62	8,04	Mn	3,29	3,14
Mn	1,07	1,02	Dy	3,75	3,49	Dy	1,41	1,35
C	0,87	0,83	Mg	1,54	1,44	Fe	1,10	1,05
O	0,66	0,63	C	0,84	0,79	C	1,04	0,99
Dy	0,52	0,50	O	0,54	0,50	Ni	0,58	0,56
Ba	0,36	0,35				Al	0,52	0,50
						O	0,50	0,48
						Ba	0,39	0,37
Total	104,92	100,00	Total	107,27	100,00	Total	104,73	100,00

5.3.1.3 Input 2b MET-2

To both the naked eye and through the electron microscope, the slag of Input 2b MET-2 from both experiments seemed to have solidified as a glass. With both EDS and EPMA, three points were measured from different places in the slag, but all had approximately the same composition. The SEM image with EDS points is shown in Figur 5-9. The results from the EDS measurements are given in. The composition as measured with EPMA is given in Table 5-11. In the metal phase shown in Figure 5-10, three different phases were distinguished, with the matrix marked as 2, the darker phase as 3 and the white specks as 1. The composition of the metal is given in Table 5-12.

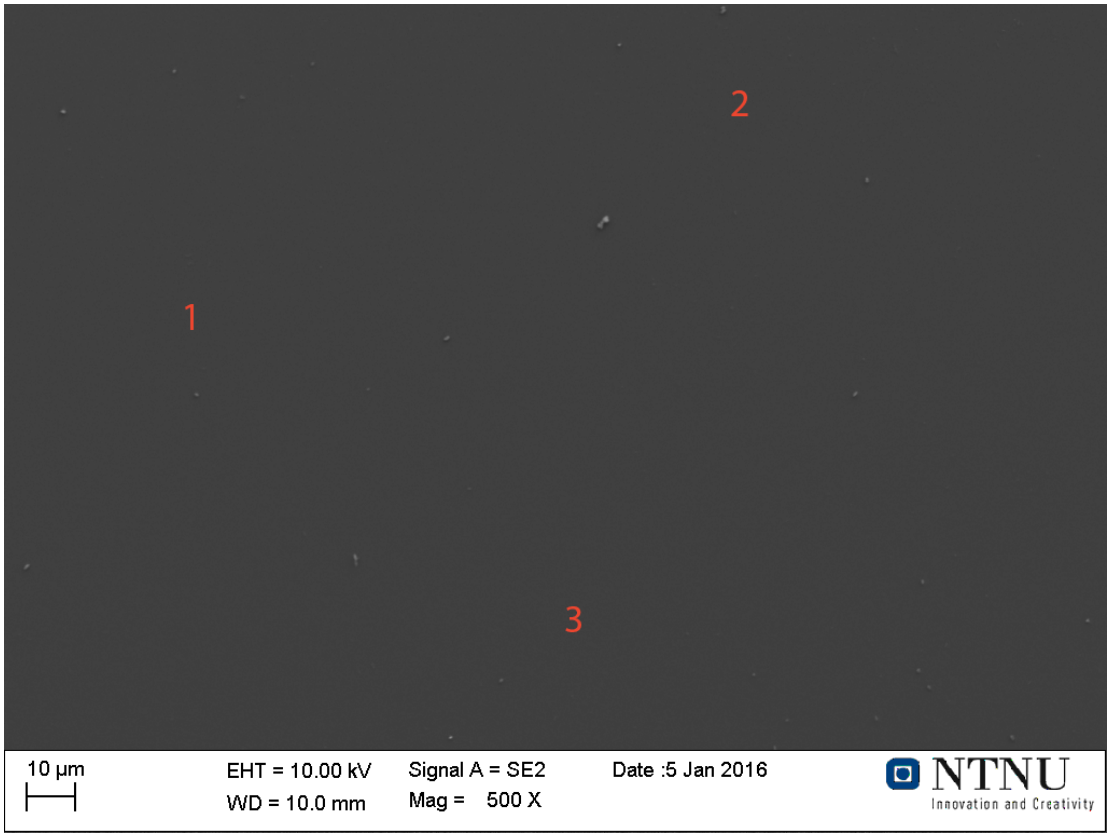

Figur 5-9 Slag of Input 2b MET-2 with EDS points.

Table 5-10 EDS measurements of slag from Input 2b MET-2.

	Point 1		Point 2		Point 3	
Element	[wt.%]	[norm. wt.%]	[wt.%]	[norm. wt.%]	[wt.%]	[norm. wt.%]
O	26,40	33,95	25,94	33,94	26,26	32,77
Si	15,03	19,33	14,91	19,51	15,99	19,96
Al	10,10	12,99	9,83	12,86	10,70	13,36
Mn	7,20	9,26	6,90	9,03	7,40	9,24
Mg	6,76	8,70	6,73	8,80	7,24	9,04
Ba	4,51	5,80	4,66	6,10	7,04	8,78
Ca	4,22	5,42	4,06	5,31	4,39	5,48
C	2,06	2,65	1,97	2,57	1,10	1,38
Ti	1,48	1,91	1,42	1,86		
Sum:	77,75	100,00	76,42	100,00	80,14	100,00

Table 5-11 EPMA results for slag from Input 2b MET-2.

Element	Average wt%	Normalized wt%
O	40,43	40,81
Si	15,22	15,36
Al	12,61	12,73
Mg	7,99	8,07
Mn	6,11	6,17
Ba	5,52	5,58
Ca	4,85	4,89
Dy	2,89	2,92
Ti	1,70	1,72
Sr	0,84	0,85
C	0,39	0,39
Zr	0,23	0,23
Eu	0,16	0,16
W	0,13	0,13
Total	99,08	100,00

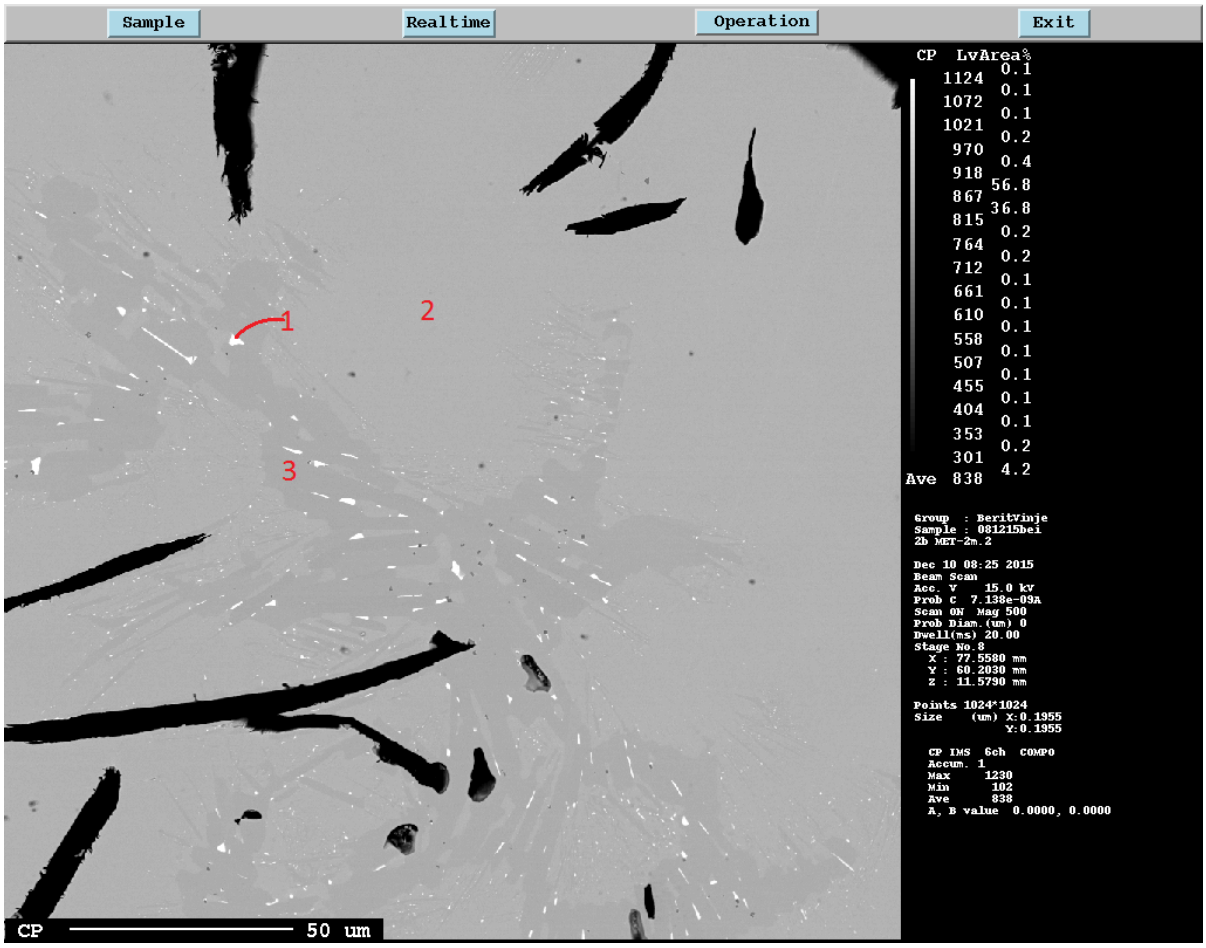

Figure 5-10 Input 2b MET-2 metal.

Table 5-12 EPMA results for metal from Input 2b MET-2.

Point 1			Point 2			Point 3		
	wt%	Norm. wt%		wt%	Norm. wt%		wt%	Norm. wt%
Sn	41,69	38,27	Fe	87,39	83,22	Fe	80,69	79,38
Cu	39,71	36,44	Mn	6,13	5,84	Mn	11,45	11,27
Ni	9,00	8,26	Dy	3,39	3,23	Dy	5,71	5,62
Fe	8,51	7,81	Cu	2,70	2,57	Cr	1,78	1,75
Mn	6,28	5,76	Ni	2,61	2,49	C	0,94	0,93
Dy	2,46	2,26	Sn	1,07	1,02	Ni	0,63	0,62
O	0,41	0,38	Si	0,64	0,61	O	0,17	0,16
C	0,30	0,28	C	0,42	0,40	Cu	0,15	0,15
Ba	0,29	0,27	Cr	0,39	0,37	Eu	0,12	0,12
Cr	0,21	0,19	O	0,26	0,25			
Y	0,11	0,10						
Total	108,95	100,00	Total	105,01	100,00	Total	101,64	100,00

5.3.1.4 Input 2c MET-1

The SEM image with EDS points for Input 2c MET-1 is shown in Figure 5-11. The corresponding results are given in Table 5-13. The EPMA image from Input 2c MET-1 is shown in Figure 5-12, with results shown in Table 5-14.

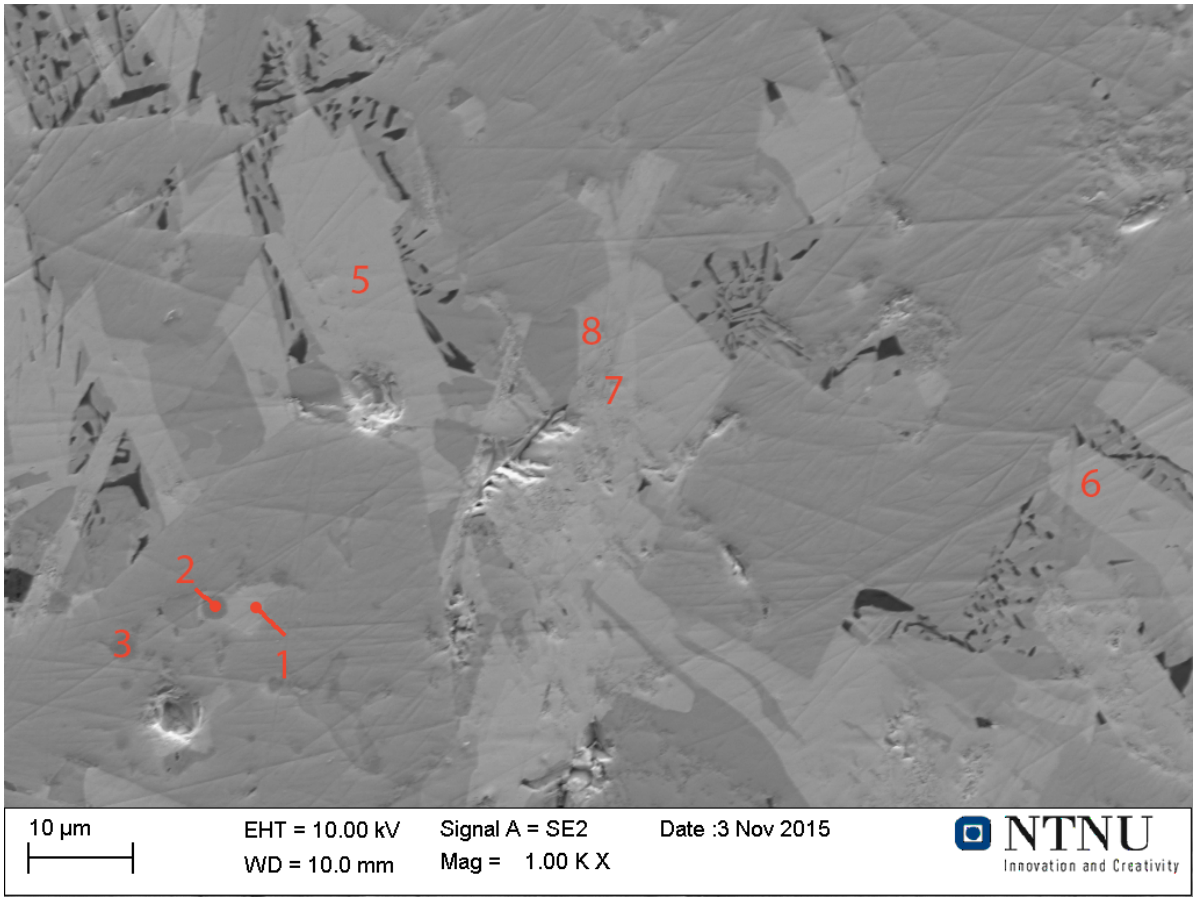

Figure 5-11 Slag from Input 2c MET-1 with EDS points.

Table 5-13 EDS results for Input 2c MET-1

Point 1			Point 2			Point 3		
Element	[wt.%]	[norm. wt.%]	Element	[wt.%]	[norm. wt.%]	Element	[wt.%]	[norm. wt.%]
Nd	67,38	71,15	Fe	65,08	66,41	Fe	73,60	72,74
O	11,01	11,62	Cr	26,87	27,42	Cr	19,20	18,98
La	3,36	3,55	C	6,04	6,16	C	5,92	5,85
C	2,49	2,63				Mn	2,46	2,44
Ar	2,22	2,34						
Mn	1,96	2,07						
Cu	1,75	1,84						
Cr	1,69	1,79						
Zn	1,48	1,56						
Ba	1,37	1,45						
Sum:	94,71	100	Sum:	97,99	100,00	Sum:	101,18	100,00

Point 4			Point 5			Point 6			Point 7		
Element	[wt.%]	[norm. wt.%]	Element	[wt.%]	[norm. wt.%]	Element	[wt.%]	[norm. wt.%]	Element	[wt.%]	[norm. wt.%]
Nd	67,85	72,11	Nd	67,20	71,66	Nd	70,45	73,62	Nd	66,57	71,38
O	11,49	12,21	O	11,23	11,97	O	9,28	9,70	O	12,37	13,26
La	3,13	3,33	La	3,13	3,34	La	3,19	3,33	La	3,61	3,87
C	2,86	3,04	C	2,51	2,67	Ar	2,93	3,06	C	3,02	3,24
Ar	2,23	2,37	Ar	2,09	2,23	C	2,56	2,67	Ar	2,70	2,90
Cu	1,70	1,80	Cu	1,63	1,74	Zn	1,76	1,84	Mn	1,96	2,10
Mn	1,64	1,75	Zn	1,59	1,69	Mn	1,70	1,78	Zn	1,63	1,75
Zn	1,64	1,74	Mn	1,56	1,66	Cu	1,48	1,55	Cu	1,40	1,50
Cr	1,56	1,66	Cr	1,54	1,64	Ba	1,31	1,37			
			Ba	1,31	1,40	Ge	1,04	1,08			
Sum	94,10	100,00	Sum	93,78	100,00	Sum	95,71	100,00	Sum	93,26	100,00

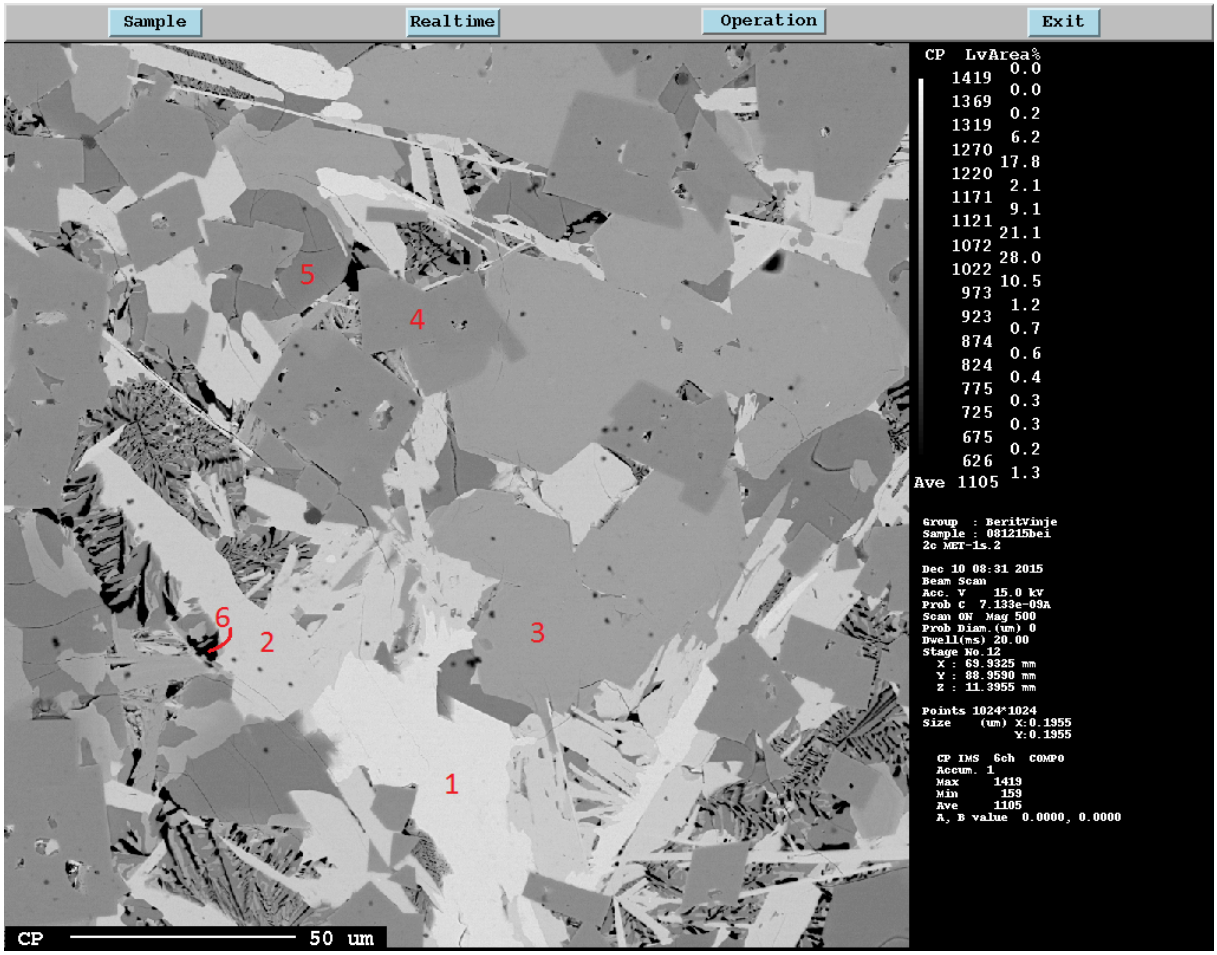

Figure 5-12 Input 2c MET-1 slag

Table 5-14 EPMA results for slag from Input 2c MET-1.

Point 1			Point 2			Point 3		
	wt%	Norm. wt%		wt%	Norm. wt%		wt%	Norm. wt%
Nd	29,79	52,29	Nd	27,94	51,13	Nd	24,45	37,84
O	12,98	22,78	O	15,19	27,79	O	20,67	32,00
Dy	6,41	11,25	Dy	4,46	8,16	Si	6,39	9,89
Eu	2,90	5,08	Eu	2,72	4,97	Sr	3,17	4,91
Pr	2,03	3,56	Pr	2,11	3,86	Eu	2,55	3,94
W	1,09	1,91	W	0,70	1,28	Pr	1,95	3,02
C	0,65	1,14	C	0,67	1,23	Dy	1,60	2,48
Zr	0,53	0,92	Zr	0,32	0,58	Ca	1,07	1,66
Ba	0,20	0,35	Ba	0,27	0,49	Al	1,03	1,60
Si	0,16	0,29	Si	0,14	0,26	C	0,81	1,25
Mn	0,14	0,25	Sr	0,13	0,23	Ba	0,45	0,70
Ca	0,10	0,18				W	0,35	0,53
						Mn	0,11	0,18
Total	56,96	100,00	Total	54,65	100,00	Total	64,60	100,00

Point 4			Point 5		
	(wt%)	Normalized wt%		(wt%)	Normalized wt%
Nd	24,27	37,26	O	21,95	30,99
O	20,45	31,39	Sr	17,16	24,22
Al	11,03	16,93	Nd	13,92	19,65
Eu	2,45	3,76	Ba	9,20	12,99
Pr	1,88	2,89	Ca	3,35	4,72
Ti	1,32	2,02	Eu	1,48	2,09
C	0,98	1,51	Pr	1,23	1,73
Dy	0,84	1,29	Dy	1,05	1,48
Sr	0,71	1,08	C	0,77	1,09
Mg	0,31	0,48	W	0,32	0,45
Ca	0,25	0,39	Ti	0,31	0,44
Ba	0,23	0,35	Al	0,11	0,15
Total	64,72	99,35	Total	70,84	100,00

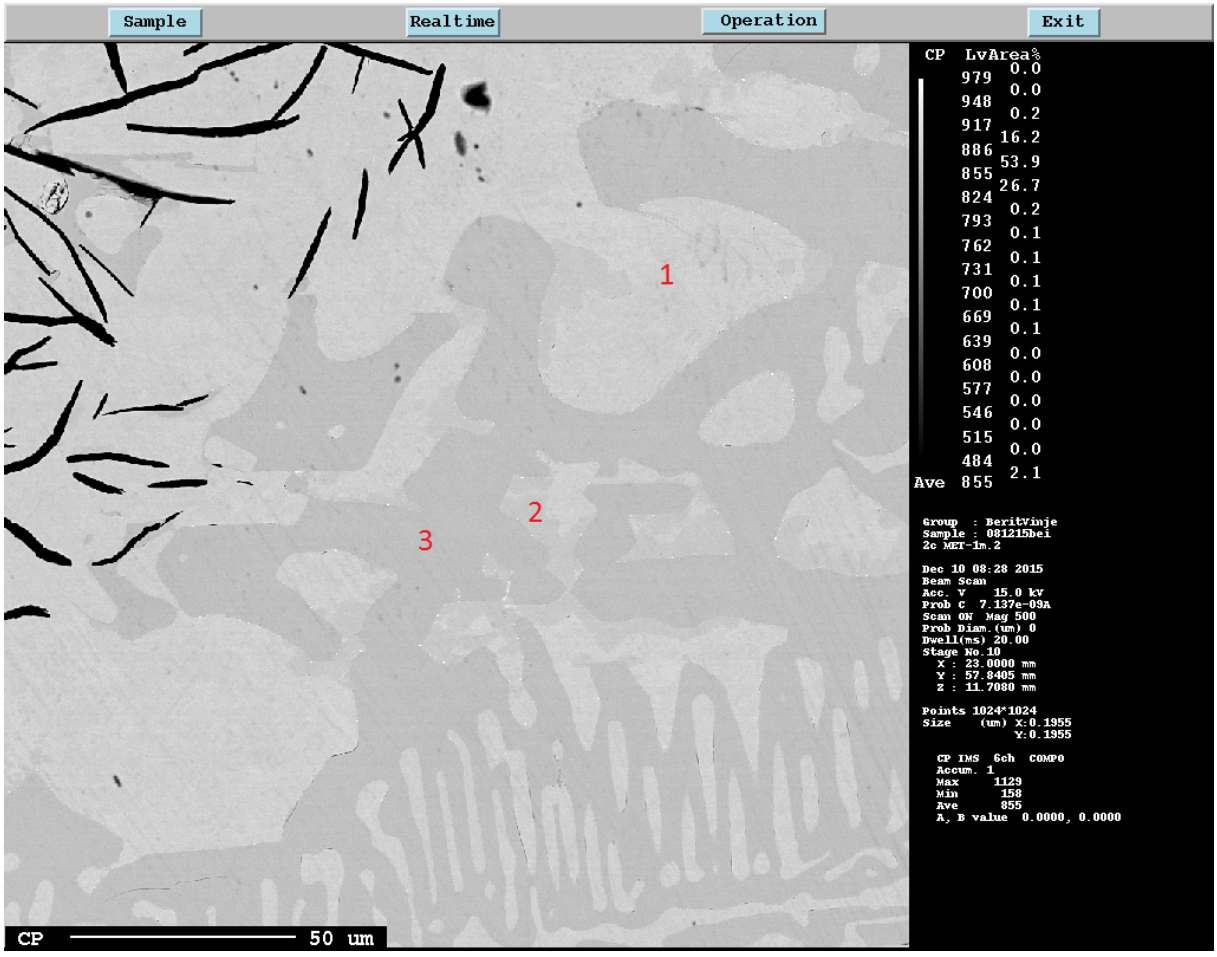

Figure 5-13 Input 2c MET-1 metal.

The metal from Input 2c MET-1 is given in Figure 5-13. Notice that there were two different phases within the lighter phase. The results are shown in Table 5-15.

Table 5-15 EPMA results for the metal from Input 2c MET-1.

Point 1			Point 2			Point 3		
	wt%	Norm. wt%		wt%	Norm. wt%		wt%	Norm. wt%
Fe	96,35	92,37	Fe	92,64	89,57	Fe	90,34	91,37
Mn	2,59	2,48	Mn	3,36	3,25	Mn	4,25	4,30
Dy	1,48	1,42	Dy	1,86	1,80	Dy	2,25	2,28
Ni	1,38	1,33	Sn	1,75	1,69	C	1,03	1,04
Cu	1,04	1,00	Ni	1,73	1,67	Ni	0,46	0,46
Sn	0,56	0,53	Cu	1,17	1,13	O	0,34	0,34
C	0,54	0,52	C	0,50	0,48	Cr	0,21	0,21
O	0,36	0,35	O	0,42	0,41			
Total	104,31	100,00	Total	103,42	100,00	Total	98,88	100,00

5.3.1.5 Input 2c MET-2

The SEM image with EDS points for Input 2c MET-2 is shown in. The results are given in. The EPMA image for the slag from The EPMA image for the slag from Input 2c MET-2 is shown in Figure 5-15 with the corresponding results given in

Table 5-17.

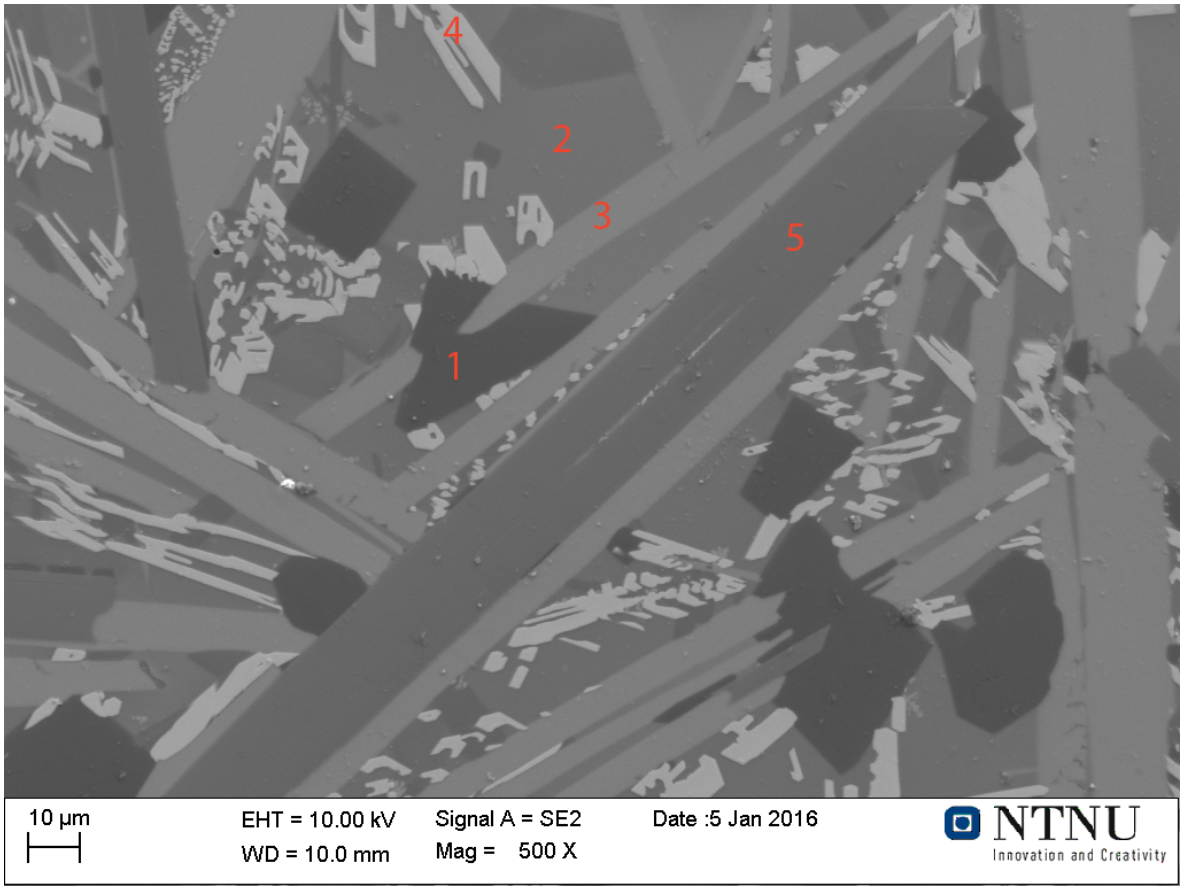

Figure 5-14 SEM image of the slag from Input 2c MET-2 with EDS points.

Table 5-16 EDS results for the slag of Input 2c MET-2.

Point 1			Point 2			Point 3		
Element	[wt.%]	[norm. wt.%]	Element	[wt.%]	[norm. wt.%]	Element	[wt.%]	[norm. wt.%]
Al	28,90	38,93	O	26,57	37,25	Ba	33,35	38,97
O	26,51	35,70	Si	11,87	16,63	O	21,17	24,74
Mg	11,40	15,36	Ca	10,22	14,33	Si	16,44	19,22
Mn	5,10	6,87	Mn	7,38	10,35	Al	12,79	14,94
C	2,33	3,14	Al	7,23	10,14	C	1,82	2,13
			Ti	3,57	5,00			
			C	2,06	2,89			
			Zn	1,40	1,97			
			Mg	1,03	1,45			
Sum:	74,24	100,00	Sum:	71,33	100,00	Sum:	85,58	100,00

Point 4			Point 5		
Element	[wt.%]	[norm. wt.%]	Element	[wt.%]	[norm. wt.%]
Nd	49,83	55,46	Al	34,41	44,52
O	17,63	19,63	O	26,90	34,80
Si	10,87	12,10	Nd	11,07	14,33
Ca	6,69	7,44	Mg	2,27	2,94
Z	1,85	2,06	C	1,40	1,81
C	1,58	1,76	Ca	1,24	1,61
Ar	1,39	1,55			
Sum:	89,85	100,00	Sum:	77,29	100,00

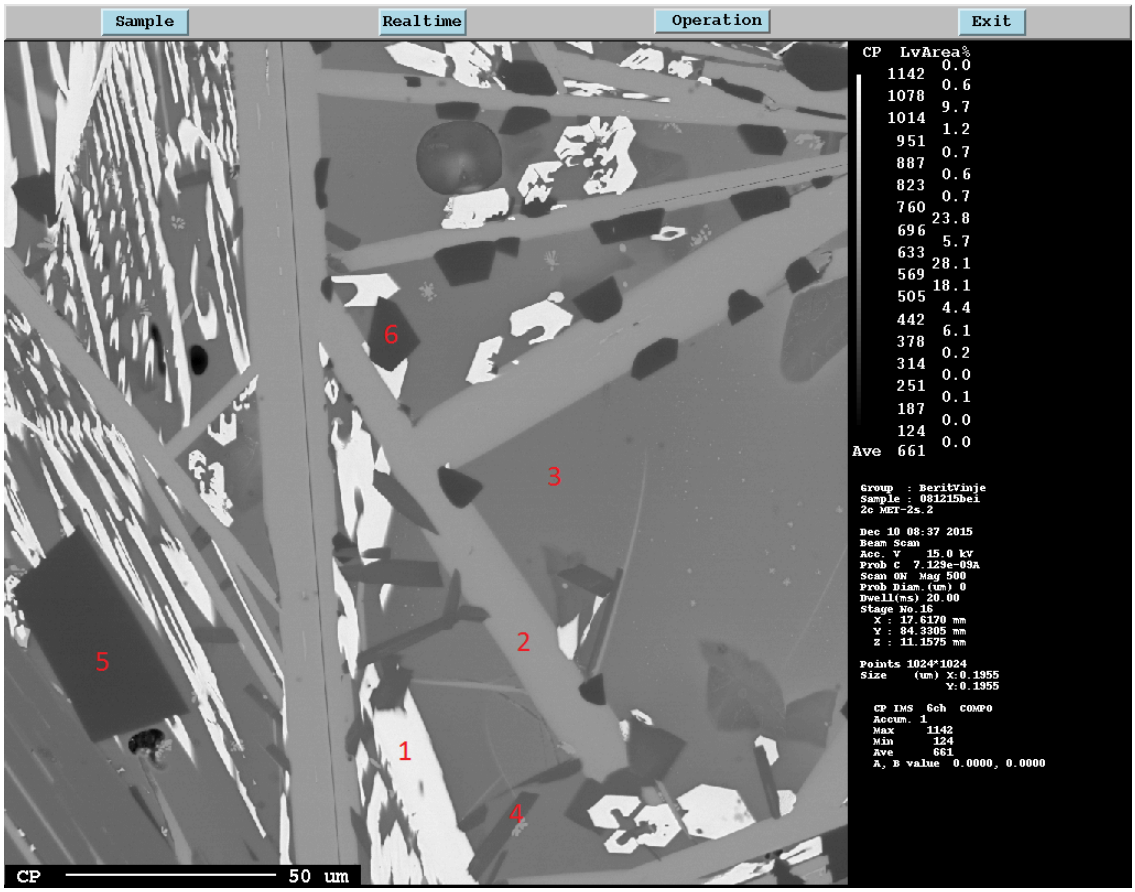

Figure 5-15 Input 2c MET-2 slag.

Table 5-17 EPMA results for the slag from Input 2c MET-2.

Point 1			Point 2			Point 3		
	wt%	Norm. wt%		wt%	Norm. wt%		wt%	Norm. wt%
O	25,83	35,41	O	35,46	34,40	O	37,58	39,95
Nd	20,69	28,37	Ba	34,24	33,22	Si	11,87	12,62
Si	9,27	12,71	Al	16,08	15,60	Ca	11,58	12,31
Ca	6,52	8,94	Si	14,71	14,27	Al	11,29	12,00
Dy	2,96	4,06	Ti	1,21	1,18	Mn	5,59	5,95
Eu	1,97	2,70	Sr	0,74	0,72	Ti	3,38	3,59
Pr	1,42	1,95	Ca	0,34	0,33	Nd	3,05	3,24
Mn	0,90	1,23	C	0,29	0,28	Dy	3,00	3,19
Ba	0,67	0,91				Ba	2,33	2,48
Al	0,57	0,78				Sr	1,89	2,01
S	0,56	0,77				Zr	1,40	1,49
Ti	0,34	0,46				Mg	0,71	0,75
Zr	0,32	0,44				Eu	0,38	0,40
C	0,31	0,42						
Sr	0,31	0,42						
W	0,30	0,41						
Total	72,94	100,00	Total	103,08	100,00	Total	94,06	100,00

Point 4			Point 5			Point 6		
	wt%	Norm. wt%		wt%	Norm. wt%		wt%	Norm. wt%

O	41,46	43,25	O	39,36	39,50	O	44,86	43,18
Al	39,22	40,93	Al	20,54	20,61	Al	38,34	36,90
Nd	4,80	5,01	Ti	11,43	11,47	Mg	13,26	12,76
Mg	2,15	2,24	Ca	8,11	8,14	Mn	4,08	3,93
Ca	1,61	1,68	Si	6,39	6,41	Dy	2,09	2,01
Ti	1,58	1,65	Mg	4,66	4,67	Ti	0,80	0,77
Ba	0,99	1,03	Mn	4,22	4,24	C	0,46	0,44
Si	0,75	0,79	Dy	2,49	2,49			
Mn	0,75	0,78	Nd	1,25	1,25			
Dy	0,61	0,64	Ba	0,46	0,46			
Eu	0,55	0,58	C	0,39	0,39			
C	0,50	0,52	Zr	0,36	0,36			
Sr	0,46	0,48						
Pr	0,40	0,42						
Total	95,84	100,00	Total	99,64	100,00	Total	103,88	100,00

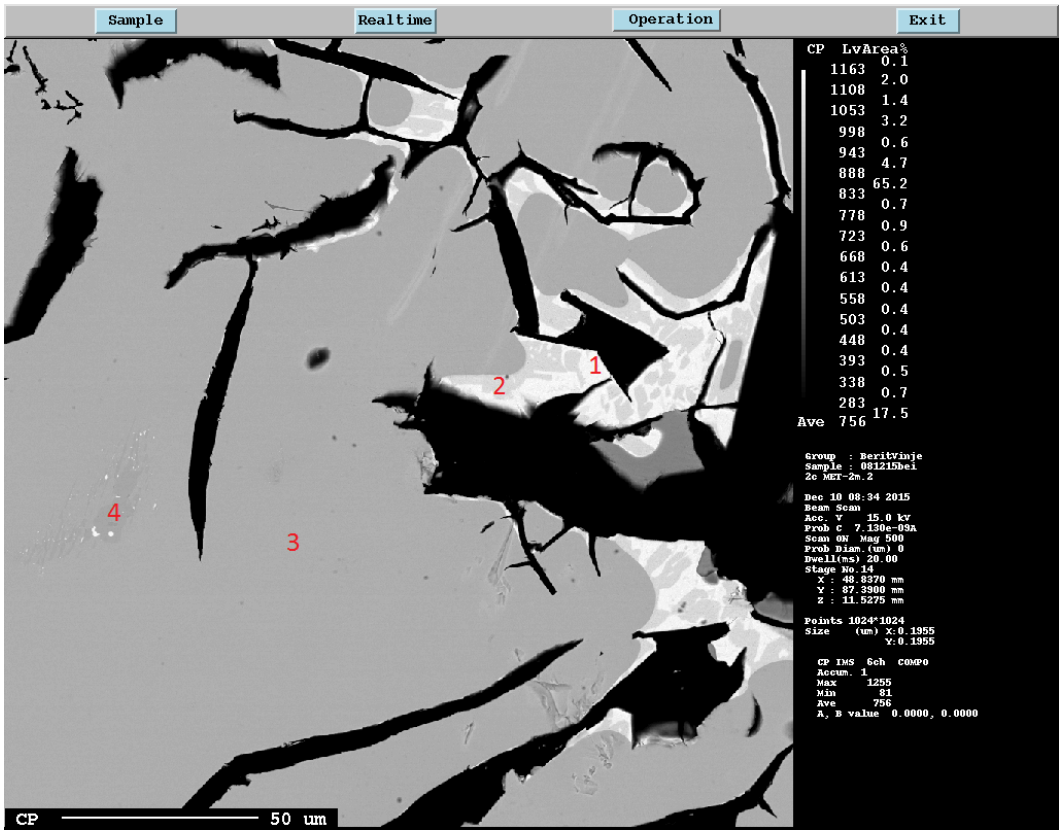

Figure 5-16 Input 2c MET-2 metal.

The metal is shown in Figure 5-16. A slightly darker phase can be seen within the matrix, these are marked as points 4 and 3, respectively. Likewise, the light areas around the carbide had two different hues. The results are shown in Table 5-18.

Table 5-18 EPMA results for the metal from Input 2c MET-2.

Point 1			Point 2			Point 3			Point 4		
	wt%	Norm. wt%		wt%	Norm. wt%		wt%	Norm. wt%		wt%	Norm. wt%
Cu	54,19	55,34	Cu	78,50	76,51	Fe	83,54	79,73	Fe	80,80	80,83
Sn	30,22	30,86	Sn	12,15	11,85	Ni	7,30	6,96	Mn	8,93	8,94
Ni	4,84	4,94	Mn	3,93	3,83	Cu	5,50	5,25	Dy	4,52	4,52
Mn	3,88	3,96	Fe	3,23	3,15	Mn	3,90	3,72	Cr	3,12	3,12
Fe	1,93	1,97	Dy	1,98	1,93	Dy	2,10	2,00	Ni	1,67	1,67

Dy	1,81	1,84	Ni	1,70	1,66	Si	0,80	0,76	C	0,92	0,92
O	0,55	0,56	C	0,57	0,55	Sn	0,65	0,62			
C	0,52	0,53	O	0,52	0,51	C	0,51	0,48			
						Cr	0,49	0,47			
Total	97,93	100,00	Total	102,60	100,00	Total	104,79	100,00	Total	99,96	100,00

Point 4			Point 5		
	wt%	Norm. wt%		wt%	Norm. wt%
Fe	83,54	79,73	Fe	80,80	80,83
Ni	7,30	6,96	Mn	8,93	8,94
Cu	5,50	5,25	Dy	4,52	4,52
Mn	3,90	3,72	Cr	3,12	3,12
Dy	2,10	2,00	Ni	1,67	1,67
Si	0,80	0,76	C	0,92	0,92
Sn	0,65	0,62			
C	0,51	0,48			
Cr	0,49	0,47			
Total	104,79	100,00	Total	99,96	100,00

5.3.2 XRF

The XRF results are presented in the tables below. The amounts are given in mass percent. It is important to note that XRF does not provide exact amounts of any of the compounds given here. One might argue that the compounds with concentrations lower than 1 % should have been removed. Due to the low concentration, they may very well not have been present. Because many of them were very likely to be found in the scrap, such as Tb_2O_3 from NdFeB magnets, they have after all been included.

Table 5-19 Input 2a MET-1. An experiment with this input was conducted prior to this project, and the results are included for comparison.

Prior experiment		Normalized	Experiment 1	Date: 30.09.15	Normalized
Nd2O3	28,8700 %	28,2237 %	Nd2O3	26,3900 %	25,0731 %
Al2O3	19,6800 %	19,2394 %	Al2O3	20,8100 %	19,7715 %
SrO	18,3600 %	17,9490 %	SrO	14,8400 %	14,0994 %
BaO	9,9100 %	9,6881 %	SiO2	10,8900 %	10,3466 %
SiO2	8,2200 %	8,0360 %	BaO	9,8300 %	9,3395 %
CaO	5,4800 %	5,3573 %	CaO	5,1900 %	4,9310 %
Pr6O11	4,0400 %	3,9496 %	Pr2O3	4,0500 %	3,8479 %
MgO	1,9500 %	1,9063 %	FeO	3,9700 %	3,7719 %
Fe	1,2800 %	1,2513 %	MgO	2,1500 %	2,0427 %
Dy2O3	1,1200 %	1,0949 %	TiO2	2,0400 %	1,9382 %
TiO2	1,1000 %	1,0754 %	MnO	1,2500 %	1,1876 %
Cr2O3	0,8400 %	0,8212 %	Dy2O3	1,0700 %	1,0166 %
La2O3	0,5800 %	0,5670 %	Cr2O3	0,8200 %	0,7791 %
S	0,3200 %	0,3128 %	ZrO2	0,6300 %	0,5986 %
MnO	0,1200 %	0,1173 %	MoO3	0,4600 %	0,4370 %
ZrO2	0,1200 %	0,1173 %	WO3	0,3500 %	0,3325 %
W	0,1100 %	0,1075 %	SO3	0,1700 %	0,1615 %
Tb4O7	0,0955 %	0,0934 %	NiO	0,1500 %	0,1425 %

Pd	0,0478 %	0,0467 %	CuO	0,1100 %	0,1045 %
Cu	0,0317 %	0,0310 %	Tb2O3	0,0824 %	0,0783 %
Ni	0,0123 %	0,0120 %			
Sum	102,29 %	100,00 %	Sum	105,25 %	100,00 %
Total REO		33,93 %	Total REO		30,02 %

Table 5-20 XRF results for Input 2b MET-1.

Experiment 2	Date: 10.12.15	Normalized
Al2O3	46,7600 %	44,0439 %
MgO	26,6600 %	25,1115 %
CaO	11,2000 %	10,5494 %
FeO	7,8900 %	7,4317 %
SiO2	3,4300 %	3,2308 %
Nd2O3	3,2400 %	3,0518 %
Cr2O3	1,7200 %	1,6201 %
SrO	1,6000 %	1,5071 %
BaO	1,1000 %	1,0361 %
MnO	0,4900 %	0,4615 %
Pr2O3	0,4900 %	0,4615 %
MoO3	0,3600 %	0,3391 %
TiO2	0,3500 %	0,3297 %
WO3	0,2200 %	0,2072 %
ZrO2	0,2200 %	0,2072 %
CuO	0,2100 %	0,1978 %
NiO	0,1300 %	0,1224 %
Dy2O3	0,0967 %	0,0911 %
Sum	106,1667 %	100,00 %
Total REO		3,60 %

Table 5-21 XRF results for Input 2b MET-2.

Experiment 1	Date: 14.10.15	Normalized	Experiment 2	Date: 04.11.15	Normalized
SiO2	33,4700 %	32,2945 %	SiO2	32,2100 %	30,5582 %
Al2O3	26,8800 %	25,9359 %	Al2O3	25,1500 %	23,8602 %
MgO	13,5900 %	13,1127 %	MgO	14,1300 %	13,4054 %
MnO	9,1400 %	8,8190 %	MnO	8,1000 %	7,6846 %
CaO	7,2200 %	6,9664 %	CaO	6,3700 %	6,0433 %
BaO	5,7900 %	5,5866 %	BaO	5,8600 %	5,5595 %
Nd2O3	3,0100 %	2,9043 %	Nd2O3	2,7100 %	2,5710 %
TiO2	2,2000 %	2,1227 %	FeO	2,5900 %	2,4572 %
SrO	0,8900 %	0,8587 %	TiO2	2,4100 %	2,2864 %
ZrO2	0,6800 %	0,6561 %	MoO3	2,3800 %	2,2579 %
Pr2O3	0,3400 %	0,3281 %	CeO2	1,0300 %	0,9772 %
FeO	0,1800 %	0,1737 %	SrO	0,9000 %	0,8538 %
SO3	0,0931 %	0,0898 %	ZrO2	0,8200 %	0,7779 %
Dy2O3	0,0645 %	0,0622 %	Pr2O3	0,3100 %	0,2941 %
Y2O3	0,0554 %	0,0535 %	Cr2O3	0,1700 %	0,1613 %
CuO	0,0265 %	0,0256 %	NiO	0,1000 %	0,0949 %
NiO	0,0111 %	0,0107 %	CuO	0,0825 %	0,0783 %
			Dy2O3	0,0525 %	0,0498 %
			Y2O3	0,0305 %	0,0289 %
Sum	103,64 %	100,00 %	Sum	105,41 %	100,00 %
Total REO		3,3480 %	Total REO		4,8693 %

Table 5-22 XRF results for Input 2c MET-1.

Experiment 1	Date: 21.10.15	Normalized	Large crucible no. 1		Normalized
Nd2O3	72,1100 %	66,1630 %	Nd2O3	72,4000 %	66,9914 %
Pr2O3	8,1500 %	7,4779 %	Pr2O3	7,8400 %	7,2543 %
Al2O3	5,6900 %	5,2207 %	SiO2	5,9700 %	5,5240 %
SiO2	4,9800 %	4,5693 %	Al2O3	4,8500 %	4,4877 %
SrO	4,7600 %	4,3674 %	SrO	4,0800 %	3,7752 %
FeO	2,7400 %	2,5140 %	BaO	3,1000 %	2,8684 %
BaO	2,6500 %	2,4315 %	Dy2O3	2,4100 %	2,2300 %
Dy2O3	2,3800 %	2,1837 %	CaO	1,9200 %	1,7766 %
CaO	1,6000 %	1,4680 %	MnO	1,6900 %	1,5638 %
MgO	1,4900 %	1,3671 %	MgO	1,2900 %	1,1936 %
TiO2	0,7100 %	0,6514 %	TiO2	1,1400 %	1,0548 %
Cr2O3	0,6500 %	0,5964 %	FeO	0,5500 %	0,5089 %
MnO	0,4100 %	0,3762 %	Tb2O3	0,2800 %	0,2591 %
ZrO2	0,3400 %	0,3120 %	SO3	0,2200 %	0,2036 %
Tb2O3	0,1800 %	0,1652 %	ZrO2	0,2100 %	0,1943 %
CoO	0,0690 %	0,0633 %	CoO	0,0722 %	0,0668 %
SO3	0,0325 %	0,0298 %	CuO	0,0318 %	0,0294 %
CuO	0,0253 %	0,0232 %	NiO	0,0195 %	0,0180 %
NiO	0,0216 %	0,0198 %			
Sum	108,99 %	100,00 %	Sum	108,07 %	100,00 %
Total REO		75,9897 %	Total REO		76,7348 %

Table 5-23 XRF results for Input 2c MET-2.

Experiment 1	Date: 05.11.15	Normalized
Al2O3	25,9200 %	24,4935 %
FeO	19,2600 %	18,2000 %
SiO2	16,8100 %	15,8848 %
Nd2O3	11,6800 %	11,0372 %
BaO	8,3800 %	7,9188 %
MnO	6,0600 %	5,7265 %
CaO	5,2600 %	4,9705 %
TiO2	3,7000 %	3,4964 %
MgO	2,9900 %	2,8254 %
Pr2O3	1,2600 %	1,1907 %
Cr2O3	1,0800 %	1,0206 %
SrO	0,8400 %	0,7938 %
NiO	0,8400 %	0,7938 %
ZrO2	0,4000 %	0,3780 %
CuO	0,3200 %	0,3024 %
Dy2O3	0,3200 %	0,3024 %
MoO3	0,3000 %	0,2835 %
P2O5	0,1300 %	0,1228 %
SO3	0,0807 %	0,0763 %
SnO2	0,0776 %	0,0733 %
WO3	0,0745 %	0,0704 %
Y2O3	0,0414 %	0,0391 %
Sum	105,82 %	100,00 %
Total REO		12,5693 %

5.3.3 XRD

The XRD was initially performed to establish if the slag phase from Input 2b MET-2 was in fact glassy. In XRD, glass generally appears as blunt but still distinguishable peaks (K. Høydalsvik, personal communication, Fall 2015). The result for Input 2b MET-2 shows that it was not glassy after all. It is worth noting that preparation for XRD requires skill and may give false indications of structure if not done with proper care. The sharp peaks seen in FIGURE may therefore result from the author's poor experience in sample preparation. XRD is a "fingerprint" technique, meaning that all peaks must be accounted for. This was not possible for any of the samples, and the preferred and suggested matches in the software made no sense compared to the XRF results. Because the structure of the slag from Input 2b MET-2 was the original purpose of the measurements, the XRD results of that sample are shown here, although it has been incompletely identified like all the other samples. The rest of the XRD results are included in Appendix. As seen from the EDS, EPMA and XRF results, the samples contained a very high number of different elements, and this could be the reason why the peaks are so hard to identify.

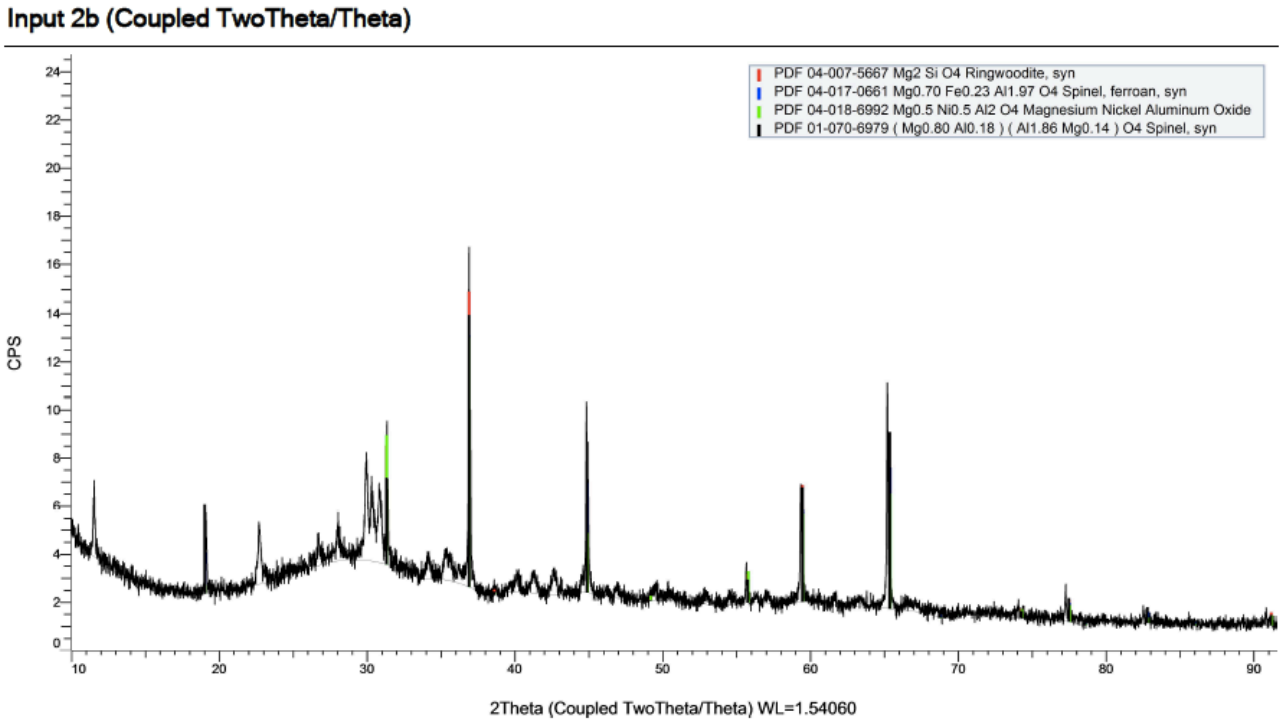

Figure 5-17 XRD results for Input 2b MET-2.

5.3.4 Sessile Drop technique

The pictures taken during the wetting experiments are presented in the tables below. The melting temperature is found at the time when the material forms a near-perfect circle. The three pictures selected for each of the samples illustrate its shape before melting, the temperature at which it started melting and the temperature at which it was completely melted. Except for Input 2b MET-1, metal and slag were melted separately for all fractions.

5.3.4.1 Input 2a

The metal was melted at 1100°C, indicating carbon saturation. As seen, there were shell-like carbides or oxides on the surface of the metal that were not completely melted. This does not represent the overall composition of the metal, since the samples used for the sessile drop technique are minute. The slag from Input 2a MET-1 was completely melted at 1600°C.

Table 5-24 Results of wetting experiment with the Input 2a MET-1 metal phase.

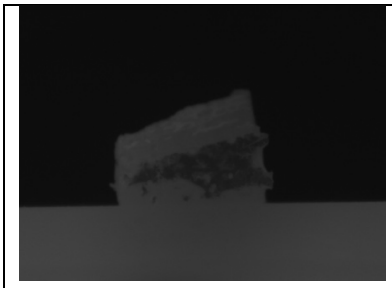	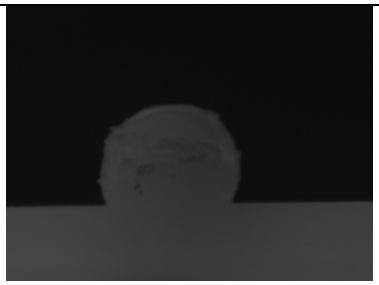	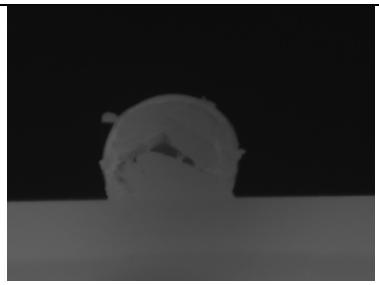
1093°C	1097°C	1313°C

Table 5-25 Results of wetting experiment with the Input 2a MET-1 slag phase.

		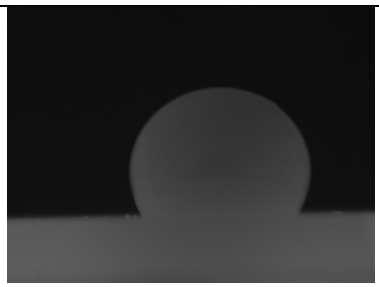
1512°C	1536°C	1606°C

5.3.4.2 Input 2b

The temperature needed for the second experiment with Input 2b MET-1 was established here. Because slag and metal were not separated in the first experiment, they were melted together in this particular experiment.

Table 5-26 Results of wetting experiment with material from the first experiment with Input 2b MET-1.

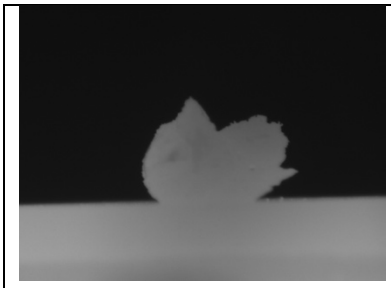	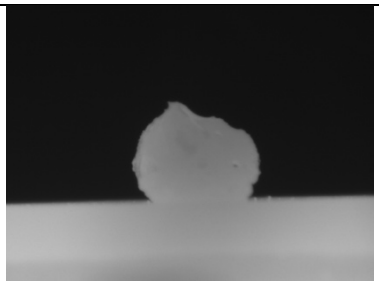	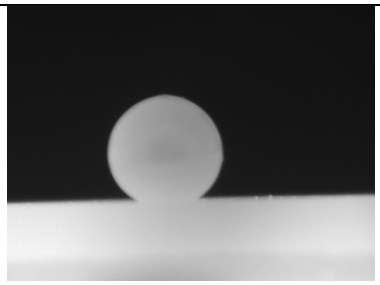
1710°C	1747°C	1800°C

As with the metal from Input 2a MET-1, the metal from Input 2b MET-2 was melted at 1100°C. The experiment was run until all impurities were melted.

Table 5-27 Results of wetting experiment with the Input 2b MET-2 metal phase.

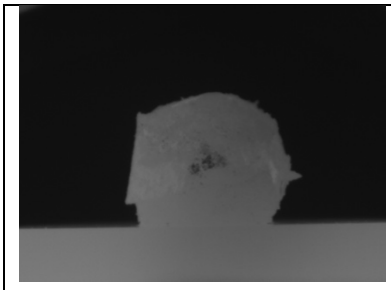	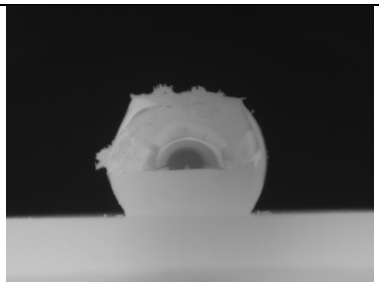	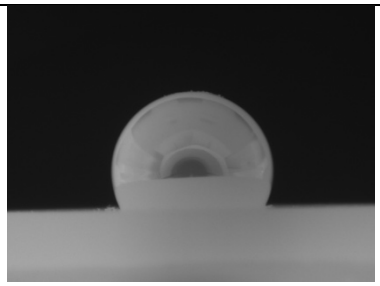
1094°C	1500°C	1704°C

The slag from Input 2b MET-2 melted at the lowest temperature of all input materials: 1170°C.

Table 5-28 Results of wetting experiment with the Input 2b MET-2 slag phase.

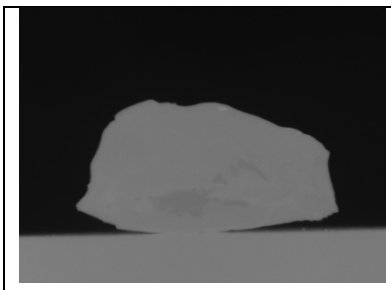	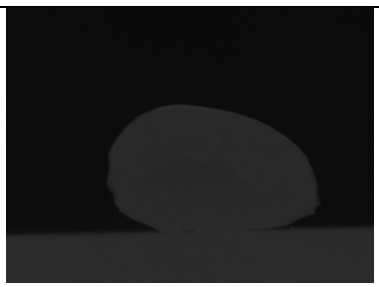	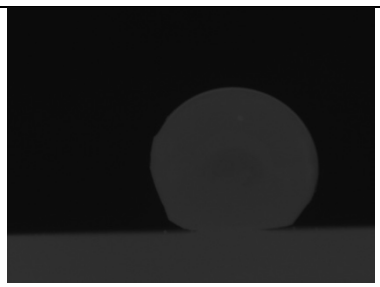
1136°C	1160°C	1170°C

5.3.4.3 Input 2c

The metal sample from Input 2c MET-1 was melted around 1100°C, like the other metal samples. The slag melted at 1550°C.

Table 5-29 Results of wetting experiment with the Input 2c MET-1 metal phase.

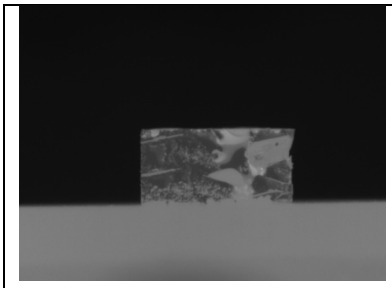	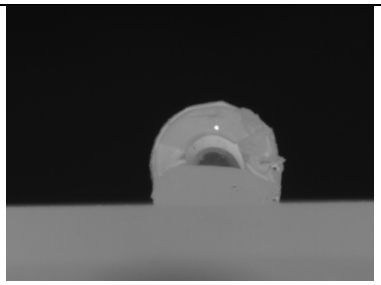	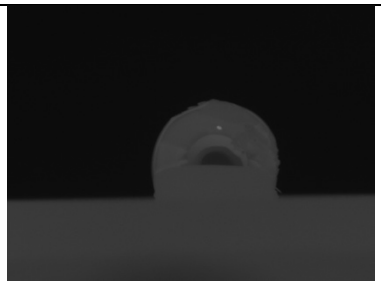
1070°C	1076°C	1111°C

Table 5-30 Results of wetting experiment with the Input 2c MET-1 slag phase.

	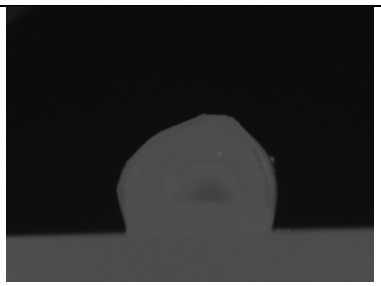	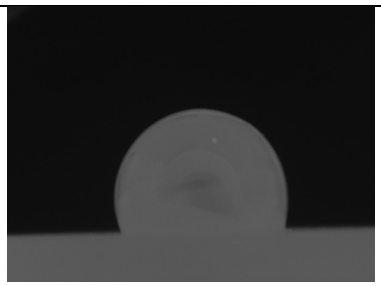
1503°C	1520°C	1548°C

The metal from Input 2c MET-2 was not completely melted until at 1400°C, however it may have been very impure, as it clearly starts melting at around the same temperature as the other metal samples. The slag melted already at 1450°C.

Table 5-31 Results of wetting experiment with the Input 2c MET-2 metal phase.

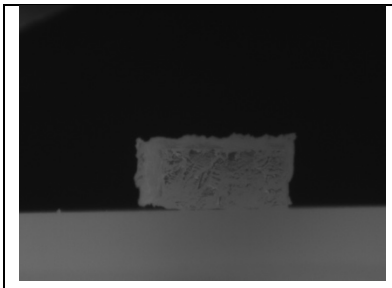	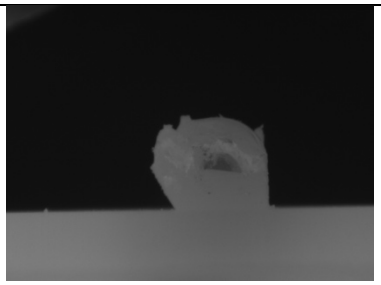	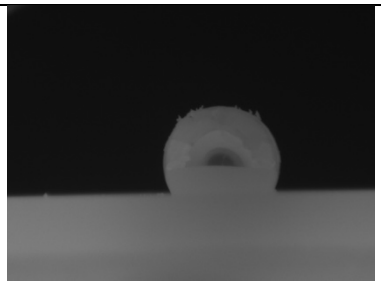
1077°C	1097°C	1400°C

Table 5-32 Results of wetting experiment with the Input 2c MET-2 slag phase.

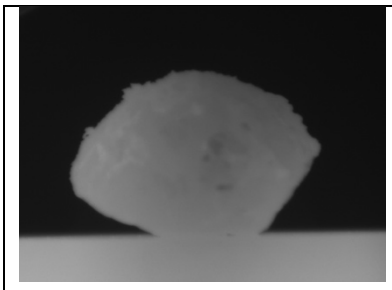	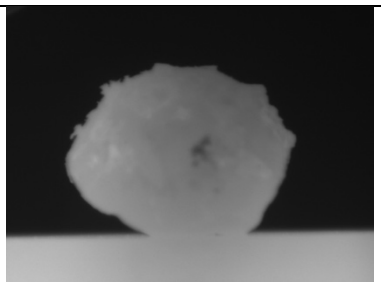	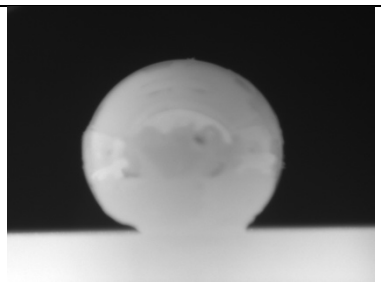
1382°C	1404°C	1457°C

6 DISCUSSION

The three different inputs gave very different results, and the following discussion tries to give possible explainations for the differences. It is impossible to say which of the inputs is nearest to an average without collection and analyses of more fractions. From the results, it is clear that the main source of rare earths was NdFeB magnets.

Using the mass balances from the Smelting and the XRF results from the second experiment for inputs 2a MET-1, 2b MET-1 and 2b MET-2, as well as the pre-smelting analyses of the Input Materials for the same fractions, Table 6-1 shows a comparison of expected yield and actual yield from the smelting experiments. Only a few elements are comparable, because as the EPMA results showed, several elements such as Dy and Mn were present in both metal and slag. The expected yield is found using the analyses from before the experiments and multiplying the percentage with the total amount of material that was melted. The actual yield was found using the relative amounts of each element and multiplying it with the percentage found in the XRF measurements, then multiplying it with the amount of slag achieved in the experiments. For instance, Al_2O_3 consists of 52,93 wt% Al and 47,07 wt% O, so with a content of 19,77 wt% Al_2O_3 in Input 2a MET-1, the relative amount of Al is 10,46 wt% and the actual Al yield in the experiment is 0,145 g. The iron content is more of a guess: assuming carbon saturation and no other elements in the metal phase but iron, the amount of iron is assumed to be approximately 96% of the total amount of metal plus the amount from the FeO in the slag. This guess gives a higher-than-expected amount of iron for 2a MET-1 and 2b MET-2, but a lower amount for 2b MET-1. For all the other elements except Mn, the actual yields are also higher than expected. Because the compositions seem higher than first measured, it is hard to back-calculate to find out if some of the rare earths have gone elsewhere than the slag.

The waste is very inhomogeneous. It is no wonder the concentrations are higher in the slag than in the material as a whole, but since the yield also becomes higher, it raises the question of which sample measurements were most presise and also of which could be considered representative to the sample as a whole. The amount of slag produced in the experiment with Input 2b MET-1 means the Nd yield is higher than in the experiment with 2a MET-1. However, the 2b MET-1 slag is much more difficult, and at first glance seems rather undesireable to recycle. The economy of the method was beyond the scope of this thesis.

Table 6-1 Comparison of expected yield from analyses made before and after the experiments.

Input 2a MET-1				
Element	Analysis before:	Relative amount in slag from XRF	Expected yield	Actual yield
Nd	0,6489 %	21,4965 %	0,20693421	0,303100161
Dy	0,0246 %	0,8858 %	0,00784494	0,012489572
Al	0,15 %	10,4641 %	0,047835	0,147543769
Fe	80,30 %	5,7767 %	25,60767	27,50693987
Mn	0,76 %	0,3574 %	0,242364	0,012968657

Input 2b MET-1				
Element	Analysis before	Relative amount in slagfrom XRF	Expected yield	Actual yield
Nd	0,4039 %	2,6165 %	0,148076202	0,341986187
Dy	0,0162 %	0,0794 %	0,005939179	0,010373064
Fe	59,1000 %	5,7767 %	21,6670056	16,96752415
Al	5,2700 %	23,3103 %	1,93206632	3,046772822
Mg	--	15,1431 %	0	1,979280143
Ca	--	7,5396 %	0	0,985462764
Si	--	1,5102 %	0	0,197387311

Input 2b MET-2				
Element	Analysis before	Relative amount in slag from XRF	Expected yield (g)	Actual yield (g)
Nd	0,2016 %	2,20 %	0,061841212	0,064585245
Al	1,2465 %	12,63 %	0,382303116	0,37000196
Fe	59,2917 %	1,91 %	18,18475387	20,1967623
Mn	4,3765 %	5,95 %	1,342280863	0,174376211
Mg	--	8,08 %	0	0,236858922
Si	--	14,59 %	0	0,427473627
Ca	--	4,32 %	0	0,126549984

Input 2b MET-1 had not beforehand been analysed with regards to 3 of its 5 most important elements, Mg, Ca and Si. If it had, the prediction of its melting temperature might have been easier. Normalizing the Al_2O_3, MgO and CaO content to fit the pure Al_2O_3-MgO-CaO system shown in Figure 6-1, the expected melting temperature would be 1900°C. SiO_2 and FeO both have the effect on Al_2O_3 of lowering the melting temperature [24], which may explain why the temperature is not higher than 1800°C.

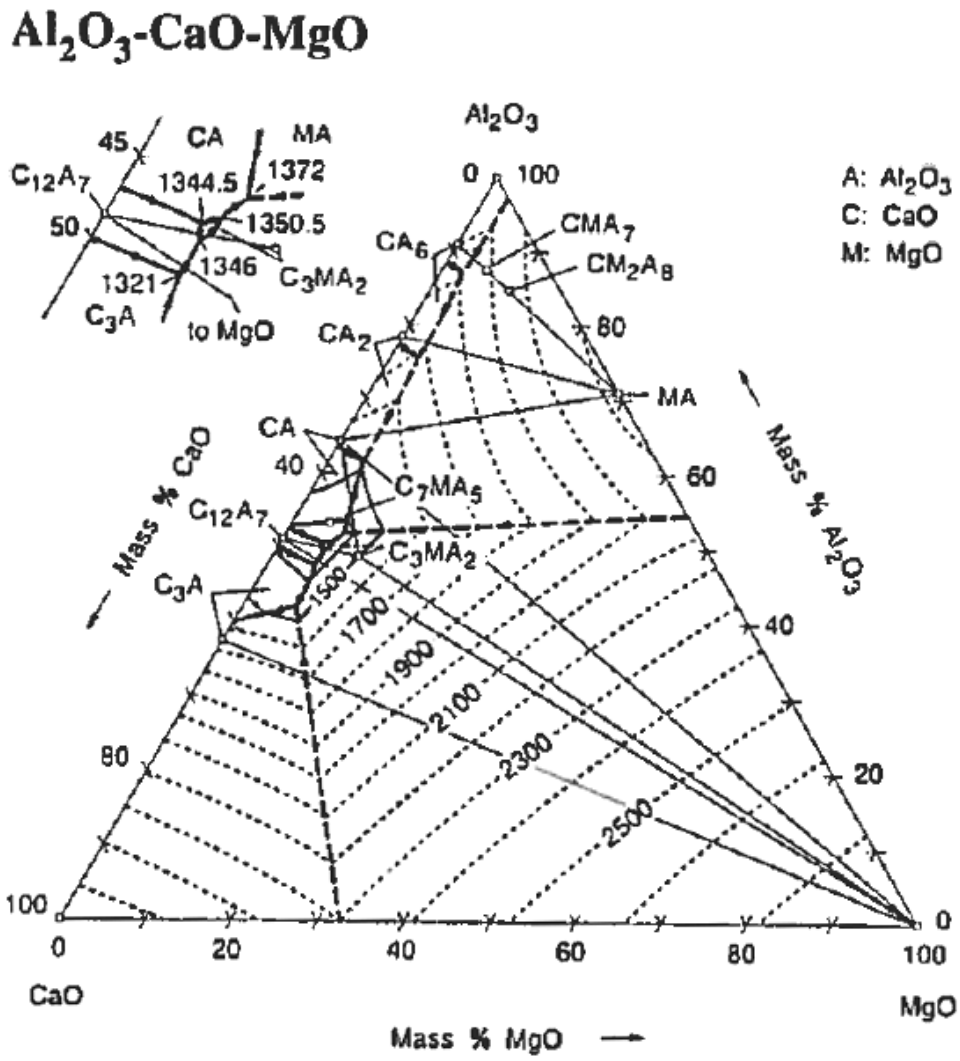

Figure 6-1 The ternary phase diagram of the Al_2O_3-MgO-CaO system. [24]

The results from the smelting of Input 2c were very promising. Although differing results from initial and final analyses for inputs 2a MET-1 and 2b MET-1 and Met-2 may be explained by the inhomogeneity of the material, the small-scale and large-scale smelting experiments on input 2c MET-1 had very consistent XRF results. The small differences may be explained by the differing conditions for the experiments, as they were melted in different furnaces and the larger crucibles were probably not made from such a fine material as the smaller crucibles. The REO yield from Input 2c MET-1 and MET-2 may be calculated using the mass balances and the XRF results. The yield is then 800g REO from the total amount of MET-1 and 156g from MET-2, or 4% and 2%, respectively.

Although it is unfortunate that the inputs were sieved to different fractions, it is unlikely that 9,5 mm vs. 2 mm made much difference. There is clearly a lower concentration of REOs in the MET-2 fractions than in the MET-1 fractions, but the MET-1 fractions seem to only contain iron or steel with crushed magnets. A greater share of iron through a larger sieve would only result in a larger fraction of metal after smelting, and not in a lower concentration of REOs in the slag.

The condensate that was observed on the graphite tube that was used a holder and protection for the thermocouples should have been analysed for better insight into what is fumed off.

The demagnetization of the input materials clearly producted and released toxic and environmentally hazardous gas as predicted in the litterature survey. Industry processes for cleaning off-gases and standardized and good, and a potential industrial-scale version of this process, the off-gas cleaning could easily be designed so as to capture all hazardous substances and recover the energy.

As the EDS and EPMA-WDS results show, certain phases in the slags are enriched in REOs, and if these phases could be first mechanically separated from the rest of the slag, it might facilitate the further processing more.

7 CONCLUSION AND FUTURE WORK

In this thesis, three different input materials, denoted as Input 2a, Input 2b and Input 2c, were collected from the ferrous stream at an industrial recycling process. The materials were sorted into fractions larger and smaller than 60 mm and named MET-1 and MET-2, respectively. They were then demagnetized and sieved. Input 2a was sieved to -9,5 mm, Input 2b was sieved to -3,35 mm and Input 2c was sieved to -2 mm. The total number of materials was then 5. The small fractions were melted in a graphite tube furnace with the result of easily separable slag and metal phases. Input 2c was also melted in larger batches in an induction furnace. All samples except Input 2b MET-1 were melted at 1600°C, while Input 2b MET-1 required 1800°C to melt due to its high Al_2O_3, MgO and CaO content. The slag phases were analysed by SEM and EDS, EPMA-WDS, XRD, XRF and the sessile drop method, while the metal was analysed by EPMA-WDS and the sessile drop method. The results show that the rare earth oxides have almost exclusively ended up in the slag, while the metal phase mostly containes iron. There are great differences in the REO contents of the three inputs, and it is not possible to say which one is closer to a typical average composition. Some phases in the slags were enriched in rare earths, and the possibility of mechanical separation before further hydrometallurgical processing should be investigated.

The author is to continue working on the REEcover project, and will start by analysing the condensate collected from the larger-scale smelting of Input 2c. Inputs 2d, e, f, and so on, will also be collected and analysed to establish the average composition of the WEEE. Input 2b was early on selected as the material for demo tests, and it will be smelted in larger-scale experiments to test the method's feasibility on an industry scale.

Will continue to work on project.

- Include future work at all?
- Analyse condensate
- Do more tests on inputs 2d, e, f and so on to establish typical contents.
- Do large-scale tests on Input 2b.

8 REFERENCES

1. EURARE. *What are Rare Earth Elements?* 2015 06/04/2015]; Available from: http://www.eurare.eu/RareEarthElements.html.
2. Binnemans, K., et al., *Recycling of rare earths: a critical review.* Journal of Cleaner Production, 2013. **51**: p. 1-22.
3. Krishnamurthy, N. and C.K. Gupta, *Extractive metallurgy of rare earths*. 2015: CRC press.
4. Haxel, G.B., J.B. Hedrick, and G.J. Orris. *Rare Earth Elements—Critical Resources for High Technology*. 2005 06/04/2015]; Available from: http://pubs.usgs.gov/fs/2002/fs087-02.
5. Shiraishi, P.A., *The rare earths revolution: The dirty secret of green technologies*. 2012.
6. U.S. Department of Energy. *Critical Materials Strategy*. 2010 06/01/2015]; Available from: http://energy.gov/sites/prod/files/edg/news/documents/criticalmaterialsstrategy.pdf.
7. Walters, A. and P. Lusty, *Rare Earth Elements*, B.G. Survey, Editor. 2010.
8. Survey, U.S.G. *Rare Earths Statitics and Information*. 2015 06/09/2015]; Available from: http://minerals.usgs.gov/minerals/pubs/commodity/rare_earths/.
9. Navarro, J. and F. Zhao, *Life-Cycle Assessment of the Production of Rare-Earth Elements for Energy Applications: A Review.* Frontiers in Energy Research, 2014. **2**: p. 45.
10. Hurst, C., *China's Rare Earth Elements Industry: What Can the West Learn?* 2010, DTIC Document.
11. *China's Rare Earth Dominance*. 2010 06/10/2015]; Available from: http://www.wikinvest.com/concept/China's_Rare_Earth_Dominance.
12. Bontron, C., *En Chine, les terres rares tuent des villages*, in *Le Monde*. 2012.
13. Goodship, V. and A. Stevels, *Waste electrical and electronic equipment (WEEE) handbook*. 2012: Elsevier.
14. Commission, E. *Waste Electrical and Electronic Equipment (WEEE)*. 2015 [cited 2016 27.01]; Available from: http://ec.europa.eu/environment/waste/weee/index_en.htm.
15. Coolrec. *WEEE Recycling*. [cited 2016 27/1]; Available from: http://www.coolrec.eu/dienstverlening/weee-recycling.aspx.
16. Bonomini, P., *WEEE Man*. 2006.
17. *The Digital Dump: Exporting Re-use and Abuse to Africa*. 2007: Seattle.
18. Wikipedia. *Basel Convention*. [cited 2016 12.01]; Available from: https://en.wikipedia.org/wiki/Basel_Convention.
19. Hense, P., et al., *Pyrolysis of waste electrical and electronic equipment (WEEE) for recovering metals and energy: previous achievements and current approaches.* Environmental Engineering and Management Journal, 2015. **14**(7): p. 1637-1647.
20. Cui, J. and L. Zhang, *Metallurgical recovery of metals from electronic waste: A review.* Journal of hazardous materials, 2008. **158**(2): p. 228-256.
21. Hitachi, *Press Release: Hitachi Develops Recycling Technologies for Rare Earth Metals*, in *Hitachi Ltd*. 2010.
22. Yang, X., et al., *Pyrolysis and dehalogenation of plastics from waste electrical and electronic equipment (WEEE): A review.* Waste Management, 2013. **33**(2): p. 462-473.
23. Hoshi, H., Miyamoto, Y., & Furusawa, K. (2014). Technique for Separating Rare Earth Elements from R-Fe-B Magnets by Carbothermal Reduction Method. *JOURNAL OF THE JAPAN INSTITUTE OF METALS*, *78*(7), 258-266.
24. Keene, B. J., Mills, K. C., & Susa, M. (1995). Slag atlas. *Verlag Stahleisen, Düsseldorf*.

Appendix I

NTNU HSE	Hazardous activity identification process	Prepared by HSE section Approved by The Rector	Number HMSRV2601E	Date 09.01.2013 Replaces 01.12.2006

Unit: **Department of Materials Science and Engineering** **Date:** **01.10.2015**

Line manager: Jostein Mårdalen

Participants in the identification process (including their function)**: Berit Johansen Vinje (Master student), Gabriella Tranell (Supervisor)**

Short description of the main activity/main process: Master project for student Berit Johansen Vinje. Recycling of REO from WEE.

Is the project work purely theoretical? (YES/NO): **NO** *Answer "YES" implies that supervisor is assured that no activities requiring risk assessment are involved in the work. If YES, briefly describe the activities below. The risk assessment form need not be filled out.*

Signatures: *Responsible supervisor:* *Student:* Berit Vinje

ID nr.	Activity/process	Responsible person	Existing documentation	Existing safety measures	Laws, regulations etc.	Comment
1	Handling of demagnetized, iron-rich and BaO containing powder from scrap.	Berit Johansen Vinje	None, only training	Safety gloves, safety glasses, fume hood	NTNU- SINTEF Laboratory and workshop handbook	
2	*Preparation for SEM*: sputter coating of powder.	Berit Johansen Vinje	Training, documentation in room	Safety glasses, safety gloves	NTNU- SINTEF Laboratory and workshop handbook	Not considered hazardous apart from handling of powder.
3	*Furnace TF3 in room E-118 in Bergbygget:* Fill graphite crucible with iron-rich powdered WEEE.	Berit Johansen Vinje	None, only training	Safety gloves, safety glasses, fume hood	NTNU- SINTEF Laboratory and workshop handbook	Same as point no 1.
4	Put sealed graphite crucible into furnace and close furnace.	Berit Johansen Vinje	None, only training	Safety glasses, safety gloves	NTNU- SINTEF Laboratory and workshop handbook	
5	Evacuate and refill chamber with argon gas.	Berit Johansen Vinje	None, only training	Safety glasses. The backfill pressure is restricted to 1 bar.	NTNU- SINTEF Laboratory and workshop handbook	
6	Turn on furnace and heat sample.	Berit Johansen Vinje	None, only training	Safety glasses. Separate safety switch turns off furnace if it gets too hot.	NTNU- SINTEF Laboratory and workshop handbook	

7	Turn off furnace and let it cool for 1 hour and 15 minutes to room temperature before taking out sample.	Berit Johansen Vinje	None, only training	Safety glasses, heat resistant gloves.	NTNU- SINTEF Laboratory and workshop handbook	
8	*Chamber furnace* Loading of BaO containing WEEE scrap into furnace.	Berit Johansen Vinje	None	Gloves, lab coat, safety glasses, dust mask.	NTNU- SINTEF Laboratory and workshop handbook	
9	Heating of scrap in furnace. Scrap contains various types of plastics (most importantly ABS, PC, HIPS, PPO, PE, PP and PVC, all or some containing BFRs and PBDE) in small, but varying and unknown amounts.	Berit Johansen Vinje	None	Gloves, lab coat, safety glasses, ventilation	NTNU- SINTEF Laboratory and workshop handbook	
10	Take out scrap from furnace after heating.	Berit Johansen Vinje	None	Gloves, lab coat, safety glasses, dust mask.	NTNU- SINTEF Laboratory and workshop handbook	
11	*Sling mill* Crush demagnetized scrap.	Berit Johansen Vinje	None, only training	Dustmask, earplug, safety glasses, protection lid, ventilation, lab coat	NTNU- SINTEF Laboratory and workshop handbook	
12	Sieve scrap.	Berit Johansen Vinje	None	Dustmask, safety glasses, ventilation, lab coat	NTNU- SINTEF Laboratory and workshop handbook	

Note:
ABS = Acrylonitrile Butadiene Styrene
PC = Polycarbonate
HIPS = High Impact Polystyrene
PPO = Polyphenylene Oxide Blends
PE = Polyethylene
PP = Polypropylene
PVC = Polyvinylchloride
BFR = Brominated flame retardant
PBDE = Polybrominated diphenyl ethers

NTNU HSE/KS	Risk assessment	Prepared by	Number	Date
		HSE section	HMSRV2603E	04.02.2011
		Approved by		Replaces
		The Rector		01.12.2006

Unit: *(Department)* **Department of Materials Science and Engineering** **Date:** **01.10.2015**

Line manager: Jostein Mårdalen

Participants in the identification process (including their function): **Berit Johansen Vinje (Master student), Gabriella Tranell (Supervisor)**

Short description of the main activity/main process: Master project for student Berit Johansen Vinje. Recycling of REO from WEE.

Signatures: *Responsible supervisor:* *Student:* Berit Vinje

Activity from the identification process form	**Potential undesirable incident/strain**	**Likelihood:**	**Consequence:**			**Risk Value (human)**	**Comments/status Suggested measures**
		Likelihood (1-5)	Human (A-E)	Environment (A-E)	Economy/ material (A-E)		
Handling of demagnetized, iron-rich and BaO containing powder from scrap.	Irritation to skin, eyes or lungs.	3	C	A	A	C3	Use fume hood, protection glasses and protection gloves.
Preparation for SEM: sputter coating of powder.	None						
Furnace TF3 in room E-118 in Bergbygget: Fill graphite crucible with iron-rich powdered WEEE.	Inhale dust containing BaO.	2	C	A	A	C3	Fill graphite crucible in fume hood, wear protection gloves and glasses.
Put sealed graphite crucible into furnace and close furnace.	Accidentally break crucible, resulting in spreading of dust	2	C	A	A	C2	Graphite is brittle and breaks easily. Room should be evacuated if crucible breaks.
Put sealed graphite crucible into furnace and close furnace.	Accidentally break furnace parts.	3	A	A	B	A3	Graphite is brittle and may break, but there is no alternative material.
Evacuate and refill chamber with argon gas.	Too high pressure.	2	A	A	A	A2	Backfill pressure is restricted to max 1 bar.

Turn on furnace and heat sample.	Sample may destroy furnace	1	A	A	B	A1	Sample holder and crucible is non-reactive.
Turn on furnace and heat sample.	Furnace may overheat	2	A	A	C	A2	Separate switch will turn off furnace if too hot.
Turn off furnace and let it cool for 1 hour and 15 minutes to room temperature before taking out sample.	Sample may be hot	3	A	A	A	A3	Use heat-resistant gloves.
Chamber furnace: Loading of BaO containing WEEE scrap into furnace.	Irritation to skin, eyes or lungs from BaO. Scrap must in general not be touched.	3	C	A	A	C3	Use gloves, safety glasses, dust mask.
Heating of scrap in furnace.	Get burns from furnace.	1	B	A	A	B1	Furnace is simple in operation and touching it during experiment is unnecessary and easy to avoid.
Heating of scrap in furnace.	From pyrolysis of plastics, NH_3, HBr, HCN and HF are likely to be created. Risk of inhalation of these and of corrosion of furnace by the same compounds. The uncertainty concerning amounts is also a risk.	3	C	B	C	C3	Gas mask should be used. Heating of low amounts of scrap at a time until gases have been measured and effects on furnace have been estimated.
Take out scrap after heating.	Chlorine and bromine distribute over the products of pyrolysis: gas, oil and char. Scrap may be toxic.	3	C	A	A	C2	Wear gloves, lab coat, safety glasses, gas mask.

Sling mill Crush demagnetized scrap.	BaO dust and noise	3	B	A	A	B3	Use dustmask, earplug, safety glasses, protection lid, ventilation, lab coat
Sieve scrap.	BaO dust and noise	3	B	A	A	B3	Use dustmask, earplug, safety glasses, protection lid, ventilation, lab coat

Likelihood, e.g.:
1. *Minimal*
2. *Low*
3. *Medium*
4. *High*
5. *Very high*

Consequence, e.g.:
A. *Safe*
B. *Relatively safe*
C. *Dangerous*
D. *Critical*
E. *Very critical*

Risk value (each one to be estimated separately):
Human = Likelihood x Human Consequence
Environmental = Likelihood x Environmental consequence
Financial/material = Likelihood x Consequence for Economy/materiel

NTNU HSE/KS	Risk assessment	Prepared by HSE section Approved by The Rector	Number HMSRV2603E	Date 04.02.2011 Replaces 01.12.2006	

Potential undesirable incident/strain

Identify possible incidents and conditions that may lead to situations that pose a hazard to people, the environment and any materiel/equipment involved.

Criteria for the assessment of likelihood and consequence in relation to fieldwork

Each activity is assessed according to a worst-case scenario. Likelihood and consequence are to be assessed separately for each potential undesirable incident. Before starting on the quantification, the participants should agree what they understand by the assessment criteria:

Likelihood

Minimal 1	Low 2	Medium 3	High 4	Very high 5
Once every 50 years or less	Once every 10 years or less	Once a year or less	Once a month or less	Once a week

Consequence

Grading	Human	Environment	Financial/material
E Very critical	May produce fatality/ies	Very prolonged, non-reversible damage	Shutdown of work >1 year.
D Critical	Permanent injury, may produce serious serious health damage/sickness	Prolonged damage. Long recovery time.	Shutdown of work 0.5-1 year.
C Dangerous	Serious personal injury	Minor damage. Long recovery time	Shutdown of work < 1 month
B Relatively safe	Injury that requires medical treatment	Minor damage. Short recovery time	Shutdown of work < 1week
A Safe	Injury that requires first aid	Insignificant damage. Short recovery time	Shutdown of work < 1day

The unit makes its own decision as to whether opting to fill in or not consequences for economy/materiel, for example if the unit is going to use particularly valuable equipment. It is up to the individual unit to choose the assessment criteria for this column.

Risk = Likelihood x Consequence

Please calculate the risk value for "Human", "Environment" and, if chosen, "Economy/materiel", separately.

About the column "Comments/status, suggested preventative and corrective measures":

Measures can impact on both likelihood and consequences. Prioritise measures that can prevent the incident from occurring; in other words, likelihood-reducing measures are to be prioritised above greater emergency preparedness, i.e. consequence-reducing measures.

MATRIX FOR RISK ASSESSMENTS at NTNU

CONSEQUENCE						
	Extremely serious	E1	E2	E3	E4	E5
	Serious	D1	D2	D3	D4	D5
	Moderate	C1	C2	C3	C4	C5
	Minor	B1	B2	B3	B4	B5
	Not significant	A1	A2	A3	A4	A5
		Very low	Low	Medium	High	Very high
		LIKELIHOOD				

Principle for acceptance criteria. Explanation of the colours used in the risk matrix.

Colour		Description
Red		Unacceptable risk. Measures must be taken to reduce the risk.
Yellow		Assessment range. Measures must be considered.
Green		Acceptable risk Measures can be considered based on other considerations.

Appendix II

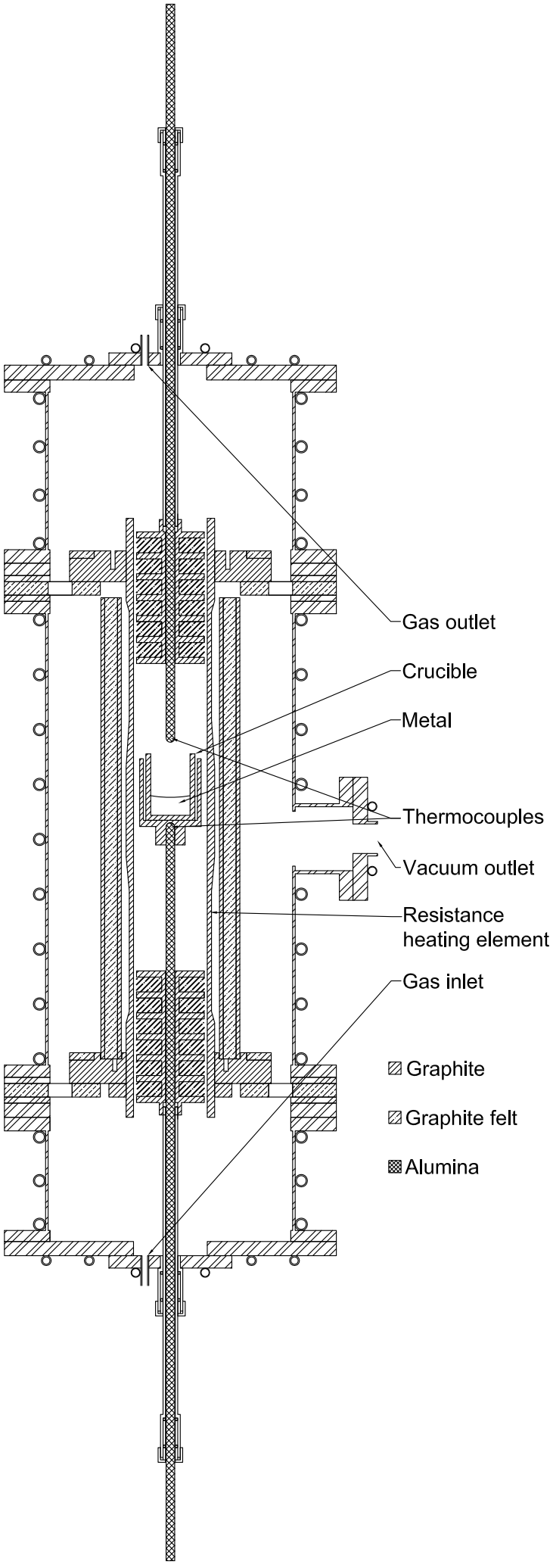
Gas outlet
Crucible
Metal
Thermocouples
Vacuum outlet
Resistance
heating element
Gas inlet
Graphite
Graphite felt
Alumina

Appendix III

Input 2a MET1 (Coupled TwoTheta/Theta)

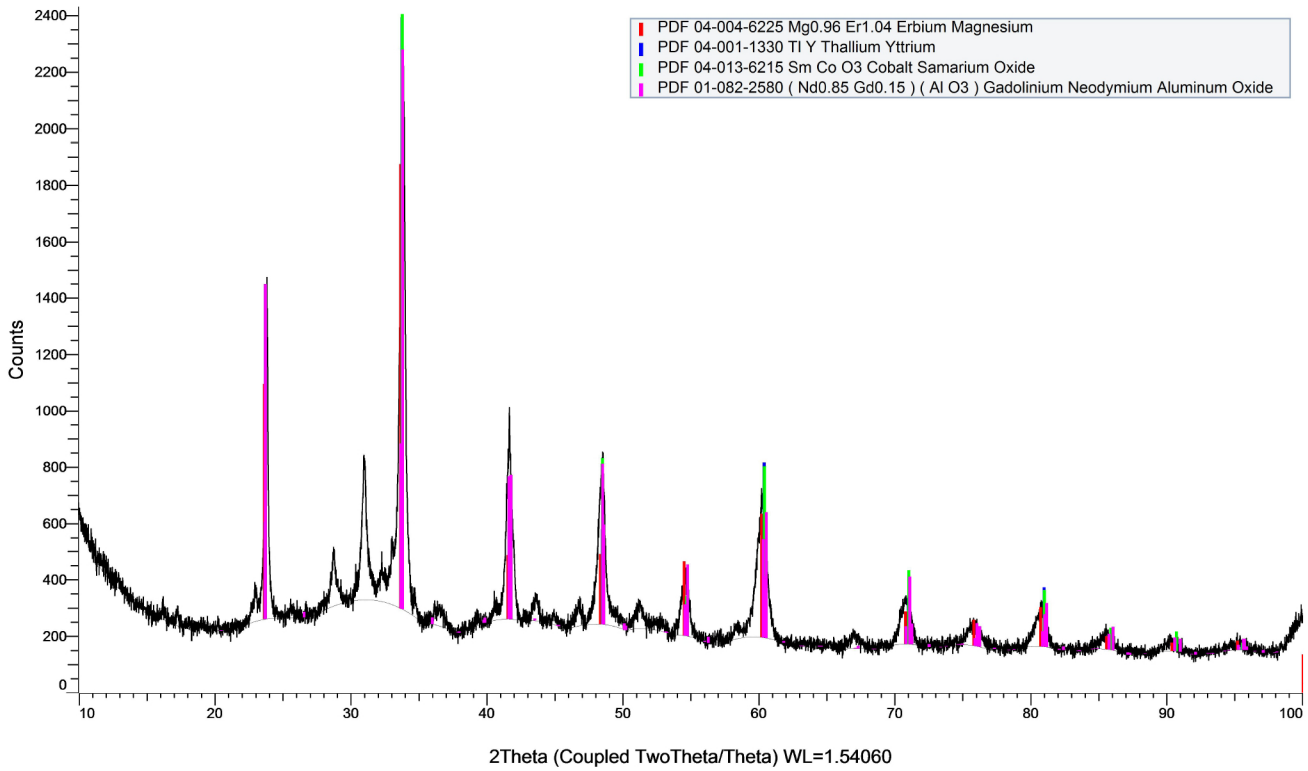

Input 2b MET 1 (Coupled TwoTheta/Theta)

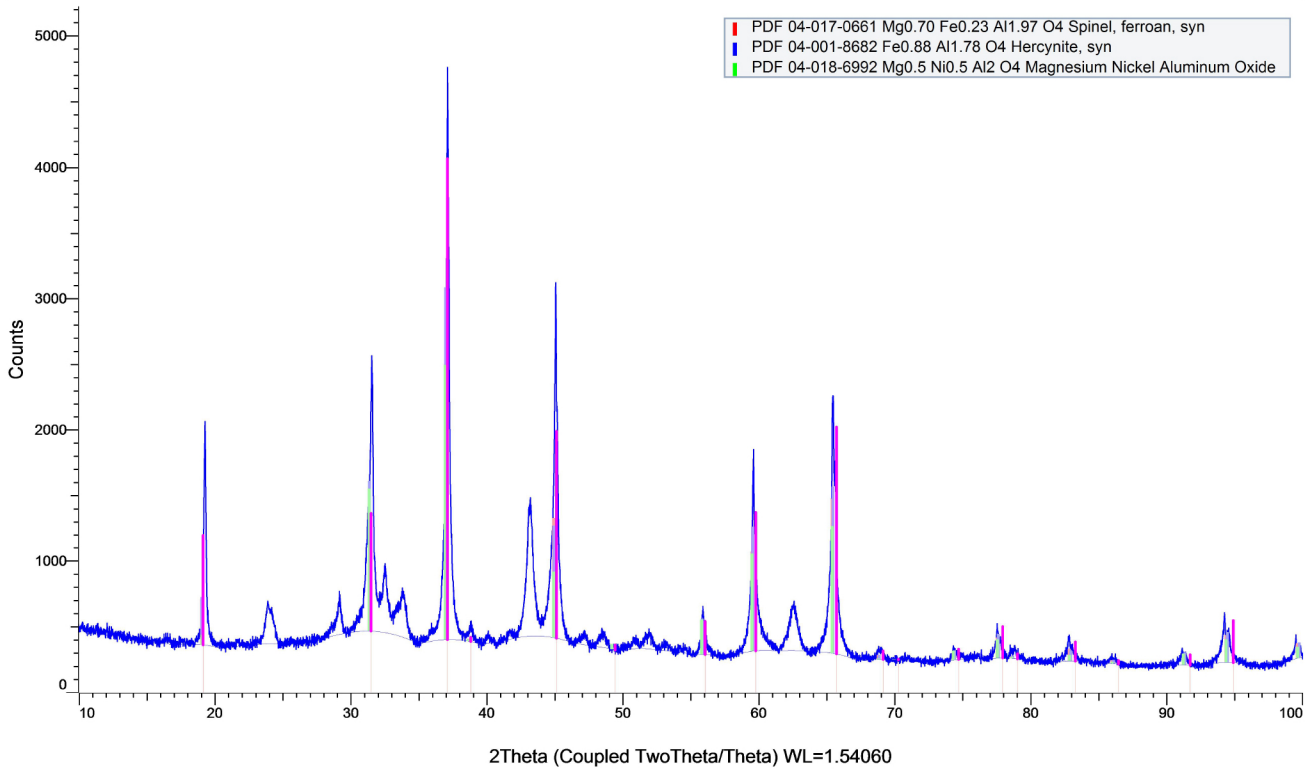

Input 2c MET1 (Coupled TwoTheta/Theta)

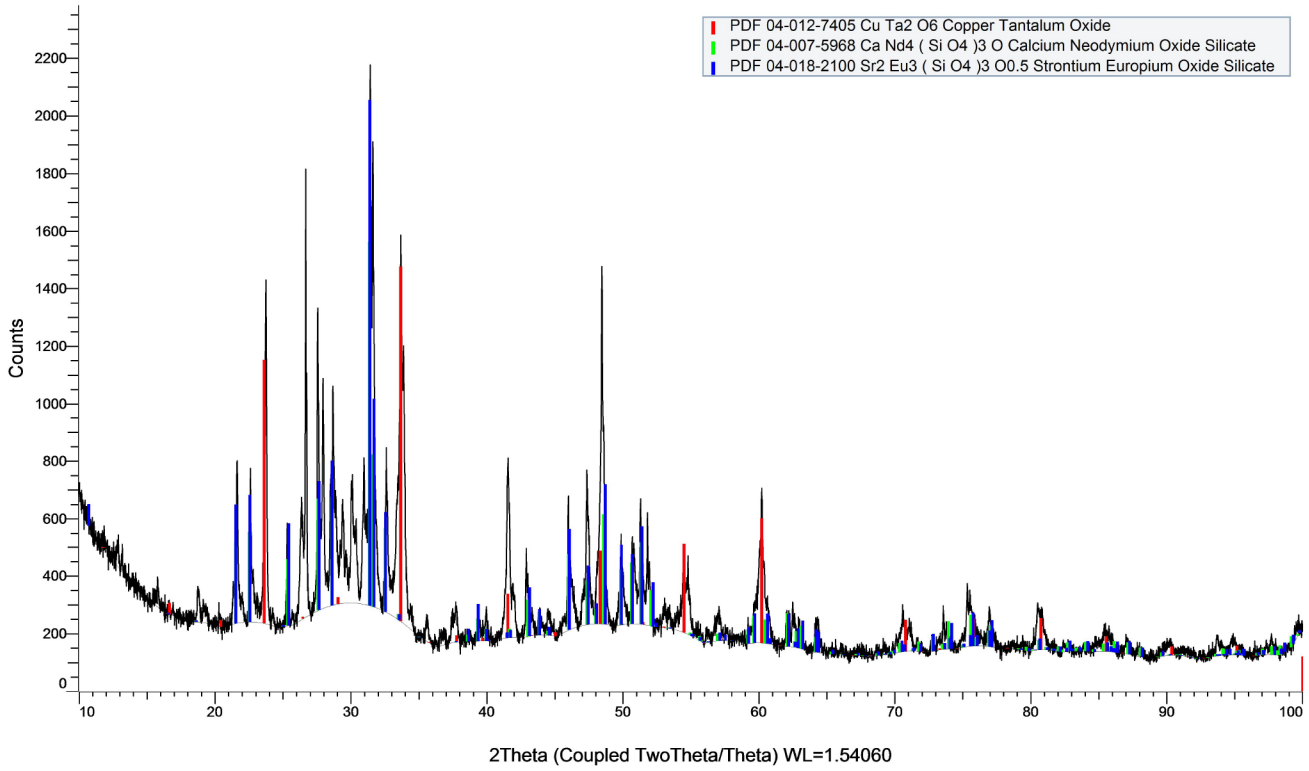

Input 2c MET2 (Coupled TwoTheta/Theta)